Middle-Infrared Laser Sources

by

Wayne Sean Koen

Dissertation presented for the degree of

Doctor of Philosophy

in the Faculty of Science at

Stellenbosch University

Supervisor: Prof. M.J. Daniel Esser

Co-supervisors: Prof. Erich G. Rohwer, Dr. Hencharl J. Strauss, Dr. Lourens R. Botha

March 2016

DECLARATION

By submitting this dissertation electronically, I declare that the entirety of the work contained therein is my own original work, that I am the sole author thereof (save to the extent explicitly otherwise stated), that reproduction and publication thereof by Stellenbosch University will not infringe any third party rights and that I have not previously in its entirety or in part submitted it for obtaining any qualification.

DECLARATION

This dissertation includes 5 original papers published in peer reviewed journals, proceedings or books and 1 unpublished publication. The development and writing of the papers (published and unpublished) were the principal responsibility of myself and, for each of the cases where this is not the case, a declaration is included in the dissertation indicating the nature and extent of the contributions of co-authors.

ABSTRACT

Both bulk solid-state mid-infrared lasers and amplifier systems based on Tm^{3+} and Ho^{3+}, as well as mid-infrared optically pumped molecular gas lasers based on HBr were developed and studied.

An efficient high-power Ho:YLF laser which was end-pumped by a commercially available Tm:fibre laser was designed and demonstrated. The holmium laser delivered 45.1 W of average power in a near diffraction-limited beam when pumped with 84.7 W, resulting in a record optical-to-optical efficiency of 53 %.

A compact 60.2 W Ho:YLF master oscillator power amplifier system pumped by two unpolarised Tm:fibre lasers was subsequently developed. The seed laser delivered a maximum average output power of 24 W with a beam quality factor (M^2) equal to 1.06. The two-crystal, single-pass amplifier delivered a gain of 2.5 and M^2 of 1.09. The amplifier utilised the transmitted pump from the seed lasers' single fibre laser in addition to a second fibre laser, resulting in an optical-to-optical efficiency of 55.5 %. Under Q-switched operation, laser pulse lengths of between 43 and 113 ns at pulse repetition rates from 15 to 40 kHz were measured.

An optical pump source for molecular HBr lasers was developed collaboratively, which comprised of a double-pass, single-frequency Ho:YLF slab amplifier that delivered 350 ns long pulses of up to 330 mJ at 2064 nm, with a maximum M^2 of 1.5 at 50 Hz. It was end-pumped with an in-house developed diode-pumped Tm:YLF slab laser and seeded with up to 50 mJ of single-frequency laser pulses from an injection-seeded, single-frequency Ho:YLF ring-laser.

Subsequently an optically end-pumped HBr master oscillator power amplifier was demonstrated for the first time. It produced a record output energy of up to 10.3 mJ, operating simultaneously at 4.20 and 4.34 µm when pumped with the single-frequency Ho:YLF slab amplifier. Wavelength selection with the use of an intra-cavity CO_2 absorption cell was also demonstrated, forcing the oscillator to emit at 3.89, 4.13 and 4.16 µm simultaneously, with a maximum output energy of 6.5 mJ per pulse after amplification.

Lastly, an optically pumped tuneable HBr molecular laser was demonstrated for the first time. Laser oscillation was demonstrated on nineteen molecular transition lines including both the R-branch (3870 nm to 4015 nm) and the P-branch (4070 nm to 4453 nm) by the use of an intra-cavity diffraction grating. This was also the first time laser operation on the R-branch of HBr was demonstrated. The highest output energy from the laser was 2.4 mJ at 4134 nm.

OPSOMMING

Beide vastetoestand mid-infrarooi laser- en versterker-stelsels gebaseer op Tm^{3+} en Ho^{3+}, sowel as mid-infrarooi opties-gepompte molekulêre gas lasers gebaseer op HBr, is ontwikkel en bestudeer.

'n Doeltreffende hoë-energie Ho:YLF laser, wat ge-entpomp is deur 'n kommersieel beskikbare Tm:vesel laser is ontwerp en gedemonstreer. Die holmium laser het tot 45.1 W se gemiddelde krag gelewer in 'n diffraksie-beperkte laser-bundel wanneer dit gepomp is met 84.7 W. Die ontwerp het gelei tot 'n rekord optiese-tot-optiese doeltreffendheid van 53%.

'n Kompakte 60.2 W Ho:YLF meester ossillator en versterker-stelsel gepomp deur twee ongepolariseerde Tm:vesel lasers is daarna ontwikkel. Die ossillator het 'n maksimum gemiddelde uitsetkrag van 24 W gelewer, met 'n laser-bundel gehalte-faktor (M^2) gelyk aan 1.06. Die twee-kristal, enkel-gang versterker het 'n versterkingsfaktor van 2.5 en M^2 van 1.09 gehad. Die versterker het die ongeabsorbeerde pomplig van die ossillator se enkele vesel-laser in kombinasie met die pomplig van ‘n tweede vesel-laser gebruik. Die pomp skema het gelei tot 'n optiese-tot-optiese doeltreffendheid van 55.5%. Onder Q-skakeling is laser pulslengtes van tussen 43 en 113 ns vir puls repetisie frekwensies van 15 tot 40 kHz gemeet.

'n Optiese pomp bron vir molekulêre HBr lasers is gesamentlik ontwikkel. Dit het bestaan uit 'n dubbel-gang, enkel-frekwensie Ho:YLF versterker wat 350 ns lang pulse van tot 330 mJ per puls gelewer het by 2064 nm, met 'n maksimum M^2 van 1.5 teen ‘n repetisie tempo van 50 Hz. Dit is gepomp met 'n Tm:YLF blad laser.

Daarna is 'n opties ge-entpompte molekulêre HBr meester-ossillator drywingsversterker vir die eerste keer gedemonstreer. Dit het 'n rekord uitset energie van tot 10.3 mJ gelewer, en gelyktydig ossilleer by 4.20 en 4.34 μm. Die HBr stelsel is gepomp met die enkel-frekwensie Ho:YLF blad versterker. Golflengte-seleksie met die gebruik van 'n CO_2 absorbsie-sel is ook gedemonstreer, wat die laser gedwing het om gelyktydig uit te straal by 3.89, 4.13 en 4.16 μm, met 'n maksimum uitset energie van 6.5 mJ per puls na versterking.

Laastens is 'n opties gepompte, golflentge-verstelbare HBr molekulêre laser vir die eerste keer gedemonstreer. Laser ossillasie is gedemonstreer op negentien oorgange, insluitende beide die R-transisies (3870 nm tot 4015 nm) sowel die P-transisies (4070 nm tot 4453 nm) deur die gebruik van 'n diffraksierooster. Dit is die eerste keer wat laser-emissie op die R-transisies van HBr gedemonstreer is. Die hoogste uitset energie van die laser was 2.4 mJ per puls by 4134 nm.

Aan my Liefste,

Ernst

ACKNOWLEDGEMENTS

I would like to express my sincere gratitude to, and acknowledge:

- The CSIR National Laser Centre that sponsored my formal studies and afforded me the time to complete this dissertation.
- The CSIR Young Researcher Establishment Fund.
- ARMSCOR for their substantial financial support of laser development at the CSIR National Laser Centre.
- The National Research Foundation for financial aid through a Thuthuka Grant.
- The Novel Lasers group members at the NLC for their technical ideas and contributions, particularly Cobus Jacobs, Gary King, Lorinda Wu, Hencharl Strauss, Dieter Preussler, and Corrie van der Westhuizen.
- Christoph Bollig, for setting me on this great adventure in the first place.
- My supervisors, Prof. Daniel Esser, Dr. Hencharl Strauss, Prof. Erich Rohwer, and posthumously, Dr. Lourens Botha. Your knowledge, encouragement, and assistance have allowed me to become the scientist I am today.
- My family and friends whose interest and encouragement helped me complete this dissertation with maximum vigour (if not always the greatest enthusiasm).

Finally, I would like to thank the love of my life, Ernst. Without your unwavering love and support, this endeavour would simply have been impossible to take on and complete.

TABLE OF CONTENTS

Declaration i

Declaration ii

Abstract iii

Opsomming iv

Acknowledgements vi

Table of Contents vii

List of Figures xi

List of Tables xviii

List of Symbols and Abbreviations xix

1 Introduction 22

1.1 Research problem 23

1.2 Overview of the dissertation 26

2 Introduction to Tm:fibre Laser Pumped Ho:YLF Lasers 29

2.1 Three approaches to designing holmium lasers: A brief overview 29

2.2 Properties of Ho:YLF 34

2.2.1 Absorption spectra and energy levels 34

2.2.2 Mechanical and optical properties of Ho:YLF laser crystals 37

2.2.3 Quenching of the laser transition: Ho-Ho energy transfer 38

2.3 Power and energy scaling of Tm pumped Ho:YLF solid state lasers and amplifiers 40

2.4 Conclusions 51

3 Development of an Efficient 45 W Ho:YLF Laser Pumped by a Tm:fibre Laser 54

3.1 Introduction 54

3.2 Experimental design and setup 56
3.2.1 The Ho:YLF laser crystals 57
3.2.2 Pump source and design 59
3.2.3 Resonator design 61
3.3 Experimental results 65
3.4 Discussion 68
3.5 Conclusion 70
4 Development of a 60 W Ho:YLF Oscillator-Amplifier System 72
4.1 Introduction 72
4.2 Design and experimental setup of the Ho:YLF MOPA system 74
4.2.1 Pump design 74
4.2.2 Selection of the Ho:YLF laser crystals 76
4.2.3 Resonator design 76
4.2.4 Design of the two-crystal amplifier 78
4.3 Experimental results of the Ho:YLF MOPA system 80
4.3.1 Oscillator results 81
4.3.2 Amplifier Results 83
4.4 Discussion 84
4.5 Conclusion 87
5 Single-frequency Ho:YLF Slab Amplifier Pumped by a High-power Tm:YLF Slab Laser . 90
5.1 Introduction 90
5.2 Development of a Tm:YLF slab laser as pump source for a Ho:YLF slab amplifier 92
5.3 The single-frequency Ho:YLF seed laser 99
5.4 The double-pass Ho:YLF slab amplifier design and setup 100

5.5 Performance of the Tm:YLF slab laser pumped Ho:YLF slab amplifier system 103
5.6 Conclusion 107
5.7 Contributions 108
6 Introduction to Mid-infrared Optically Pumped Molecular Lasers Based on HBr Gas 111
6.1 Optically pumped HBr lasers as mid-infrared laser sources 111
6.2 Properties of HBr gas as an optically pumped laser medium 113
6.2.1 Pumping transitions 114
6.2.2 Laser transitions 117
6.3 Optically pumped HBr molecular lasers in literature 118
6.4 Discussion 123
6.5 Conclusion 126
7 Development of an Optically Pumped HBr Master Oscillator Power Amplifier 128
7.1 Introduction 128
7.2 Experimental design and setup 129
7.2.1 Pump design and setup 130
7.2.2 Resonator design and setup 133
7.2.3 Amplifier design and setup 136
7.3 Experimental results 138
7.3.1 Absorption measurements 139
7.3.2 Oscillator performance 141
7.3.3 Amplifier performance 146
7.4 Discussion 151
7.5 Conclusion 152
8 Design & Development of an Optically Pumped Tuneable HBr Laser 155

8.1 Introduction 155
8.2 Experimental design and setup 157
8.2.1 The single-frequency pump source 158
8.2.2 Design and setup of the tuneable HBr laser 159
8.3 Experimental results and discussion 162
8.4 Conclusion 166
9 Closing Remarks 168
9.1 Summary of significant results 168
9.1.1 Efficient 45 W Ho:YLF Laser Pumped by a Tm:fibre Laser 168
9.1.2 60 W Ho:YLF Oscillator-Amplifier System 169
9.1.3 High-energy, Single-frequency Ho:YLF Slab Amplifier 170
9.1.4 Optically Pumped Mid-Infrared HBr Master Oscillator Power Amplifier System 171
9.1.5 Optically Pumped Tuneable HBr Laser 171
9.2 Conclusion 172
10 References 175
11 List of Publications 181

LIST OF FIGURES

Figure 1: Atmospheric transmission of light from 1 to 6 µm, as generated by IRTRANS4 (4.2 km propagation distance from space to ground), provides a good indication where lasers may operate for free space propagation (UKIRT 2013). 23

Figure 2: Pumping scheme and relevant energy levels in a flash lamp-pumped co-doped Cr, Tm, Ho:YLF 2 µm system (Rustad & Stenersen 1996; Sorokina & Vodopyanov 2003).. 30

Figure 3: Pumping scheme and relevant energy levels in a diode-pumped co-doped Tm, Ho:YLF 2 µm system (W. Koen, H. J. Strauss, et al. 2010). 31

Figure 4: Schematic and pumping scheme of a laser diode-pumped Tm laser pumping a Ho laser (W. Koen, H. J. Strauss, et al. 2010). 33

Figure 5: Absorption and emission cross sections for the $^5I_7$ manifold of Ho:YLF on the π- and σ-sigma polarisations from 1850 to 2100 nm (Walsh et al. 1998). 35

Figure 6: Scheme of the energy levels of interest for pumping Ho:YLF with a Tm:fibre laser, reproduced from (Koen 2010). 36

Figure 7: Ho-Ho energy transfer process (marked p_{77}) where two holmium ions can interact so that one of the ions is excited from the $^5I_7$ manifold to the $^5I_5$ manifold and the second ion is de-excited from $^5I_7$ to $^5I_8$. The reverse self-quenching process (p_{58}) also exists where a holmium ion in the $^5I_5$ state and another ion in the $^5I_8$ state can interact, resulting both ions ending up in $^5I_7$ (Barnes et al. 2003). 39

Figure 8: Schematic of a Ho:YLF laser end-pumped by a commercially sourced, unpolarised 100 W Tm:fibre laser. The unpolarised laser light from the fibre laser was split into vertical and horizontally polarised light with a polarising beam splitter (PBS) in order to separately pump the two Ho:YLF crystals in the laser (Dergachev et al. 2005). ... 43

Figure 9: Schematic layout of a Tm:fibre laser pumped Ho:YLF Master Oscillator Power Amplifier (MOPA) (Dergachev et al. 2007). The unpolarised laser light from the fibre laser is split into vertically and horizontally polarised beams to pump the oscillator and amplifier crystals seperately. 44

Figure 10: Schematic layout of the two crystal Ho:YLF amplifier pumped by a single Tm:fibre laser, developed by Dergachev et al.. Two of these amplifiers amplified a Ho:YLF MOPA's output to 170 mJ at a PRF of 50 Hz (Dergachev et al. 2008). 45

Figure 11: A schematic of the Ho:YLF MOPA system reported upon in (W Koen et al. 2010). The system utilised the unpolarised beam from a Tm:fibre laser to pump two Ho:YLF crystals in series. 46

Figure 12: The single-frequency Ho:YLF ring laser and single-pass amplifier developed subsequently to (W Koen et al. 2010). The MOPA system also used the full unpolarised beam from the same Tm:fibre laser to pump multiple Ho:YLF crystals whose c-axes were orientated perpendicular with regard to each other (Bollig et al. 2009). 48

Figure 13: A Tm:fibre laser pumped Ho:YLF MOPA reported on by Kwiatkowski et al. in 2015 (Kwiatkowski et al. 2015) 49

Figure 14: A single-frequency Ho:YLF ring-laser developed by Gibert et al. to do CO_2 DIAL measurements in the atmosphere (Gibert et al. 2014). 50

Figure 15: Simulated average output power of a Q-switched Ho:YLF laser (25 kHz PRF) as a function of mode size in the Ho:YLF crystals for a constant 84.7 W of incident pump power (Jacobs 2013b). An increase in average output power with a decrease in pump and mode size is clearly evident. 56

Figure 16: A Ho:YLF crystal rod mounted in a water cooled copper mount. A more compact variation of the mount design that was used in subsequent work is shown in the background. 58

Figure 17: The commercially sourced thulium fibre laser used as pump source (Model TLR-80-1940, from *IPG Photonics*) 58

Figure 18: The IPG thulium fibre laser's spectral output superimposed with the atmospheric transmission of light through 1 meter of air with a relative humidity of 50 %, at 300K (Koen 2010). 59

Figure 19: Beam profiles of the thulium fibre laser taken 1.85 m away from the fibre collimator, as measured by an *Ophir Spiricon Pyrocam III* (Koen 2010). The left profile is with the laser set at 50 % output power while the right profile is at 100 %. The thermal blooming at the lower power is attributed to a shift in the output wavelength of the laser, increasing the overlap with a strong water absorption line. 61

Figure 20: Schematic of the experimental layout of the 45 W Ho:YLF laser. 61

Figure 21: The *Gooch & Housego* AOM used for q-switching the laser. 63

Figure 22: Two Ho:YLF crystals inside the same cavity, their c-axes rotated 90° with regard to each other in order to increase the total amount of pump light being absorbed. 64

Figure 23: A top-view photo of the constructed Ho:YLF laser. The input coupler mirror is on the top left of the photo, followed by the two crystals in the water cooled copper mounts and the folding mirror. The AOM and output coupler mirror is shown bottom right. 66

Figure 24: The Ho:YLF measured laser slope (cw) as a function of incident pump power. The simulated results are also shown. The difference between the simulated cw and Q-switched results can be attributed to AOM insertion losses (Jacobs 2013b)..... 67

Figure 25: (left) Laser beam profile at full power and (right) the pulse trace of the laser when being Q-switched at a pulse repetition frequency of 50 kHz. The green trace is the AOM trigger while the cyan trace is the measured laser pulse. 68

Figure 26: Schematic diagram of the Ho:YLF Master Oscillator Power Amplifier system..... 74

Figure 27: The system control rack containing the two air-cooled Tm:fibre lasers and other electronic components 75

Figure 28: A screen shot of the Resonator design within *Psst!* software (Gillies et al. 2000). The optical components are shown in blue while the fundamental resonator mode is shown in red..... 77

Figure 29: The input screen of the in-house developed beam propagation software, *EXAG*, used to design the Ho:YLF amplifier (Jacobs 2013a; Jacobs et al. 2009). 78

Figure 30: A screenshot from *EXAG* software depicting the amplifier seed beam (navy trace) and the second thulium fibre laser pump beam (cyan trace) design (Jacobs 2013a; Jacobs et al. 2009)..... 79

Figure 31: The Ho:YLF MOPA system prior to integration. The two thulium fibre lasers can be seen connected on the right. Their respective beam reducing telescopes are wrapped in plastic and flushed with dry air to prevent absorption of the laser light by water vapour from causing thermal blooming..... 80

Figure 32: A photo of the Ho:YLF MOPA system integrated into its portable case. The MOPA occupied less than half of the box, with the rest occupied by a three-channel optical switching system and two optical parametric oscillators..... 81

Figure 33: Oscillator output power versus absorbed fibre pump power under cw lasing conditions. The solid line is a linear fit of the measured data points, indicating a slope of 75 % with regards to absorbed pump power. 82

Figure 34: Oscillator and amplifier output energy (left axis) and FWHM pulse lengths (right axis) as a function of the pulse repetition rate at full pump power..... 83

Figure 35: Temporal pulse trace of the MOPA output at a PRF of 15 kHz and full pump power. The FWHM pulse length was 43 ns. The spatial intensity profile of the MOPA output

beam at full pump power, as measured by an *Ophir Spiricon Pyrocam III*, is shown in the inset. 84

Figure 36: The optical transmission graph of uncoated zinc germanium phosphate crystals (Inrad 2015). A photo of AR coated ZGP crystals is shown in the insert. 87

Figure 37: Schematic showing the inter-dependencies of the systems described in this as well as subsequent chapters. The Tm:YLF slab laser is described in Section 5.2 while the single-frequency Ho:YLF ring-laser is discussed in Section 5.3. The Ho:YLF slab amplifier, which is pumped by the thulium laser and seeded by the ring-laser, is presented in Section 5.4. Various configurations of the HBr system, which is optically pumped by the amplifier, are presented in Chapters 8 and 7..... 91

Figure 38: A schematic of the initial Tm:YLF slab laser setup. The beam intensity profile of the laser is shown in the insert, bottom left (W. Koen, H. J. Strauss, et al. 2010b). 93

Figure 39: Ho:YLF and Ho:LuLF absorption spectra on the σ- and π-polarisation. Laser wavelengths of the Tm:YLF slab laser (σ- and π-polarisation) as well as a typical Tm:fibre laser output wavelength is also shown (as used in Chapters 3 and 4), indicating which of these sources are appropriate for pumping these crystals. (Reproduced from (W. Koen, H. J. Strauss, et al. 2010b))..... 94

Figure 40: The calculated laser threshold pump power density (absorbed) of the Tm:YLF laser for a 10 % output coupler, with and without a Brewster plate inducing loss on only the sigma polarisation. This work was based on an approach developed by (Fan & Byer 1987) and subsequently expanded on by (Stoneman & Esterowitz 1995). Spectroscopic data from (Walsh et al. 1998) was used in the calculations. 96

Figure 41: Schematic of the redesigned Tm:YLF slab laser. A top-view photo of the laser layout is shown in the insert, bottom left (W. Koen, H. J. Strauss, et al. 2010b). 97

Figure 42: The modified Tm:YLF lab laser output power as a function of incident pump power. The laser's beam intensity profile at full power is shown in the insert. 98

Figure 43: Schematic of the optical layout of the injection-seeded, single-frequency Ho:YLF ring laser and its pre-amplifier..... 99

Figure 44: Schematic of the experimental setup for the double-pass Ho:YLF slab amplifier. A photo of the mounted slab crystals is shown in the insert. 100

Figure 45: Seed and Amplified 2064 nm output energy (left axis) and the average power of the amplified pulses (right axis) as functions of Pulse Repetition Frequency. 104

Figure 46: The amplified output energy (right axis) and gain (left axis) as functions of incident 1890 nm Tm:YLF pump power. 105

Figure 47: The amplified output energy (right axis) and gain (left axis) as functions of seed energy at a PRF of 50 Hz. 106

Figure 48: Amplified beam profile in the far field at full power (a) and the seed and amplified pulses at maximum output and a PRF of 50 Hz (b). 107

Figure 49: A schematic diagram of an optically pumped HBr laser. 112

Figure 50: Schematic depicting pumping and lasing transitions of a 2 µm pumped HBr laser. Pumping is from the ground vibrational level v=0 to the v=2 vibrational level. Lasing can occur on various P branch (J=J'+1) and R branch (J=J'-1) transitions from v=2 to v=1. After lasing, the remaining excited vibrational levels eventually relax back to v=0 through vibration-to-translation (V-T) processes, releasing heat into the gas. J' and J are the upper and lower level rotational quantum numbers respectively. 113

Figure 51: The calculated rotational (J) partition function of the vibrational ground state (v=0) at 300 K, reproduced from (Botha et al. 2009). 115

Figure 52: Atmospheric transmission in the 3.7 µm to 5 µm region (from space to ground at an altitude of 4.2 km) using the program IRTRANS4 (UKIRT 2013) with the gain cross sections of HBr superimposed upon it (Miller et al. 1994). 117

Figure 53: Schematic of the optically pumped HBr laser reported by (Miller et al. 1994). 118

Figure 54: Experimental setup of the HBr laser reported by Kletecka et al. which was optically pumped by a 1.3 µm Nd:YAG laser (Kletecka et al. 2004). 119

Figure 55: The HBr pumping and lasing scheme implemented by Kletecka et al. in 2004. The second overtone of HBr (v=0 to v=3) was excited by pumping with a temperature-tuned, frequency-stabilised Q-switched Nd:YAG laser operating at 1.3 µm. Cascade lasing was observed from the v=3 to v=2 and v=2 to v=1 vibrational levels (Kletecka et al. 2004). 120

Figure 56: Schematic layout of the HBr laser reported on by (Ratanavis et al. 2008). The HBr laser was optically pumped by a temperature-tuned, frequency-stabilised, injection-seeded 1.34 µm Nd:YAG laser from the v=0 to v=3 overtone of HBr. 121

Figure 57: Schematic layout of the Ho:YLF pumped HBr laser system reported by our group in 2009 (Botha et al. 2009). 122

Figure 58: Atmospheric transmission of light through air in the 1.2 to 1.4 µm region, showing the sharp drop in transmission from 1.3 µm onwards (4.2 km propagation from space to ground) (UKIRT 2013). 123

Figure 59: The single-frequency ring-laser and amplifier system used as pump source (left) and the HBr MOPA setup with the gas handling system (right). 130

Figure 60: Schematic layout of the HBr oscillator and amplifier. 131

Figure 61: Screen grab of *PSST!* laser resonator software displaying the calculated fundamental resonator mode of the HBr oscillator. The software allows one to design oscillator cavities by specifying various mirror curvatures, intra-cavity lenses, propagation distances and laser wavelengths. The resulting fundamental mode of the cavity is shown in red, while the optics are shown in blue. 133

Figure 62: Experimental layout of the HBr oscillator with a CO_2 absorption cell. 134

Figure 63: Photo of the modified HBr oscillator containing an absorption cell (black tube) filled with CO_2 gas at ambient pressure. 135

Figure 64: Proposed 2 µm seed beam shaping design as generated by *EXAG* software (Jacobs 2013a). The x-axis indicates the distance from the Ho:YLF amplifier while the two purple lines indicate the region of interest for the HBr system. The vertical and horizontal pump beam radii are shown in red and blue respectively. 136

Figure 65: The amplifier pump and seed beam diameters, as measured by an *Ophir Spiricon PyroCam III* (90/10 knife edge calculation). The HBr amplifier cell position is depicted by the blue cylinder. 137

Figure 66: A photo of the HBr MOPA system. The oscillator is shown at the bottom of the photo while the amplifier is shown at the top. 138

Figure 67: Comparison of the single-pass absorption of the HBr amplifier (seeded) and the HBr oscillator (lasing and non-lasing) as a function of HBr pressure. The pump energy was kept fixed at 43 mJ for the HBr oscillator cell, and 200mJ for the HBr amplifier cell. 139

Figure 68: Double-pass absorbed 2 µm pump energy (left axis) in the HBr oscillator cell and total absorption (right axis) as a function of HBr pressure at a fixed pump energy of 43 mJ 140

Figure 69: The 4 µm laser output energy as a function of HBr pressure for an incident 2 µm pump energy of 50 mJ. 141

Figure 70: HBr Oscillator output energy as a function of incident 2 µm energy. The laser had a slope efficiency of 2.3 % with regards to incident pump energy. Optical damage of the HBr cell's front window occurred during the experiment where indicated. 142

Figure 71: The 4 µm oscillator output energy and efficiency as a function of incident pump energy. 143

Figure 72: Emission lines of HBr obtained with a CO_2 absorption cell placed in the resonator as well as the atmospheric absorption spectrum shown in black (for a propagation distance of 2 km, 1 atm. pressure, 296 K, USA tropics model (UKIRT 2013)). 144

Figure 73: The 4 µm oscillator beam intensity profile at 50 mJ of pump power and an HBr pressure of 40 mBar, as recorded by an *Ophir Spiricon Pyrocam III*. 145

Figure 74: Amplified energy and gain as functions of the HBr pressure in the amplifier cell. . 146

Figure 75: Amplified 4 µm energy and gain as functions of the seed energy from the 4µm oscillator. 147

Figure 76: Amplified energy and gain as functions of incident 2 µm pump energy to the HBr amplifier..... 148

Figure 77: The temporal pulse shape of the 4 µm amplifier output is shown in yellow. The 2 µm pump pulse is shown in blue and the pulse from the single-frequency 2 µm laser before amplification shown in green. All trace amplitudes are arbitrary and not relative to one another. 149

Figure 78: The beam intensity profile of the 4 µm amplified beam, as recorded by an *Ophir Spiricon Pyrocam III*. 149

Figure 79: Atmospheric transmission in the 3.6 to 5 µm region (from space to ground at an altitude of 4.2 km) using the program IRTRANS4 (UKIRT 2013) with the emission cross sections of v=2 to v=1 transitions of HBr (Miller et al. 1994) superimposed upon it. The cross sections have been normalized such that the strongest line, P(4), equals 100 %. 156

Figure 80: Experimental setup of the tuneable HBr oscillator..... 158

Figure 81: A photo of the ruled intra-cavity grating mounted in a rotation stage. 160

Figure 82: Laser transition lines observed by tuning the resonator cavity with the optical grating. The output energy measured for each laser transition is depicted by the square (P-branch) and diamond markers (R-branch). 162

Figure 83: Temporal pulse traces of the pump laser (yellow) and the HBr laser (cyan). The pump and laser pulse intensities are arbitrary and not relative to each other. 163

Figure 84: The HBr cell's AR coated windows damaged by corrosion. 166

LIST OF TABLES

Table 1: Optical and physical properties of Ho:YLF (Chang & Kuo 2002; Walsh et al. 1998).... 37

Table 2: Ho:YLF laser and MOPA systems in literature. 41

Table 3: Component list of the Ho:YLF laser 62

Table 4: The Ho:YLF laser output parameters 67

Table 5: Comparison of efficient holmium YLF and YAG lasers 70

Table 6: Comparitive table of published Ho:YLF MOPA systems. 86

Table 7: HBr v=0 to v=2 band transition wavelengths and A-coefficients (Miller et al. 1994). . 116

Table 8: HBr v=2 to v=1 band transition wavelengths and A-coefficients (Miller et al. 1994). . 116

Table 9: HBr MOPA component list as labelled in Figure 60. 132

Table 10: HBr laser transitions observed from vibrational level 2 to 1. 165

LIST OF SYMBOLS AND ABBREVIATIONS

AOI	Angle of Incidence
AOM	Acousto-Optic Modulator
Amp.	Amplifier
BRM	Back Reflector Mirror
cw	Continuous Wave
CCD	Charge Coupled Device
DIAL	Differential Absorption LIDAR
DIRCM	Directed Infra-Red Counter Measures
σ_a	Effective absorption cross section
σ_e	Effective stimulated emission cross section
EOM	Electro-Optic Modulator
ETU	Energy Transfer Upconversion
ESA	Excited State Absorption
ν	Frequency
FWHM	Full Width Half Maximum
HBr	Hydrogen Bromide
Ho	Holmium
ICM	Input Coupler Mirror
LASER	Light Amplification through Stimulated Emission of Radiation
LIDAR	Light Detection And Ranging
LLF/LuLiF/LuLF	Lutetium Lithium Fluoride
M^2	Beam Quality Factor
MOPA	Master-Oscillator Power Amplifier
NA	Numerical Aperture
OCM	Output Coupler Mirror
OPA	Optical Parametric Amplifier
OPG	Optical Parametric Generator

OPML	Optically Pumped Molecular Laser
OPO	Optical Parametric Oscillator
Osc.	Oscillator
PBS	Polarising Beam Splitter
PEM	Photo-electromagnetic detector
PRF	Pulse Repetition Frequency
h	Planck's constant
g_0	Small signal gain coefficient
f	Thermal Boltzmann factor
Tm	Thulium
UKIRT	United Kingdom Infrared Telescope
λ	Wavelength
YAG	Yttrium Aluminium Garnet
YLF/YLiF	Yttrium Lithium Fluoride
ZGP	Zinc Germanium Phosphate, $ZnGeP_2$

1 Introduction

Since their first successful demonstration, lasers have become an indispensable part of not only numerous industries but of the human civilization as a whole. Billions of lasers are now in daily use, from what some may consider being frivolous applications such as entertainment, to the dire; shooting down drones and disabling landmines. The vast majority of these lasers are diode-based, operating mostly in the visible and near-infrared regions. More structurally complex lasers and architectures include bulk solid-state, fibre, gas, waveguide, and quantum-cascade lasers. The sheer usefulness of this marvel of applied physics has led to research in laser sources becoming a large field of its own within the even broader scope of photonics.

The focus of this dissertation is particularly the research and development of novel laser sources operating in the mid-infrared region, an exciting part of the spectrum that has until relatively recently been served by only a few coherent sources. Despite mid-infrared lasers having first been demonstrated many decades ago, their improvement has only been gaining momentum since high-power laser diodes have become more readily available. Subsequently, laser diodes have become a critical enabler for the development of new efficient, robust, and compact laser systems in this region. It is worth noting however that although the laser systems presented in this dissertation would not have been possible without laser diodes as a primary pump source, it is only one of many components and aspects that enable us to develop novel mid-infrared coherent sources that can serve us in a diverse range of fields. The author will address these numerous aspects throughout the dissertation, from the detailed study of the laser media, laser processes, resonator and amplifier designs, to the implementation and analysis of the subsequently developed systems.

1.1 Research problem

Laser sources in the near-infrared region (0.8-1.4 µm) gained significant market representation at the end of the previous century with the proliferation of both neodymium solid-state lasers as well as diode lasers. Mid-infrared laser sources in the 2-5 µm region lagged behind, however, in both power and availability. Even though they were demonstrated soon after the first laser was developed, significant improvement was required for their use to become more mainstream (Johnson et al. 1962b; Johnson et al. 1962a; Sorokina & Vodopyanov 2003). Today this improvement is still an ongoing process, driven by need from applications, and aided by a diverse array of different scientific domains such as material science, quantum optics, nonlinear optics and solid-state physics (to name but a few).

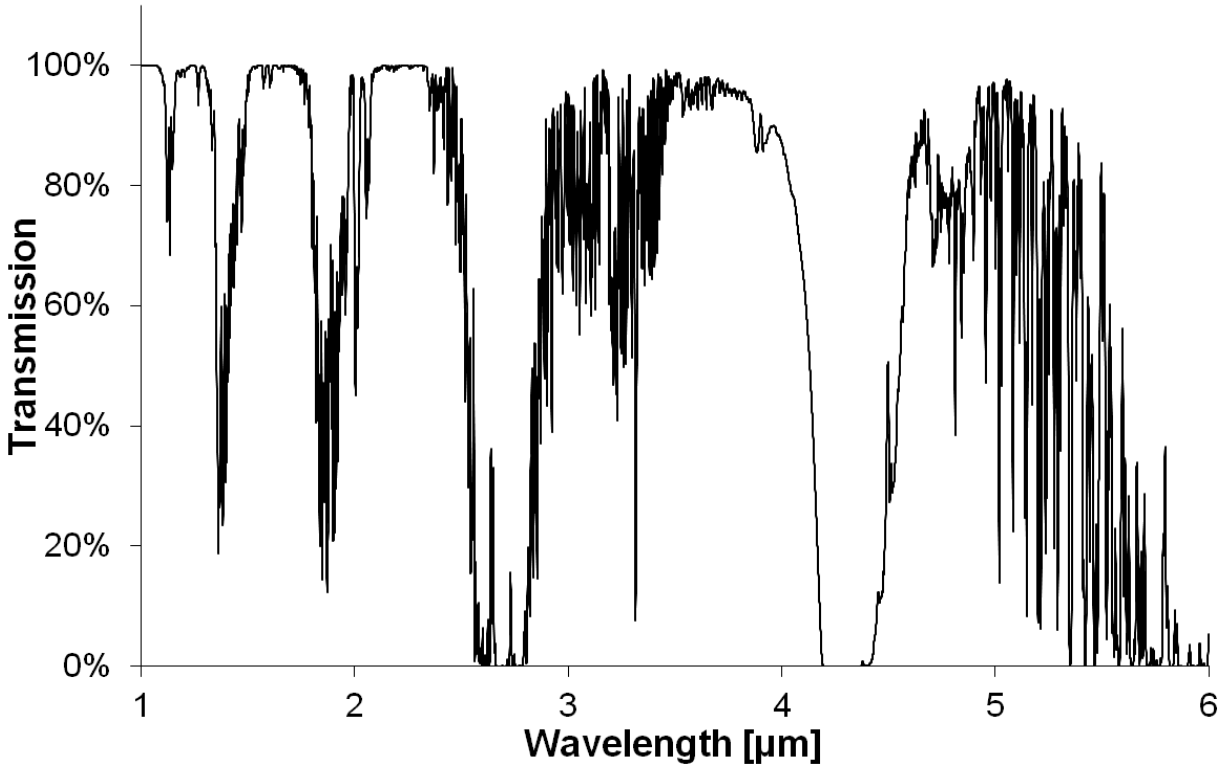

Figure 1: Atmospheric transmission of light from 1 to 6 µm, as generated by IRTRANS4 (4.2 km propagation distance from space to ground), provides a good indication where lasers may operate for free space propagation (UKIRT 2013).

Sufficient progress has since been made such that mid-infrared lasers are now used, and are considered for use, in several industries. The output wavelengths of these lasers potentially allow processing of materials that do not react in a desirable fashion to traditionally used lasers emitting at 1 µm or 10 µm. Defence applications include Directed Infrared Counter Measures (DIRCM), providing protection for aircraft from anti-aircraft missiles. Mid-infrared lasers may also be used as target designators and for range finding. In the medical field, they may be used for simultaneously cutting and cauterizing tissue, as well as for tissue ablation. Free space communication is also possible, provided the laser wavelength coincides with an atmospheric transmission window, as shown in Figure 1. Remote sensing of gases such as CO_2 as well as remote wind speed measurements are also possible. However, the need remains to improve these sources with regard to size, brightness, efficiency, and wavelength range. With the development of a wider range of lasers operating in the mid-infrared region, it is foreseen that even more applications for them will be identified.

One approach that has proven to be successful for generating laser light in the mid-infrared region is the use of thulium (Tm^{3+}) and holmium (Ho^{3+}) based solid-state lasers, where the thulium laser emitting at ~1.9 µm acts as pump source for the holmium laser that emits at ~2.1 µm.

Both thulium and holmium are part of the lanthanide series of elements (placed in the f-block of the periodic table, also known as rare earth elements). Johan Gadolin was the first person to study lanthanides in the late 1700s after receiving numerous rock samples from a feldspar mine located near the village of Ytterby, on the Swedish island of Resarö (Kean 2011). However, due to the similar properties of the lanthanides, it was very difficult to isolate the individual elements, with relatively pure samples of thulium and holmium only obtained in 1911 (Ede 2006).

An advantageous property of these trivalent ions is that their electronic transitions happen within the 4*f* shell, which is partially shielded from the host crystal lattice by the optically passive outer electronic shells, thereby reducing the influence of the host material on the wavelengths and cross sections of the optical transitions.

The properties of holmium, in a variety of host materials, make holmium lasers attractive pump sources for Optical Parametric Oscillators (OPO) and optically-pumped molecular lasers that in turn provide coherent light at even longer wavelengths in the mid-infrared region. One thing that makes this particular scheme so attractive is that thulium lasers can be efficiently pumped with readily available laser diodes operating at 792 nm. With good efficiencies obtainable at every step of the scheme, this approach does not only have the potential to lead to efficient high-powered laser systems, but also cost-effective ones, fit for use beyond the confines of a research laboratory.

The objective of this research was the development and experimental implementation of high-power and efficient holmium laser systems as well as using holmium-based laser systems as pump sources for the generation of laser light in the 3-5 µm region where efficient atmospheric transmission is also possible (Figure 1). This objective was achieved with the successful implementation of several novel laser systems, ranging from a highly efficient Ho:YLF laser and Ho:YLF MOPA system, to an optically-pumped molecular laser and amplifier which used HBr as a gain medium.

1.2 Overview of the dissertation

The dissertation consists of two parts. The first section deals with novel end-pumped, high-power, and high-energy Ho:YLF lasers and amplifiers while the second part reports on optically end-pumped HBr lasers and amplifiers.

Chapter 2 provides a discussion on the various properties of Ho:YLF relevant to its use as a gain material in this dissertation. It also provides an overview of previous published work on particularly Tm:fibre laser pumped Ho:YLF lasers. The development of a highly efficient, near diffraction-limited Ho:YLF laser with an output power in excess of 45 W is subsequently reported upon in Chapter 3. The author then continues to demonstrate the scalability of holmium YLF systems through the implementation of a novel high-powered, highly efficient Master-Oscillator Power-Amplifier (MOPA) system based on Ho:YLF. This MOPA is reported upon in Chapter 4.

Chapter 5 includes *collaborative* work on thulium and holmium laser and amplifier systems which are relevant to the subsequent chapters in which the author played a significant but not the leading role. These are:

- A 189 W Tm:YLF slab laser operating at 1890 nm.
- A single-frequency, injection-seeded Ho:YLF ring-laser operating at 2064 nm
- A 330 mJ single-frequency slab amplifier based on Ho:YLF pumped by an in-house developed Tm:YLF slab laser.

The second part of the dissertation reports on optically-pumped mid-infrared molecular lasers based on HBr gas. Chapter 6 provides an overview on the properties of HBr relevant to optically-pumped lasers as well as a review of previously published work. Scalability of HBr molecular lasers is then demonstrated in Chapter 7 by implementing the first optically pumped HBr MOPA

system. The author then reports in Chapter 8 on the first published tuneable optically pumped HBr laser.

Chapter 9 concludes the main body of the dissertation with a discussion of the findings in the preceding chapters and draws some conclusions on the outlook of future work. This is followed by the list of references in Section 10. At the end of the dissertation a list of publications of the author (first-author as well as co-authored) is provided in Section 11.

2 Introduction to Tm:fibre Laser Pumped Ho:YLF Lasers

This chapter provides a brief overview of Ho^{3+} lasers. Specific focus on Ho:YLF laser systems pumped by Tm:fibre lasers is given. The spectrographic, optical, and mechanical properties of Ho:YLF are provided and discussed. Key results and findings of Ho:YLF laser systems reported in literature, illustrating the advantages as well as challenges of Tm:fibre laser pumped Ho:YLF systems, are presented and discussed. Attention is given to energy- and power-scaling strategies.

2.1 Three approaches to designing holmium lasers: A brief overview

Initial work on holmium lasers operating in the 2 µm region involved flash-lamp pumped systems using Er, Tm, Ho and Cr, Tm, Ho co-doped crystals, as depicted in Figure 2 (Sorokina & Vodopyanov 2003). In these systems Cr^{3+} or Er^{3+} (depending on the host crystal) absorbed light from the flash lamp into the pump energy band after which the energy could be transferred to a Tm^{3+} ion. Cross relaxation between an excited thulium ion (in level $^3H_4$) and one in the ground state ($^3H_6$) would then leave both the thulium ions excited in the $^3F_4$ manifold. Energy transfer is then possible between the $^3F_4$ state of the thulium ion to the $^5I_7$ level of an adjacent Ho^{3+} ion, after which stimulated emission could occur to the $^5I_8$ level, emitting a photon with a wavelength in the 2 µm region.

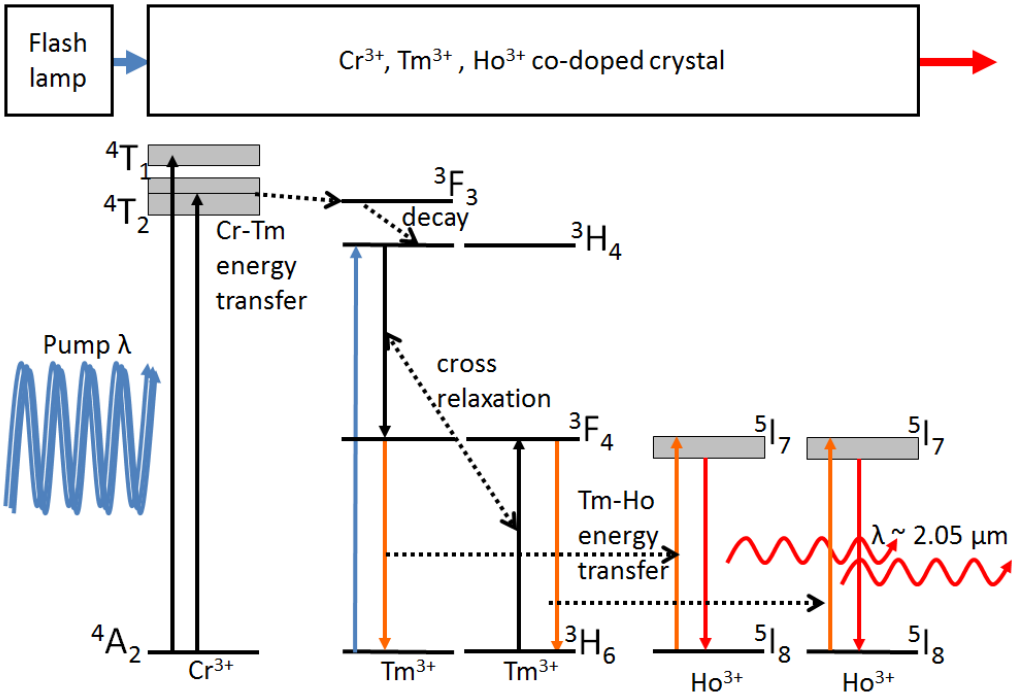

Figure 2: Pumping scheme and relevant energy levels in a flash lamp-pumped co-doped Cr, Tm, Ho:YLF 2 µm system (Rustad & Stenersen 1996; Sorokina & Vodopyanov 2003).

This approach delivered limited efficiencies however, with pump light absorption by Cr or Er being low as the flash lamp's emission spectrum is inherently broad when compared to the relevant absorption bands of the Cr or Er ions. The complexity of the flash lamp high-voltage power supplies in addition to the sheer heat load inherent to flash lamp-pumped systems did not make this design approach very desirable (Chicklis et al. 1971).

With high-power laser diodes becoming available, another approach to develop holmium lasers by using crystals co-doped with Tm^{3+} and Ho^{3+} became feasible (Fan et al. 1988). This pumping scheme is depicted in Figure 3. Since high-power, high-brightness laser diodes emitting at 1.9 µm are not yet readily available for directly pumping holmium, one may use thulium which can be pumped by commercially available laser diodes at ~ 0.8 µm as an intermediary. In this scheme a photon from the laser diode excites a thulium ion to the $^3H_4$ level. Cross relaxation between the excited thulium ion and a thulium ion in the ground state ($^3H_6$) would then leave both the thulium ions excited in the $^3F_4$ level. Depending on the efficiency by which the Tm-Tm cross relaxation can occur, one can thus obtain two thulium ions in the excited state for one pump photon; the so-called two-for-one process. Energy transfer is then possible between the $^3F_4$ state of the thulium ion to the $^5I_7$ level of an adjacent Ho^{3+} ion, after which stimulated emission can occur to the $^5I_8$ level, emitting a photon with a wavelength in the 2 µm region. As there is a good spectral overlap

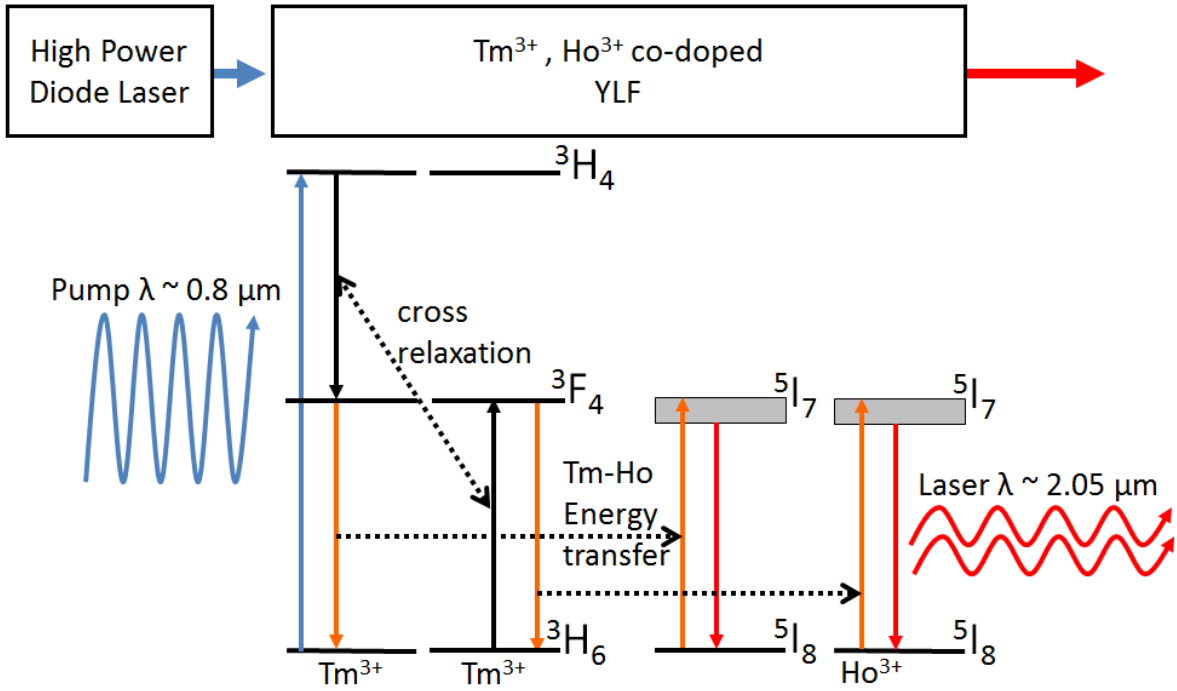

Figure 3: Pumping scheme and relevant energy levels in a diode-pumped co-doped Tm, Ho:YLF 2 µm system (W. Koen, H. J. Strauss, et al. 2010).

of the laser diode and the absorption features of thulium this approach can lead to efficient pump light absorption, aiding optical-to-optical efficiency. However, due to a strong upconversion process in which energy is transferred from the excited $^3F_4$ and $^5I_7$ states of the thulium and holmium ions respectively, co-doped systems have reduced upper-state lifetimes resulting in reduced energy storage efficiencies which are detrimental to pulsed laser performance. Upconversion also leads to an increase in thermal heat load in the laser crystal (Rustad & Stenersen 1996). This can also result in an increase in thermal lensing leading to degradation in beam quality, and even thermal fracture in severe cases.

An elegant solution to prevent this fundamental problem of parasitic energy transfer processes between the thulium and holmium ions is to host these two rare-earth ions in separate crystals (Hayward et al. 2000). This approach eliminates the upconversion processes between thulium and holmium. In addition, a more modular design where a diode-pumped thulium laser module can pump a holmium laser module is made possible. This design approach and accompanying excitation scheme is depicted in Figure 4. In this case a crystal singly-doped with thulium is optically pumped with a high power laser diode at ~0.8 µm, exciting Tm^{3+} ions from the ground state to the $^3H_4$ state. Cross relaxation between an excited thulium ion and a thulium ion in the ground state ($^3H_6$) would then leave both the thulium ions excited in the $^3F_4$ level. The thulium laser could then lase from the $^3F_4$ level to the ground state ($^3H_6$), emitting ~1.9 µm laser light. This laser light is then used to pump a laser crystal which is only doped with holmium, exciting a Ho^{3+} ion from its ground state ($^5I_8$) to the upper laser level $^5I_7$. Stimulated emission then occurs from $^5I_7$ back to the ground state $^5I_8$, emitting at ~2.05 µm.

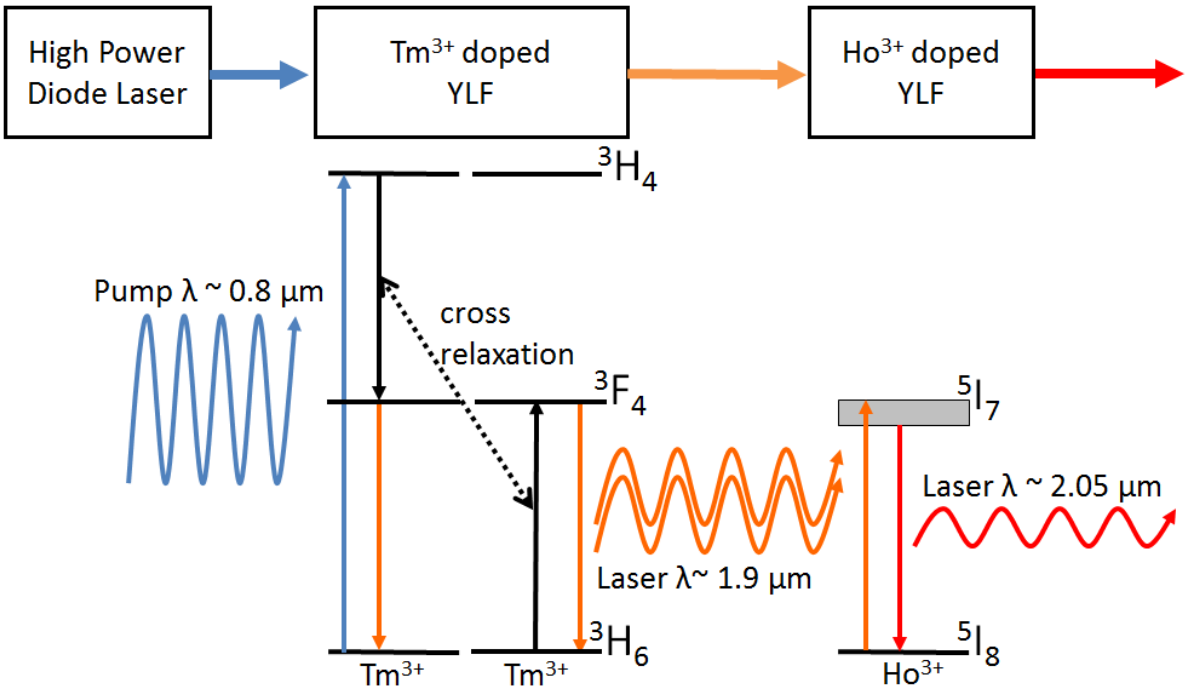

Figure 4: Schematic and pumping scheme of a laser diode-pumped Tm laser pumping a Ho laser (W. Koen, H. J. Strauss, et al. 2010).

This approach has several advantages over the first two approaches discussed in this section. The elimination of the parasitic energy transfer processes between the thulium and holmium ions in co-doped crystals leads to a decrease in heat load. The absence of these processes also increases the effective upper level lifetime of holmium, which is highly beneficial for efficient pulsed operation. The doping of the holmium laser crystals can now also be selected independently of that of the thulium, choosing a doping which is optimal for the desired holmium laser design; be it for continuous or pulsed operation. The Ho doping level can also be chosen sufficiently low to avoid detrimental Ho-Ho upconversion processes, as discussed later in Section 2.2.3. Finally, with most of the system heat load now residing in the thulium laser, and the small quantum defect between the holmium laser's pump and laser photons leading to a low heat load, the holmium

laser will experience less heat induced optical aberrations, making near-diffraction-limited laser beams at high output powers possible.

2.2 Properties of Ho:YLF

To successfully develop Ho:YLF lasers and amplifiers that exhibit desirable properties such as good beam quality, high optical-to-optical efficiency, and high power and/or energy output, to name but a few, a good knowledge and understanding of the properties of the gain material itself is needed. In this section the properties of Ho:YLF which are relevant to the work that follows in the rest of the dissertation are presented and discussed. The absorption and emission spectra are presented and the relevant cross sections of the material are discussed along with the relevant transitions. A table listing the material properties of Ho:YLF is also provided.

2.2.1 Absorption spectra and energy levels

Detailed analysis of Ho:YLF's spectroscopic properties has previously been done by (Walsh et al. 1998) and (Payne et al. 1992). The relevant polarisation dependent absorption and emission spectra reported by (Walsh et al. 1998) are shown in Figure 5. This data is for 0.5 % doped Ho:YLF crystals at a temperature of 300 K, meaning that 0.5 % of the sites where yttrium would occur in an undoped crystal are occupied by Ho^{3+} ions instead.

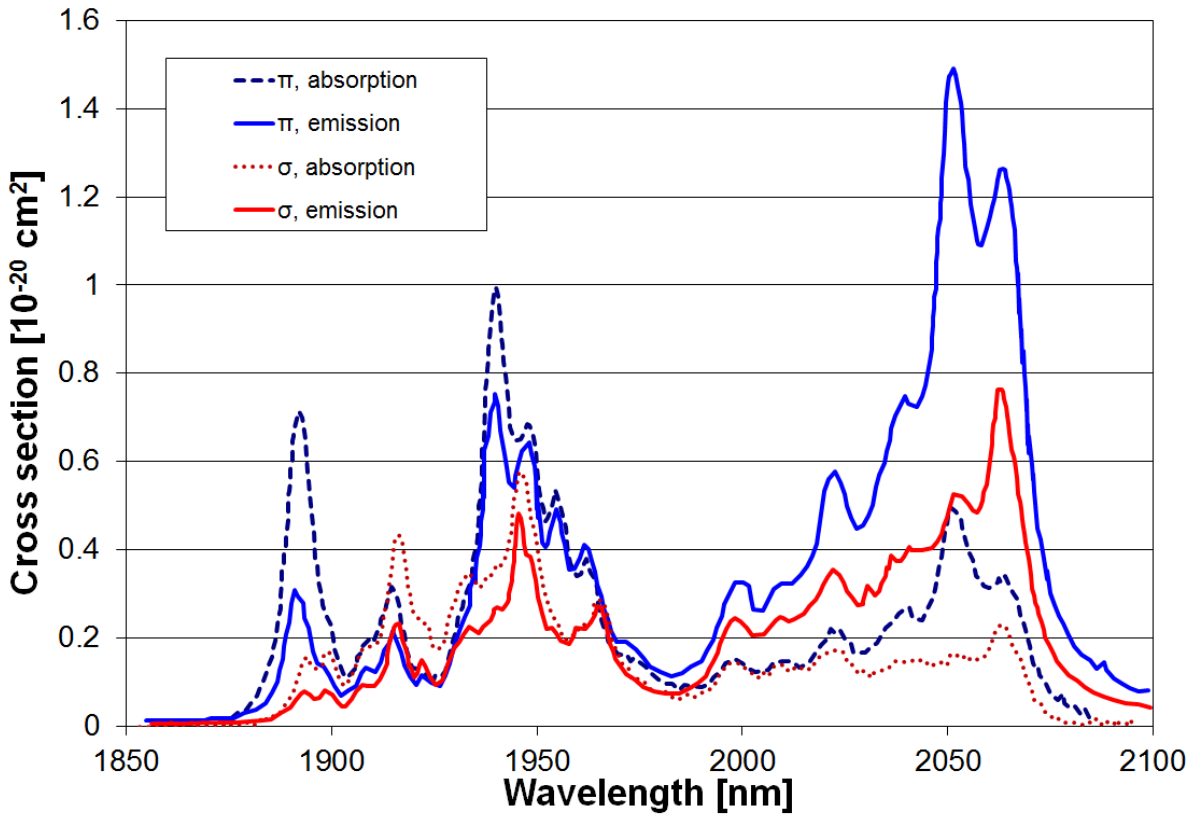

Figure 5: Absorption and emission cross sections for the $^5I_7$ manifold of Ho:YLF on the π- and σ-sigma polarisations from 1850 to 2100 nm (Walsh et al. 1998).

Of most importance to this dissertation is the 1.8 to 2.1 µm region where the $^5I_7 \leftrightarrow {}^5I_8$ transition gives rise to the spectra shown in Figure 5. For pumping Ho:YLF the two absorption peaks at 1891 nm and 1940 nm are of interest. Pumping at 1891 nm is possible with Tm:YLF lasers while 1940 nm is accessible with Tm:fibre lasers, which have been commercially available for several years now from *IPG Photonics*. However the uniaxial crystal structure of Ho:YLF results in the absorption and emission cross sections being polarisation dependent, with significant differences for σ- and π-polarisations at certain wavelengths for a-cut crystals, where the c-axis is perpendicular to the optical axis (see Figure 5). The absorption peak centered at 1891 nm has an absorption cross-section of ~0.7 x 10^{-20} cm^2 for the π-polarisation ($\boldsymbol{E} \parallel c$) while the absorption cross-section for the σ-polarisation ($\boldsymbol{E} \perp c$) at the same wavelength is less than 0.06 x 10^{-20} cm^2.

The absorption peak centered at 1940 nm has an absorption cross-section of ~0.99 x 10^{-20} cm^2 for the π-polarisation ($\boldsymbol{E} \| c$) while the absorption cross-section for the σ-polarisation ($\boldsymbol{E} \perp c$) at the same wavelength is ~0.46 x 10^{-20} cm^2. This large difference between the two polarisations for the given wavelengths is of great importance when it comes to designing an efficient pump system for Ho:YLF as one would either have to pump with a linearly polarised laser, or implement a polarisation-based pumping scheme.

Figure 6 shows a schematic of the Ho:YLF energy levels and transitions relevant to this work (namely Ho:YLF lasers and amplifiers pumped by 1940 nm Tm:fibre lasers). When pumping with ~1940 nm light (red arrows in Figure 6), holmium ions in the $^5I_8$ ground state, which absorb the

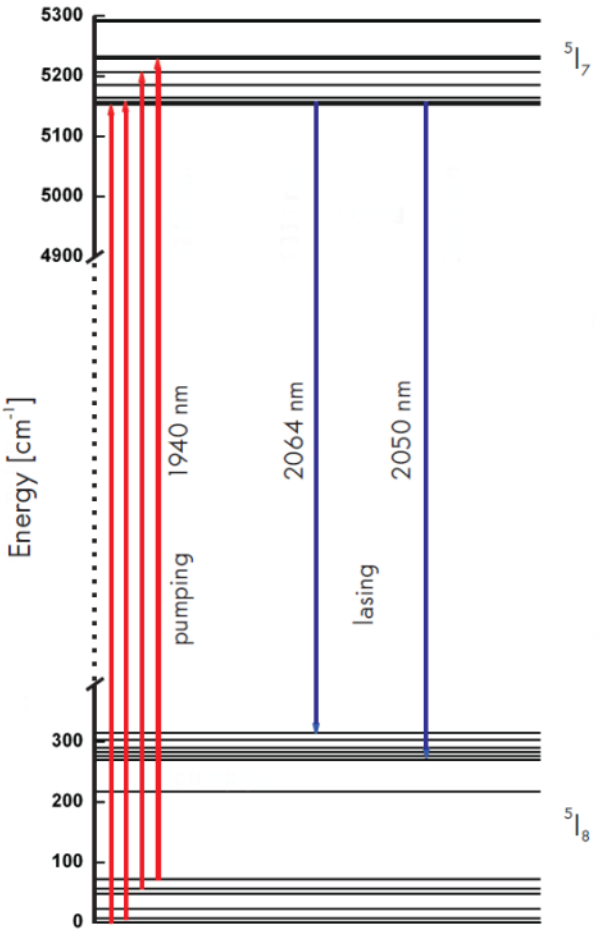

Figure 6: Scheme of the energy levels of interest for pumping Ho:YLF with a Tm:fibre laser, reproduced from (Koen 2010).

pump photons, get excited to the upper laser level $^5I_7$. This upper laser level is meta-stable with a long lifetime of ~14 ms (Walsh et al. 1998). Holmium ions in the excited state ($^5I_7$) can then decay back to the $^5I_8$ ground state through stimulated emission. Since Ho:YLF is a birefringent crystal, a Ho:YLF laser using an a-cut crystal (where the c-axis is perpendicular the optical axis) can emit at either 2050 nm, or 2064 nm, depending on the polarisation chosen in the oscillator design (blue arrows in Figure 6). Thereafter, rapid thermalisation on the picosecond scale restores the Boltzmann distribution in the ground state.

2.2.2 Mechanical and optical properties of Ho:YLF laser crystals

A summary of the optical and physical properties of a-cut Ho:YLF is provided in the table below:

Table 1: Optical and physical properties of Ho:YLF (Chang & Kuo 2002; Walsh et al. 1998).

Chemical formula	Ho^{3+}:$YLiF_4$
Crystal system	Tetragonal, uniaxial
Main absorption bands near 2 µm	1891 nm and 1940 nm
Laser wavelengths near room temperature	2050 nm and 2064 nm
Fluorescence lifetime near room temperature	~14 ms
Hardness	4-5 Mohs
Refractive index at 2 µm	n_e = 1.46, n_o = 1.44
Density	3.99 g/cm^3
Melting point	825 ºC
Thermal conductivity	6 W/mºC
Thermal expansion coefficient	8x10^{-6}/ºC ($\parallel$c), 13x10^{-6}/ºC ($\perp$c)

2.2.3 Quenching of the laser transition: Ho-Ho energy transfer

Energy transfer processes between holmium ions can lead to quenching of the efficiency in Ho:YLF lasers and amplifiers operating at ~2.1 µm (Rustad & Stenersen 1996), reducing the energy storage in the upper laser level. Figure 7 shows two Ho-Ho energy transfer processes relevant to holmium lasers which use the $^5I_7$ manifold as the upper laser level. The Ho-Ho energy transfer process marked p_{77} occurs when two holmium ions in the $^5I_7$ state (the upper laser level) interact so that one of the ions is excited from the $^5I_7$ manifold to the $^5I_5$ manifold and the second ion is de-excited from $^5I_7$ to $^5I_8$. The reverse of this process, marked p_{58}, also exists where a holmium ion in the $^5I_5$ state and another ion in the $^5I_8$ state can interact, resulting in both ions ending up in $^5I_7$. Despite the negative upconversion process p_{77} having a reverse process, p_{58}, the total effectiveness of this reverse process depends on the energy level structure in a specific host. In the case of Ho:YLF, ions in the $^5I_5$ quickly relax to $^5I_6$ and thereafter to the $^5I_7$ manifold, usually through nonradiative processes.

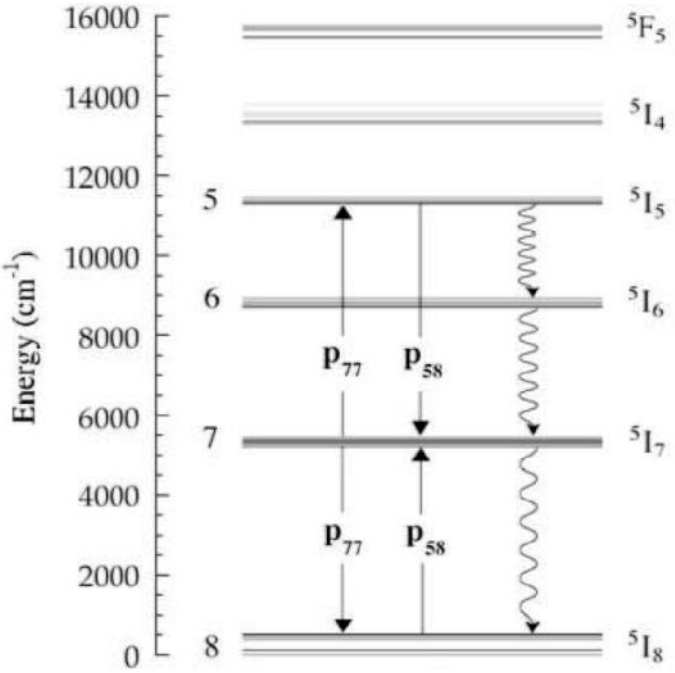

Figure 7: Ho-Ho energy transfer process (marked p_{77}) where two holmium ions can interact so that one of the ions is excited from the $^5I_7$ manifold to the $^5I_5$ manifold and the second ion is de-excited from $^5I_7$ to $^5I_8$. The reverse self-quenching process (p_{58}) also exists where a holmium ion in the $^5I_5$ state and another ion in the $^5I_8$ state can interact, resulting both ions ending up in $^5I_7$ (Barnes et al. 2003).

As the p_{77} upconversion process involves two holmium ions which are in close proximity to each other and both in the excited $^5I_7$ state, this process is most likely to happen when the population density of $^5I_7$ is high in crystals of higher doping. As this process limits energy storage in the upper laser level, it negatively affects Q-switched lasers, lowering both output energies and laser efficiency. Since upconversion is doping dependent, the use of Ho:YLF crystals with low doping can alleviate this problem, as reported in (W Koen et al. 2010).

2.3 Power and energy scaling of Tm pumped Ho:YLF solid state lasers and amplifiers

"The revolution occurred for Ho-doped materials with the commercial availability of high power continuous wave Tm:fibre lasers which enabled decoupling energy transfer between the Tm and Ho ions. It is still early to summarize all the capabilities of Ho-doped materials - partially plagued by a strong quasi-three level behavior (M. Eichhorn, 2008) - but a number of exciting results have already been reported (W. Koen et al, 2010)." - (Pires et al. 2015)

While interest in co-doped Tm-Ho lasers remains, they are typically of lower output powers and efficiencies than that of singly doped holmium lasers (Lagatsky et al. 2011; Urata et al. 2005; Feaver et al. 2013; Sato et al. 2004; Zhu et al. 2010; Zhang et al. 2013; Zhang et al. 2012). The lower efficiencies (typically less than 10 %) can be attributed to strong cooperative upconversion processes that occur between the thulium and holmium ions in the co-doped gain materials (Fan et al. 1988; Rustad & Stenersen 1996). These upconversion processes reduce the effective upper-level lifetime, and also increase the thermal load.

As stated by Pires, it was once high-power thulium fibre lasers became commercially available as pump sources to directly pump singly-doped holmium crystals that the laser research community was truly able to improve holmium lasers, as this eliminated the detrimental upconversion processes present in co-doped Tm-Ho lasers (Pires et al. 2015). For Ho:YLF lasers this can be observed from the list of published lasers and amplifiers provided in Table 2, where the vast majority are end-pumped by Tm:fibre lasers.

Table 2: Ho:YLF laser and MOPA systems in literature.

Date	Pump Source	Pumping Scheme	λ_{pump} [nm]	λ_{laser} [nm]	Laser Output Energy, Power, Peak-power	Amplifier Output	Ho:YLF Doping [%]	Crystal Length [mm]	Crystal Temp. [ºC]	PRF [Hz]	Comment	Reference
2003	2xTm:YLF slabs	End-pumped	1940	2050	37 mJ @ 100 Hz, 21 W cw	Na	0.5	40	-	100-1000	-	(Dergachev & Moulton 2003)
2004	Tm:fibre	End-pumped	1940	2065	4.8 W cw	Na	1.5	15	15	cw	-	(Shen et al. 2004)
2005	100 W Tm:fibre	End-pumped	1940	2050	45 mJ @ 200 Hz, 43 W cw	Na	2	2x20	-	200-1000	-	(Dergachev et al. 2005)
2007	120 W Tm:fibre	End-pumped	1940	2050	25 mJ @ 500 Hz, 19 W cw	55 mJ @ 500 Hz, 42 W cw	-	-	-	500-1000	-	(Dergachev et al. 2007)
2007	30 W Tm:fibre	End-pumped	1941	-	30 mJ @ 100 Hz	Na	0.5 &1.0	25 & 30	10	100	Crystals used collinearly	(Bai et al. 2007)
2008	3x120 W Tm:fibre	End-pumped	1940	2050	25 mJ @ 100 Hz, 19 W cw	170 mJ @ 100 Hz, 115 W cw	-	6 crystals, length unspecified	-	100-1000	3 amplifier stages	(Dergachev et al. 2008)
2009	40 W Tm:fibre	End-pumped	-	2051	5.8 mJ @ 1 kHz	Na	0.5 &1.0	20 & 30 mm	8.2	1000-10000	Single-frequency for DIAL	(Bai et al. 2009)

2009	82 W Tm:fibre	End-pumped	1940	2064	35 mJ	70 mJ	0.5	40 mm Osc., 50 & 30 mm Amp.	Room temp.	50 Hz	Injection seeded single-frequency ring laser	(Bollig et al. 2009)
2010	82 W Tm:fibre	End-pumped	1940	2065	10.9 mJ @ 1kHz, 12.4 W cw	21.3 mJ @ 1kHz, 23.7 W cw	0.5	30 mm Osc., 50 mm Amp.	20	1000-5000		(W Koen et al. 2010)
2011	20 W Tm:fibre	End-pumped	-	2050 & 2064	6 mJ @ 500 Hz	Na	0.5	60 mm	8.2	500-1000	Single-frequency ring laser	(Bai et al. 2011)
2011	80 W Tm:fibre	End-pumped	1938	2064	38.5 mJ @ 100 Hz, 18.1 W cw	Na	0.5	30/40 mm	15	100		(Schellhorn 2011)
2014	100 W polarised Tm:fibre	End-pumped	1940	2050	37 mJ @ 100 Hz	Na	0.5	80	15	100-10000	Single-frequency for DIAL	(Gibert et al. 2014)
2014	33 W Tm:fibre	End-pumped	1940	2051	5 mJ @ 1 kHz	Na	0.5	30	17	1000-10000		(Kwiatkowski, Swiderski, et al. 2014)
2015	83 W Tm:fibre	End-pumped	1940	2052 & 2062	11 mJ @ 1 kHz, 24.5 W cw	18.5 mJ @ 1 kHz, 30.5 W cw	0.5	30 mm Osc., 50 & 20 mm Amp.	Room temp.	1000-6000		(Kwiatkowski et al. 2015)
2015	80 W Tm:fibre	End-pumped	1938	2064	17.3 W	Na	0.5	30	-	-	Non-planar ring cavity	(Schellhorn & Eichhorn 2015)

Noteworthy Ho:YLF oscillator and amplifier systems are listed in Table 2 in order of publication (but not necessarily implementation). In 2003 Alex Dergachev and Peter Moulton from *Q-peak Inc.* reported a near-diffraction limited Ho:YLF laser that was end-pumped by two Tm:YLF slab lasers (Dergachev & Moulton 2003). The Ho:YLF laser delivered up to 21 W of cw power and up to 37 mJ of energy per pulse at a PRF of 100 Hz. In pulsed operation they used the holmium laser to pump a ZGP based OPO which delivered up to a total of 10 mJ per pulse at 3.2 and 5.7 µm. This work demonstrated that thulium slab lasers pumping a holmium laser, which in turn pumps an OPO, is an attractive approach to generate coherent light in the 3-5 µm region.

Shen et al. demonstrated in 2004 both a Ho:YLF and a Ho:YAG laser end-pumped by an unpolarised thulium fibre laser. The Ho:YAG laser delivered up to 5.8 W of polarised light while the Ho:YLF delivered up to 4.8 W. The output power of these holmium lasers was limited by the available amount of pump power from the Tm:fibre laser (Shen et al. 2004).

The reported power output from Ho:YLF lasers increased drastically after high-power thulium fibre lasers became available. In 2005 Dergachev et al. used an unpolarised Tm:fibre laser

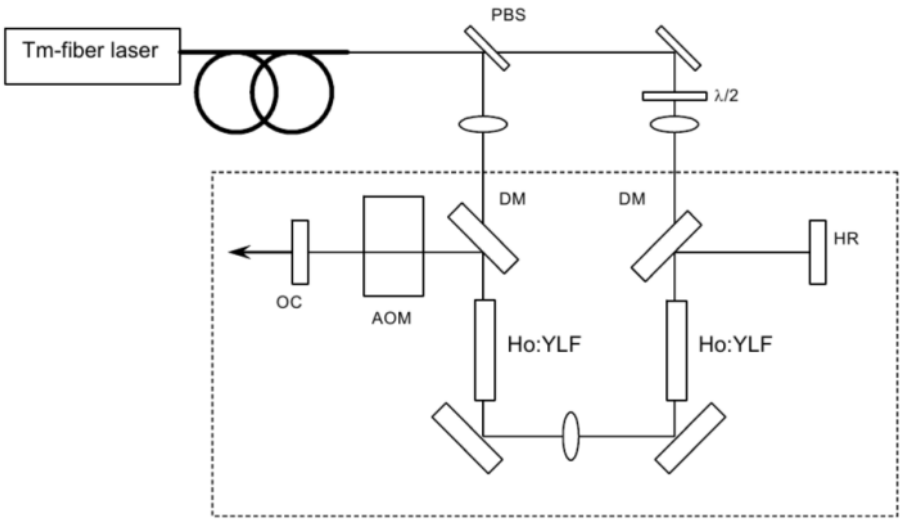

Figure 8: Schematic of a Ho:YLF laser end-pumped by a commercially sourced, unpolarised 100 W Tm:fibre laser. The unpolarised laser light from the fibre laser was split into vertical and horizontally polarised light with a polarising beam splitter (PBS) in order to separately pump the two Ho:YLF crystals in the laser (Dergachev et al. 2005).

manufactured by *IPG photonics* to end-pump a two crystal Ho:YLF laser (Dergachev et al. 2005). A schematic of the laser is shown Figure 8. The Tm:fibre laser delivered 100 W of unpolarised laser light at 1940 nm. The fibre laser's wavelength was selected to coincide with the strong π-polarisation absorption peak of Ho:YLF. But, as discussed in Section 2.2.1, absorption in Ho:YLF at 1940 nm is strongly polarisation dependent and pumping a single a-cut crystal with unpolarised light would result in inefficient pump light absorption. This was addressed by splitting the unpolarised pump light from the fibre laser into two polarised beams using a polarising beam splitter (PBS) and then pumping two Ho:YLF crystals placed in the resonator separately, as shown in Figure 8. This design approach proved highly effective, with the holmium laser producing up to 43 W of cw power and 45 mJ in the Q-switched regime.

The approach of splitting the unpolarised laser light from Tm:fibre lasers into vertically and horizontally polarised beams to pump separate Ho:YLF crystals was not limited to single oscillators containing two crystals. This approach could also be applied to Master Oscillator

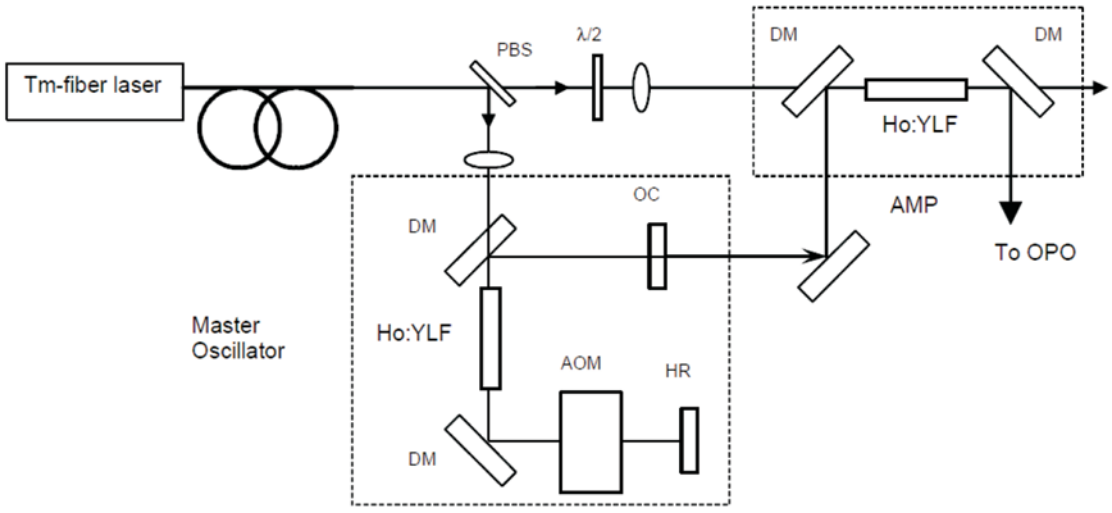

Figure 9: Schematic layout of a Tm:fibre laser pumped Ho:YLF Master Oscillator Power Amplifier (MOPA) (Dergachev et al. 2007). The unpolarised laser light from the fibre laser is split into vertically and horizontally polarised beams to pump the oscillator and amplifier crystals seperately.

Power Amplifier (MOPA) systems, as subsequently demonstrated by Dergachev et al. in 2007. A schematic showing the layout of the Ho:YLF MOPA is shown in Figure 9 (Dergachev et al. 2007). For this system a 120 W Tm:fibre laser, manufactured by *IPG Photonics*, was used to pump an oscillator and amplifier crystal by once more splitting the unpolarised pump beam into two linearly polarised beams in order to pump the two crystals separately. In addition to efficiently using an unpolarised pump source to pump birefringent crystals, the MOPA configuration was a good approach for energy scaling, decreasing the intra-cavity fluence in the oscillator when compared to the case where one would have the two crystals in a single laser cavity. This MOPA delivered up to 55 mJ at a PRF of 500 Hz when Q-switched, and 42 W of average power in cw mode.

Subsequently, Dergachev extended this pump scheme to two-crystal Ho:YLF amplifiers, as shown in Figure 10 (Dergachev et al. 2008). A single 120 W unpolarised Tm:fibre laser pumped two Ho:YLF crystals separately. The seed beam passed through both crystals once. Two of these

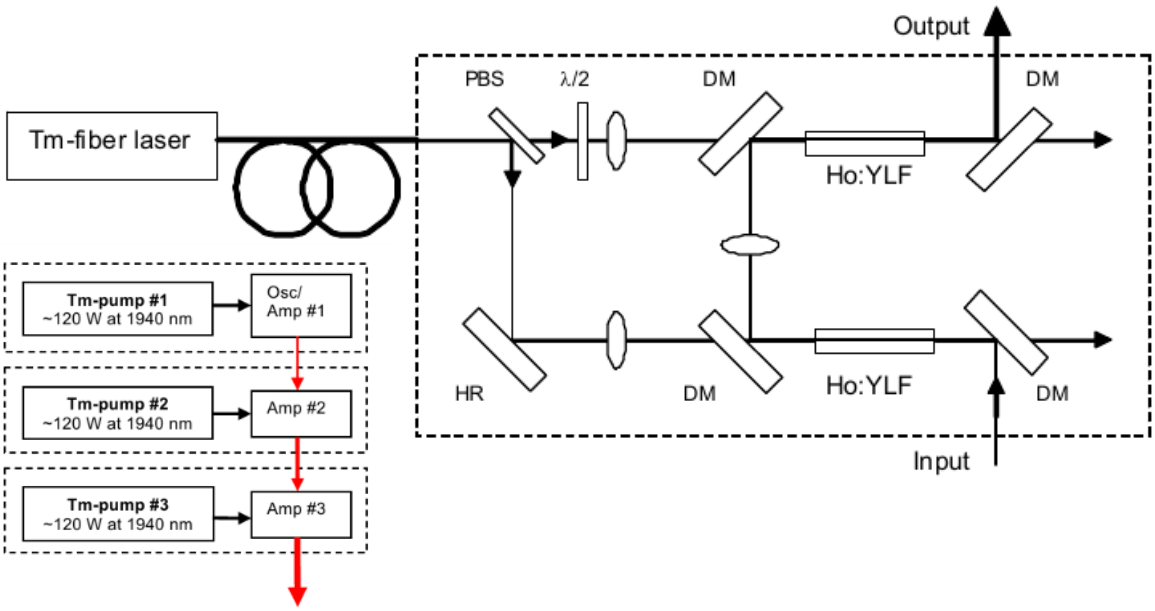

Figure 10: Schematic layout of the two crystal Ho:YLF amplifier pumped by a single Tm:fibre laser, developed by Dergachev et al.. Two of these amplifiers amplified a Ho:YLF MOPA's output to 170 mJ at a PRF of 50 Hz (Dergachev et al. 2008).

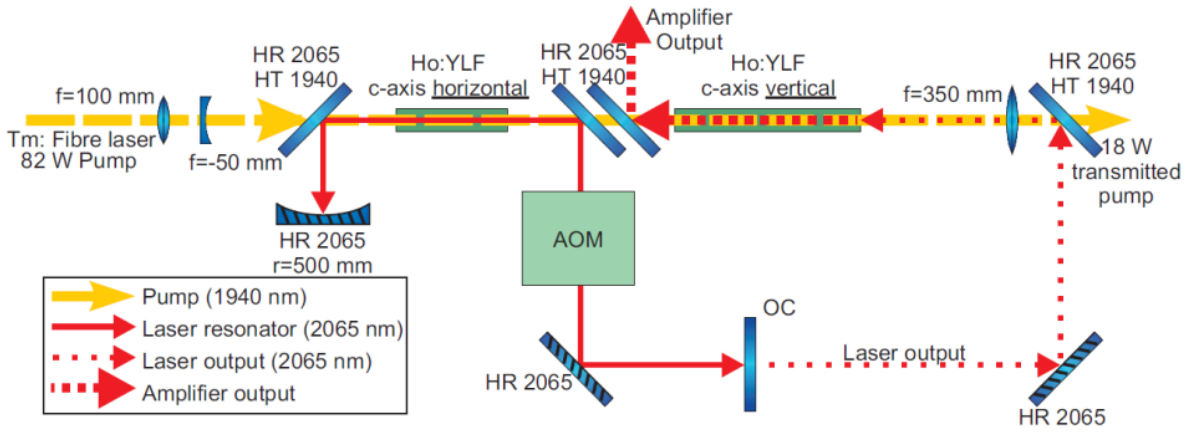

Figure 11: A schematic of the Ho:YLF MOPA system reported upon in (W Koen et al. 2010). The system utilised the unpolarised beam from a Tm:fibre laser to pump two Ho:YLF crystals in series.

amplifiers were used in series to amplify the output of a Ho:YLF MOPA similar to the one described in (Dergachev et al. 2007). This cascaded amplifier scheme delivered up to 115 W cw output, and 170 mJ per pulse at 100 Hz when the seed laser was Q-switched.

While Dergachev et al. split up the unpolarised light into two linear polarised beams in order to efficiently pump two Ho:YLF crystals separately, Bai et al. used two crystals of different doping (0.5 and 1.0 %) pumped collinearly by the same unpolarised Tm:fibre laser (Bai et al. 2009). Although this improved the effective absorption of the pump light, overall efficiency was hampered by the increased parasitic processes related to the higher doping in the second crystal. In other work, single crystal designs were also implemented, leading to decreased optical-to-optical efficiency, but with the advantage of a more simple design which did not require any polarisation-dependent optics for the unpolarised pump light (Schellhorn 2011; Bai et al. 2011).

In 2010 Koen et al. reported that it was possible to efficiently utilise the unpolarised pump light from a thulium fibre laser to pump Ho:YLF crystals (W Koen et al. 2010). This was possible by placing two a-cut Ho:YLF with their c-axes perpendicular to each other and pumping them

collinearly, as shown in Figure 11. The first crystal resided in the oscillator while the second was used as an amplifier crystal. The first crystal was orientated with its c-axis horizontal and, because the crystal absorbed pump light predominantly on its π-polarisation, it absorbed mostly horizontally polarised light. The remaining pump light transmitted through the first crystal was therefore partially vertically polarised. To maximise absorption of this partially polarised pump light, the second crystal was placed with its c-axis orientated vertically. With the oscillator forced to operate vertically polarised by the use of a polarisation-dependent 45 degree mirror, the linearly polarised seed light entering the amplifier crystal was amplified on the π-polarisation. This specific combination of crystal orientations and laser light polarisation had the advantage that the laser operated on the σ-polarisation of the first crystal, whose weak thermal lensing enabled near diffraction-limited beam quality, while the second crystal provided high gain on the π-polarisation which had the higher emission cross-section. Pumping these two crystals in series with the same pump also minimized the pump propagation distance which decreased atmospheric absorption of the pump light which could lead to detrimental effects such as thermal blooming (Koen 2010) (This is discussed in greater detail in Section 3.2.2 of the next chapter.). The oscillator-amplifier approach also led to lower fluence in the oscillator cavity, reducing the risk of optical damage.

With the oscillator emitting up to 12.4 W cw at 2065 nm, the single-pass amplifier provided a gain of nearly 2, emitting up to 23.7 W when in continuous wave mode. When pulsed, the MOPA system delivered up to 21.3 mJ at a PRF of 1 kHz. These experimental results also compared well with simulation work done by Martin Schellhorn (W Koen et al. 2010). One of the outcomes of this work was the conclusion that parasitic upconversion processes are negligible for 0.5 % doped Ho:YLF crystals. It is interesting to note that prior to this work doping percentages of Ho:YLF varied between 0.5 and 2 %, but that most other authors subsequent to this publication chose 0.5 % doped Ho:YLF crystals for their work.

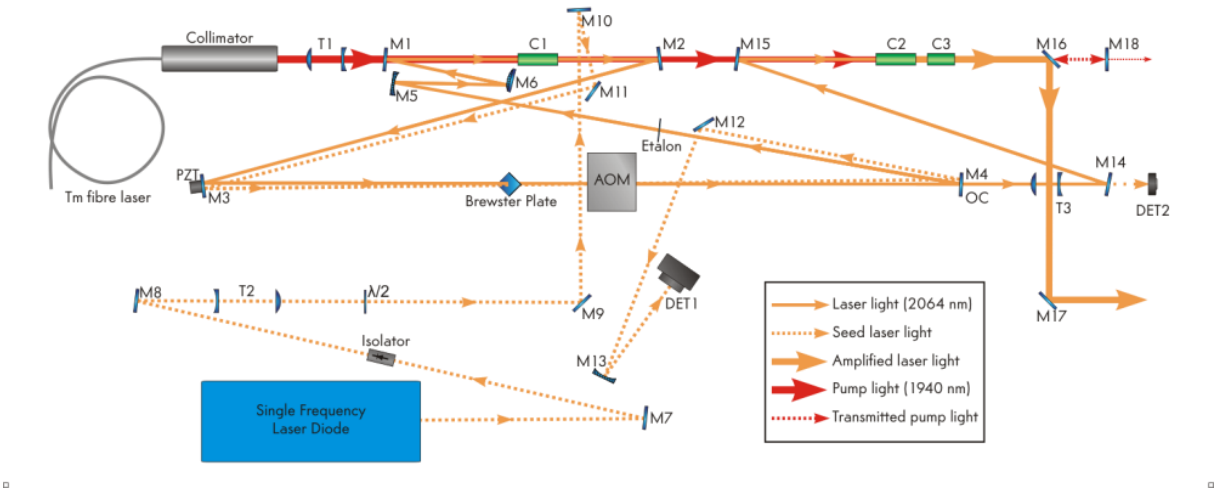

Figure 12: The single-frequency Ho:YLF ring laser and single-pass amplifier developed subsequently to (W Koen et al. 2010). The MOPA system also used the full unpolarised beam from the same Tm:fibre laser to pump multiple Ho:YLF crystals whose c-axes were orientated perpendicular with regard to each other (Bollig et al. 2009).

As the work done and reported in (W Koen et al. 2010) proved the collinear crystal pump design to be an elegant and efficient way to utilise unpolarised pump light, a single-frequency Ho:YLF ring-laser with single-pass amplifier was subsequently developed by our group, the schematic of which is shown in Figure 12 (Bollig et al. 2009). A total of three crystals were pumped in series by the same thulium fibre laser that was previously used in (W Koen et al. 2010). The oscillator contained a single a-cut Ho:YLF crystal while the amplifier consisted of two holmium YLF crystals. While up to 18 W of pump light could be transmitted through the crystals in (W Koen et al. 2010), pump light absorption on the first pass in (Bollig et al. 2009) was good enough that the total remaining pump power left was sufficiently low for it to be back-reflected into the crystals for a second pass (without feedback to the fibre laser), thereby improving overall performance. Although this system effectively absorbed all of the available pump light, its optical-to-optical efficiency was relatively low as a larger pump beam size and resonator mode was necessary in

order to prevent optical damage at the low repetition rates this system was designed to operate at (PRF from 1 to 350 Hz).

The pumping scheme reported on in (W Koen et al. 2010) was also implemented using three Ho:YLF crystals of 0.5 % doping in (Kwiatkowski et al. 2015), where one 30 mm long crystal was used in the oscillator and a 50 and 20 mm long crystal were used in a single-pass amplifier, as shown in Figure 13. The MOPA system reported in (Kwiatkowski et al. 2015) was also pumped by a single Tm:fibre laser, delivering a maximum pump power of 83 W. In continuous wave operation the oscillator delivered a maximum of 24.5 W and the amplifier 30.5 W. When the oscillator was Q-switched, it delivered a maximum output energy of 11 mJ at 1 kHz while the amplifier output was 18.5 mJ for the same PRF. While the cw performance exceeded that reported in (W Koen et al. 2010), the pulsed performance was very similar, as Koen et al. reported 10.9 mJ and 21.3 mJ from the oscillator and amplifier at 1 kHz, respectively.

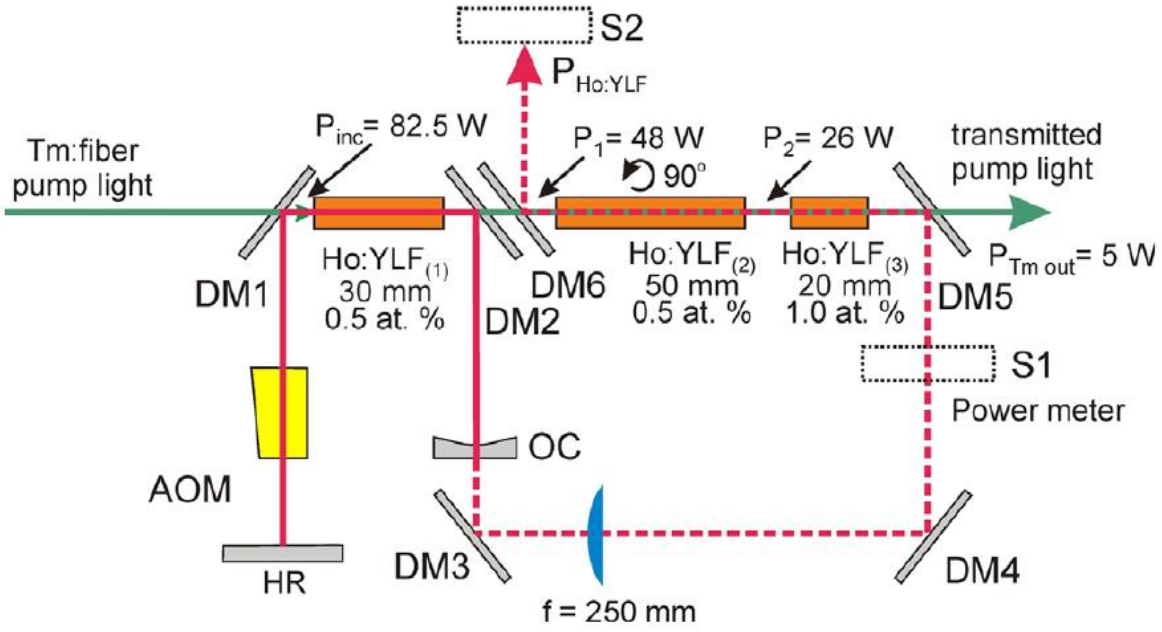

Figure 13: A Tm:fibre laser pumped Ho:YLF MOPA reported on by Kwiatkowski et al. in 2015 (Kwiatkowski et al. 2015).

Another noteworthy laser system was reported by Gibert et al. in 2014, whereby a linearly polarised Tm:fibre laser was used to pump a single-longitudinal mode Ho:YLF ring-laser used for DIAL measurements (Gibert et al. 2014). A 100 W, 1940 nm *linearly* polarised thulium fibre laser was used to pump a 0.5 % doped Ho:YLF crystal. This Ho:YLF ring laser delivered up to 37 mJ per pulse at a PRF of 100 Hz. Its wavelength was locked to a CO_2 absorption line and was successfully used to measure spatially resolved CO_2 concentrations in the atmosphere. While this laser was not ground breaking with regards to optical-to-optical efficiency, it was an excellent demonstration on how Ho:YLF lasers could be used to monitor CO_2 levels in the atmosphere, which is of fundamental importance for studies relating to climate change as CO_2 is considered an important greenhouse gas.

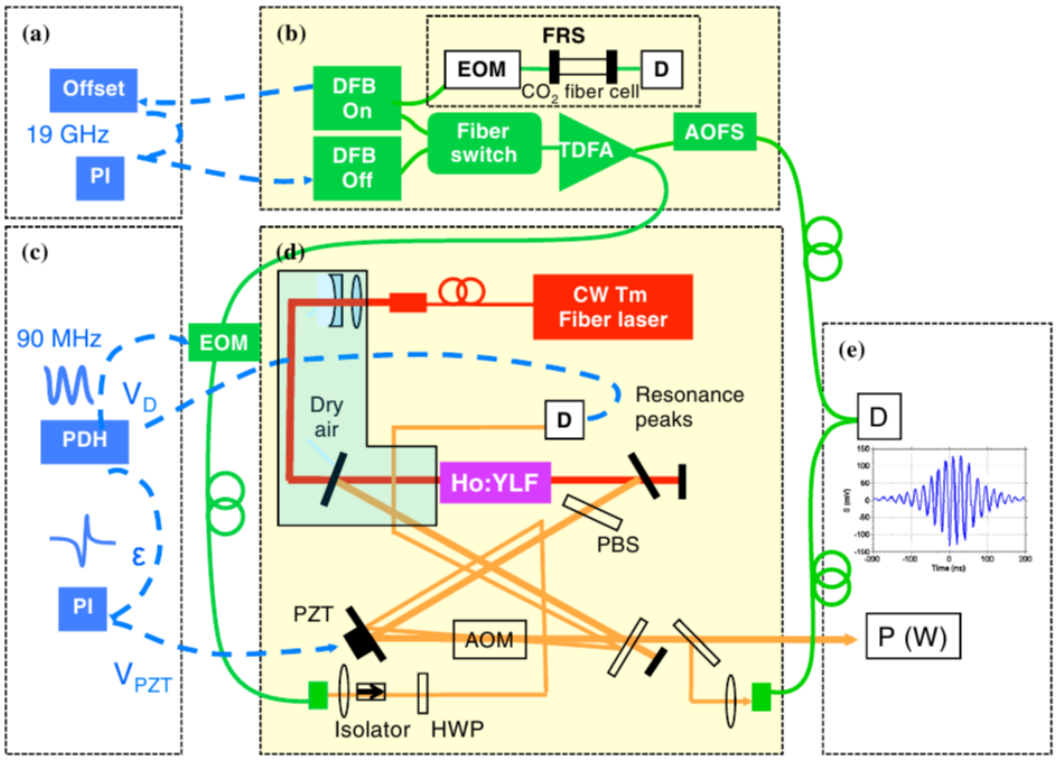

Figure 14: A single-frequency Ho:YLF ring-laser developed by Gibert et al. to do CO_2 DIAL measurements in the atmosphere (Gibert et al. 2014).

2.4 Conclusions

In this chapter three historical approaches for developing holmium lasers were discussed. It was concluded that lasers utilising singly-doped holmium crystals showed the most promise with regard to efficiency and scalability. Various spectrographic, optical and mechanical properties of specifically Ho:YLF were presented, and their implications for laser design discussed.

The literature review showed that Tm:fibre lasers are ideal pump sources for holmium laser systems, although the unpolarised laser light from most of these lasers pose a problem when it comes to pumping Ho:YLF as its pump light absorption is highly polarisation-dependent. The review also showed that there are at least two approaches for effectively using unpolarised pump light from Tm:fibre lasers to pump birefringent Ho:YLF crystals.

The first approach was demonstrated by Dergachev et al., whereby the unpolarised pump light was split into two linearly polarised beams in order to pump two holmium YLF crystals separately. Power and energy scaling was also demonstrated with the implementation of various MOPA systems.

The second approach was reported by Koen et al. whereby the unpolarised pump light from a Tm:fibre laser was used to pump multiple a-cut Ho:YLF crystals collinearly (“in series”) with the crystals’ c-axes orientated by 90 degrees with respect to each other in order to maximise absorption.

Both these approaches led to efficient pump light absorption, but the latter approach required no pump polarisation optics and resulted in a compact design. This novel approach is expanded upon in this dissertation, with both a novel intra-cavity gain medium setup demonstrated in Chapter 3, as well as an elegant and compact approach for designing a MOPA system where two unpolarised

Tm:fibre lasers are used to collinearly pump a Ho:YLF oscillator and amplifier system, as reported in Chapter 4.

3 Development of an Efficient 45 W Ho:YLF Laser Pumped by a Tm:fibre Laser

In the previous chapter various holmium lasers were presented and the properties of particularly Ho:YLF as a gain medium were discussed. In this chapter a compact and efficient high-power Ho:YLF laser which was pumped by a commercially available thulium fibre laser is presented. The holmium laser delivered 45.1 W in a near diffraction-limited beam at 2063 nm when pumped with 84.7 W at 1940 nm. The record optical-to-optical efficiency of 53 % compared favourably with similar Ho:YAG lasers which are historically more efficient than Ho:YLF lasers.

3.1 Introduction

Pumping Ho:YAG based solid-state lasers with Thulium-doped fibre lasers has been a popular approach for several years to generate coherent light at 2 µm. This approach delivered high average powers with good optical-to-optical efficiency (Lippert, Fonnum & Stenersen 2010; Elder 2009). Ho:YLF, on the other hand, was used for low pulse repetition frequency Q-switched applications (Dergachev et al. 2007; Bollig et al. 2009) due to its long upper-state lifetime of ~14 ms (Walsh et al. 1998). Ho:YLF had more limited use in high average power applications as the low thermal fracture limit of YLF could pose a problem when pumping at the high intensity levels required for efficient cw and high repetition rate pulsed operation. However, in addition to weaker thermal lensing which allows good quality beams to be obtained, Ho:YLF also does not suffer from thermally induced depolarisation losses which must be compensated for through

various techniques when using YAG crystals in high-powered lasers (Clarkson 2001). Thus, if thermal damage of Ho:YLF crystals is avoided, high-power laser configurations delivering good beam quality and high efficiency can be implemented without the need of end-capped crystals to reduce stresses from end-bulging (Elder 2009), as well as extra polarisation optics that would otherwise be needed to mitigate the effect of thermally induced birefringence, as exhibited by Ho:YAG (Lippert, Fonnum & Stenersen 2010). However, as YLF crystals are far softer than YAG, and have a lower thermal conductivity (see Table 1), avoiding thermal fracture can be challenging.

In this chapter the author proposes that it is possible to drastically increase the efficiency of Ho:YLF lasers by decreasing the mode and pump beam size in the gain medium while ensuring good pump light absorption in the gain medium. Using this approach, an efficient Ho:YLF laser which operated in both continuous and Q-switched modes is presented. The laser delivered an average power in excess of 45 W with an optical-to-optical efficiency of 53 % in a near diffraction-limited beam, demonstrating that Ho:YLF based lasers can deliver high average powers and excellent optical-to-optical efficiencies.

In Section 3.2 of this chapter the experimental design and setup is presented, followed by the experimental results in Section 3.3. The results are discussed in conjunction with the state-of-the-art Ho lasers in Section 3.4. Finally, a conclusion is drawn in Section 3.5.

3.2 Experimental design and setup

As stated earlier, smaller pump and mode sizes in conjunction with good pump absorption may increase the efficiency of Ho:YLF laser systems. This view is supported by simulation results from a rate-equation model based on such a laser, provided by Cobus Jacobs, as shown in Figure 15 (Jacobs 2013b). A novel approach to utilise the partially polarised transmitted pump light from the first Ho:YLF crystal to pump an orthogonally rotated second crystal in the same cavity in conjunction with a drastic decrease in pump beam and laser mode size is proposed. The design and implementation of this approach is described in the subsections below. Section 3.2.1 describes the gain crystals chosen, while Sections 3.2.2 and 3.2.3 describe the pump and resonator designs respectively.

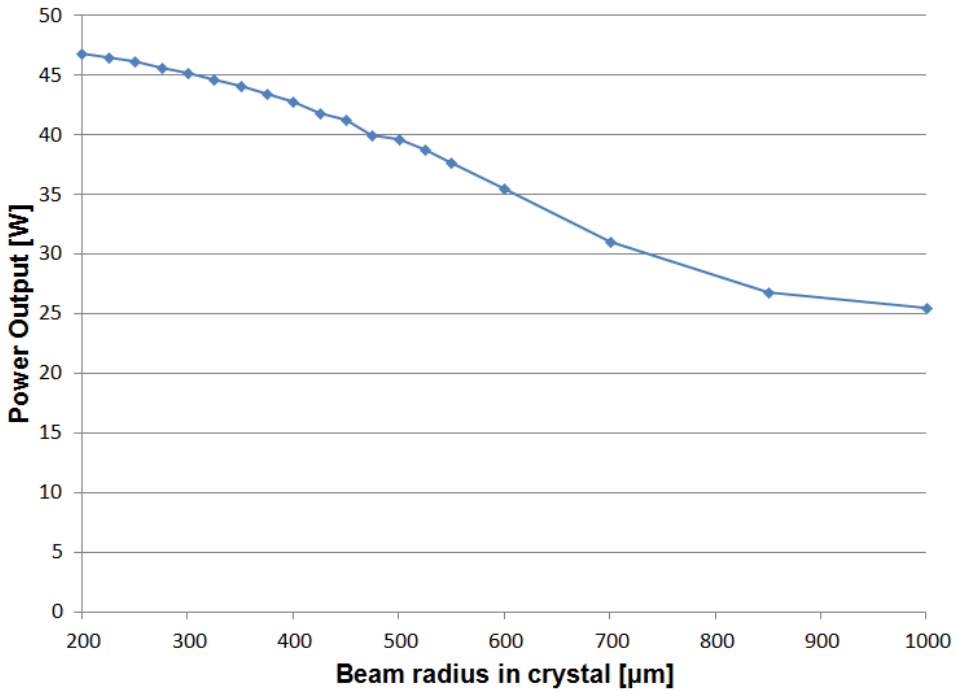

Figure 15: Simulated average output power of a Q-switched Ho:YLF laser (25 kHz PRF) as a function of mode size in the Ho:YLF crystals for a constant 84.7 W of incident pump power (Jacobs 2013b). An increase in average output power with a decrease in pump and mode size is clearly evident.

3.2.1 The Ho:YLF laser crystals

Two 0.5 % at. doped Ho:YLF crystal rods were used in the resonator cavity, as per the design discussion in the previous chapter. Both the crystals were a-cut so that their c-axis was perpendicular to the optical axis. The crystals' end-surfaces were coated to be anti-reflective (AR) for the pump and laser light. The relatively low doping of the crystals alleviated upconversion (W Koen et al. 2010) but resulted in a longer gain medium being needed for sufficient absorption of the pump light. As a consequence two crystals were used, with lengths of 50 mm and 40 mm, respectively (5 mm diameter). The longer crystals had the added benefit that the surface area of the crystals in contact with the cooling interface was increased, thereby improving cooling. The crystal rods were glued with *Norland Optical Adhesive* into round copper "sleeves" in the same manner described in (Koen 2010). Both crystal sleeves were mounted in water-cooled copper mounts (as shown in Figure 16), with a set temperature of 20 °C. Mounting the round sleeves in this fashion allowed the rotation of the crystals to align their respective c-axes to any desired angle perpendicular to the optical axis.

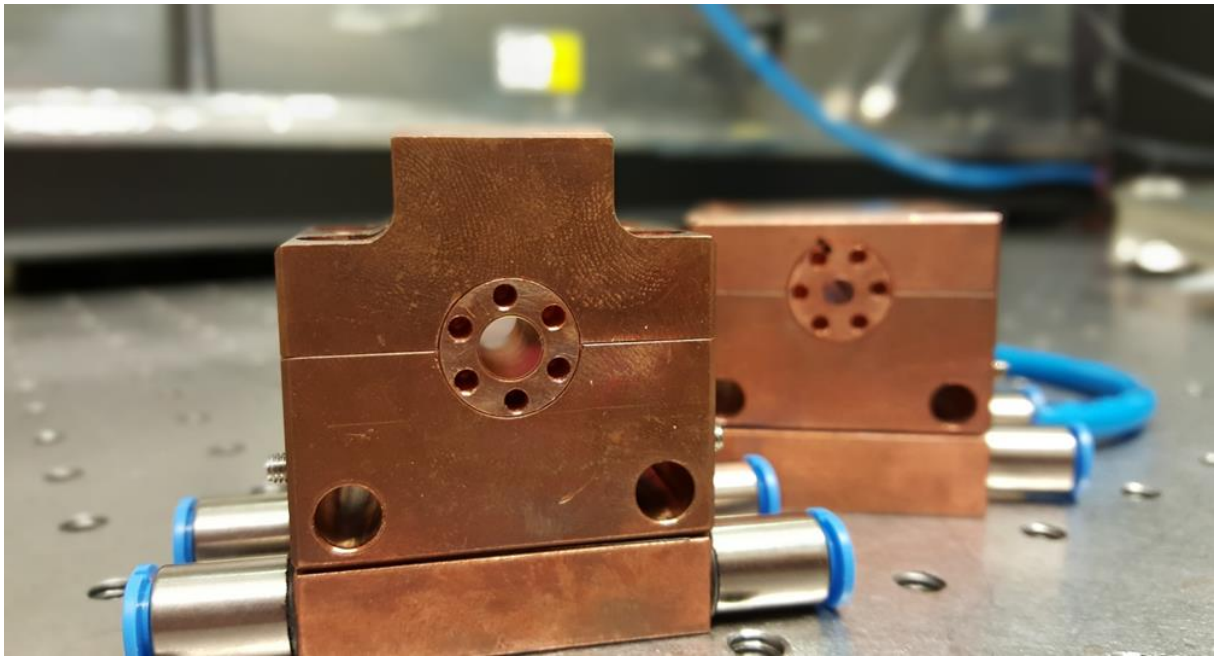

Figure 16: A Ho:YLF crystal rod mounted in a water cooled copper mount. A more compact variation of the mount design that was used in subsequent work is shown in the background.

Figure 17: The commercially sourced thulium fibre laser used as pump source (Model TLR-80-1940, from *IPG Photonics*).

3.2.2 Pump source and design

As pump source, a commercially sourced Tm-doped fibre laser (*IPG* Model TLR-80-1940, shown in Figure 17) was used, delivering up to 84.7 W of unpolarised laser light from a single-mode fibre. While the specified centre wavelength was 1940 nm, coinciding with an absorption peak of Ho:YLF, the laser had a measured laser wavelength of 1938.7 nm at full power. While this wavelength was still appropriate for good absorption in the Ho:YLF crystals, it could cause potential problems with transmission through humid air as the laser light overlapped with a few water absorption lines, as shown in Figure 18 (Koen 2010).

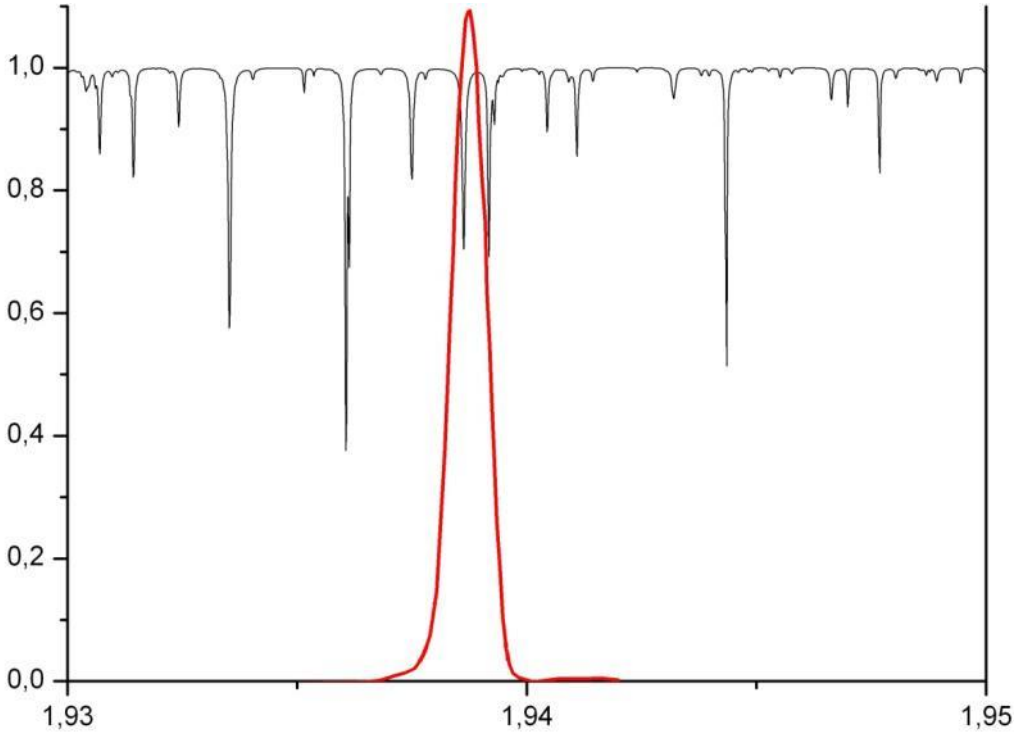

Figure 18: The IPG thulium fibre laser's spectral output superimposed with the atmospheric transmission of light through 1 meter of air with a relative humidity of 50 %, at 300K (Koen 2010).

This problem was previously confirmed by the author in (Koen 2010) where the adverse effects of thermal blooming was characterised. For illustration of the severity of the problem results from (Koen 2010) are shown in Figure 19.

In (W Koen et al. 2010) this problem was minimised by designing the pump setup so that the propagation distance between the fibre laser collimator and the laser crystals was kept to a minimum. For this work the author rather enclosed the beam path of the pump light to the first holmium crystal and purged the enclosure with dry air. This has previously been shown to be a viable solution if the relative humidity is kept below 20 % (Gibert et al. 2014; Bollig et al. 2009).

The fibre laser had a measured beam quality parameter (M^2) of 1.07 at full power (w ~1.8 mm). The fibre laser end-pumped the two Ho:YLF crystal rods which were placed one behind the other, as shown in Figure 20. Using a beam reducing telescope consisting of a plano-convex lens L_1 (f = 350 mm) and a plano-concave lens L_2 (f = -100 mm), an average pump beam radius of 310 µm was measured. This was almost half the 580 µm beam radius used previously in (W Koen et al. 2010).

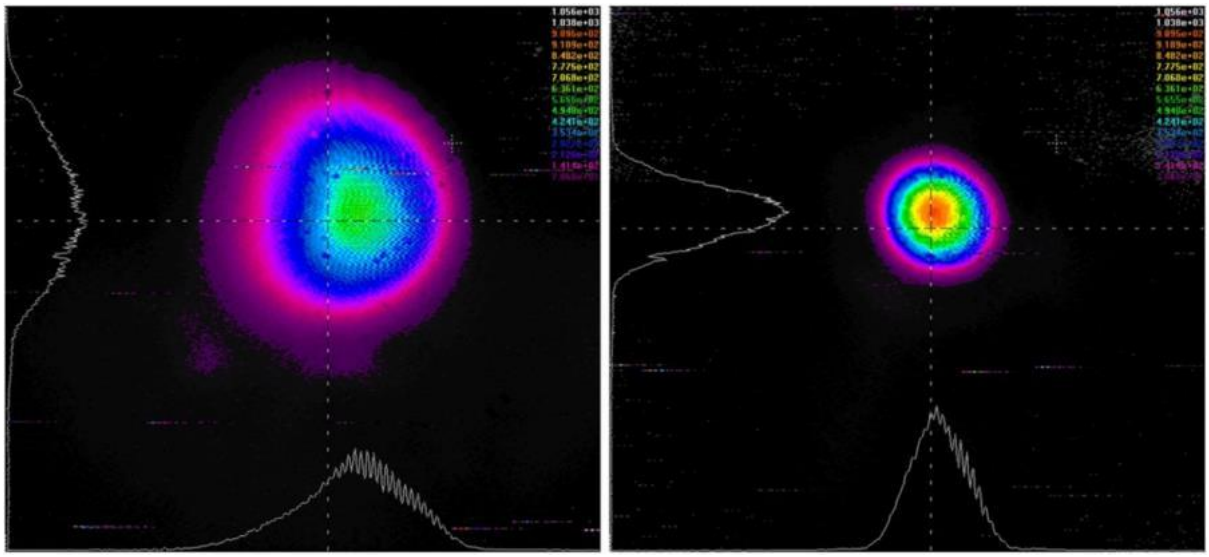

Figure 19: Beam profiles of the thulium fibre laser taken 1.85 m away from the fibre collimator, as measured by an *Ophir Spiricon Pyrocam III* (Koen 2010). The left profile is with the laser set at 50 % output power while the right profile is at 100 %. The thermal blooming at the lower power is attributed to a shift in the output wavelength of the laser, increasing the overlap with a strong water absorption line.

3.2.3 Resonator design

A schematic of the laser's layout is shown in Figure 20, with the components listed in Table 3. The cavity consisted of an input coupler mirror (M_1), a polarisation-dependent 90° folding mirror (M_2) and a concave output coupler mirror (M_3).

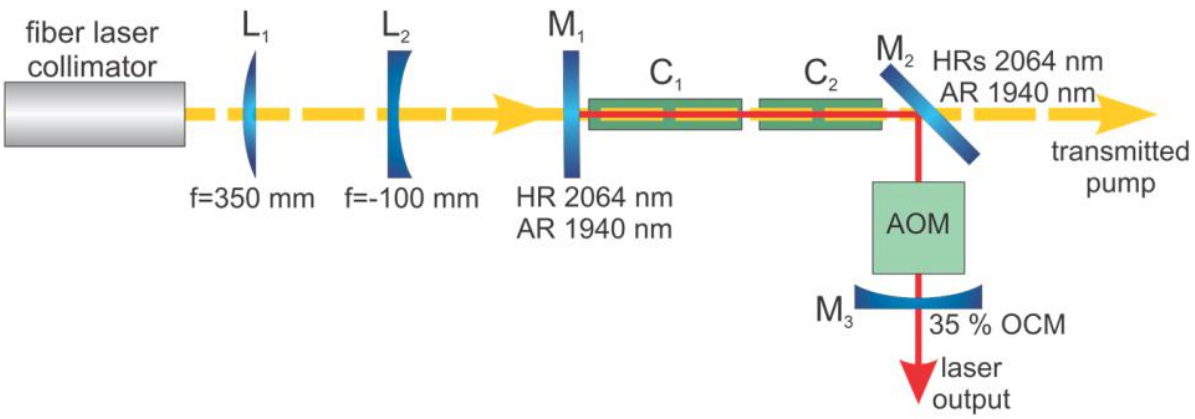

Figure 20: Schematic of the experimental layout of the 45 W Ho:YLF laser.

Table 3: Component list of the Ho:YLF laser

Component/Parameter	Specification
Lens (L_1)	f = 350 mm, AR 1900-2100 nm
Lens (L_2)	f = -100 mm, AR 1900-2100 nm
Cavity length	190 mm
ICM (M_1)	Flat AR @ 1940 nm, HR @ 2063 nm
Crystal 1 (C_1)	50 mm long a-cut 0.5% at. doped Ho:YLF
Crystal 2 (C_2)	40 mm long a-cut 0.5% at. doped Ho:YLF
Folding Mirror (M_2)	Flat AR @ 1940 nm, HRs HTp @ 2064 nm, 45º AOI
OCM (M_3)	R = 65 % @ 2064 nm, r=200mm concave
AOM	Gooch & Housego I-QS041-1.4C10V5-4-HC1

The flat input coupler mirror (M_1) had high-transmission coatings for the 1940 nm pump light while being highly reflective at the laser wavelength of 2064 nm. The flat 45° angle of incidence (AOI) folding mirror (M_2) was coated to be highly reflective at 2064 nm for the s-polarisation while being highly-transmissive for the pump light (1940 nm) as well as for p-polarised light at 2064 nm. With the mirrors placed as shown in Figure 20, the laser had a single-pass pump configuration as any pump light not absorbed in the two crystals would exit the cavity though mirror M_2. The polarisation dependent reflective coating at 2064 nm of the folding mirror (M_2, HRs & HTp at 2064 nm) also forced the laser to operate vertically polarised as it made the cavity extremely lossy for horizontally polarised light at 2064 nm (Rp < 2 % @ 2064 nm). As output coupler mirror (M_3), a concave mirror with a radius of curvature (ROC) of 200 mm and a 65 % reflectivity at 2064 nm was used. By shifting M_3, the cavity length (and thus mode size) could be varied to best match the resonator mode size with the pump beam size in the crystals. This was

done experimentally at full pump power as the exact contribution of the thermal lenses of the crystals in the cavity could only be estimated. Various output coupler curvatures were evaluated under full pumping power to determine the optimal output coupler mirror (M_3) radius of 200 mm and final cavity length of 190 mm where the resonator mode size best matched the pump size in the crystals. This allowed for efficient energy extraction while retaining excellent beam quality.

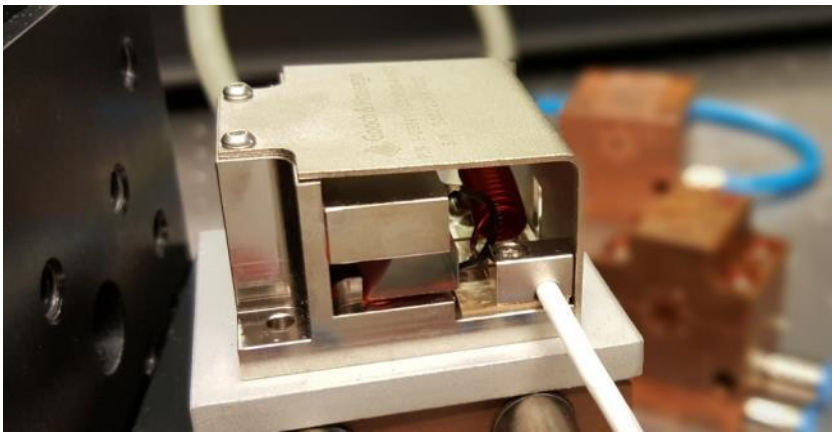

Figure 21: The *Gooch & Housego* AOM used for q-switching the laser.

For pulsed operation, a *Gooch & Housego* acousto-optic modulator (AOM, Model I-QS041-1.4C10V5) was inserted between M_2 and M_3 in order to Q-switch the laser (shown in Figure 21). The AOM was made from crystal quartz which was AR coated for 1900 to 2100 nm light. It could be driven by up to 20 W of RF power at 40.7 MHz with a rated loss modulation in excess of 65 % (1.4 mm active aperture height).

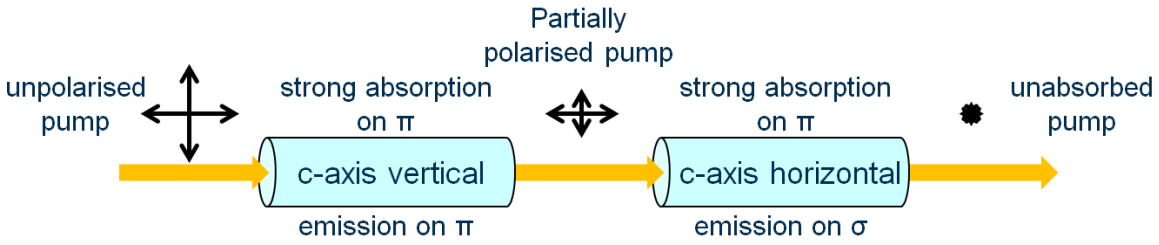

Figure 22: Two Ho:YLF crystals inside the same cavity, their c-axes rotated 90° with regard to each other in order to increase the total amount of pump light being absorbed.

Since the Ho:YLF crystals are birefringent (a-cut, with the c-axis cut perpendicular to optical axis), each crystal had to be rotated to the desired angle. First C_1 was inserted with its c-axis vertical. The polarisation dependent folding mirror M_2 (HR for vertically polarised light, HT for horizontal) would then force the laser to lase on the π-polarisation. The second crystal (C_2) was inserted behind C_1 and rotated for maximum laser output. As the maximum laser output also coincided with the least amount of transmitted pump light, it can be surmised that the second crystal's c-axis was horizontal, as the first crystal's absorption would have partially polarised the pump light of C_2 due to the polarisation-dependent absorption at 1940 nm in Ho:YLF. This concept is illustrated in Figure 22.

Previously the author has reported on a Ho:YLF MOPA system which exploited the partially polarised pump light transmitted through a laser crystal to pump an amplifier crystal by having their respective c-axes rotated by 90 ° with respect to each other (W Koen et al. 2010). This allowed efficient use of the unpolarised pump light without the need of polarisers, as used in (Dergachev et al. 2007). This is the first time, however, that the author (or anyone else, to his knowledge) has implemented this concept within a single cavity, with the first crystal lasing (providing gain) on the π-polarisation with the second shorter crystal providing gain on the σ-polarisation.

3.3 Experimental results

A photo of the constructed laser is shown in Figure 23 while the key results are listed in Table 4. The laser alignment and cavity length were optimized for maximum output power which also coincided with near diffraction-limited beam quality. The resulting power curve, taken as a function of incident pump power, is shown in Figure 24. The laser threshold was at 14.6 W of incident light, with a maximum laser power output of 45.1 W when being pumped with 84.7 W of incident light. Depending on the inclusion or omission of the laser threshold data points, the slope was between 66 and 69 % (vs. incident). These measurements do not take the losses caused by the telescope (L_1 and L_2) and input coupler mirror (M_1) into account. Figure 24 also includes the simulation results from *SimuLaser*, based on the experiment's parameters. The simulation software is based on a single element plane wave rate equation model for 3 and 4 level lasers based on two coupled rate equations (Jacobs 2013b).

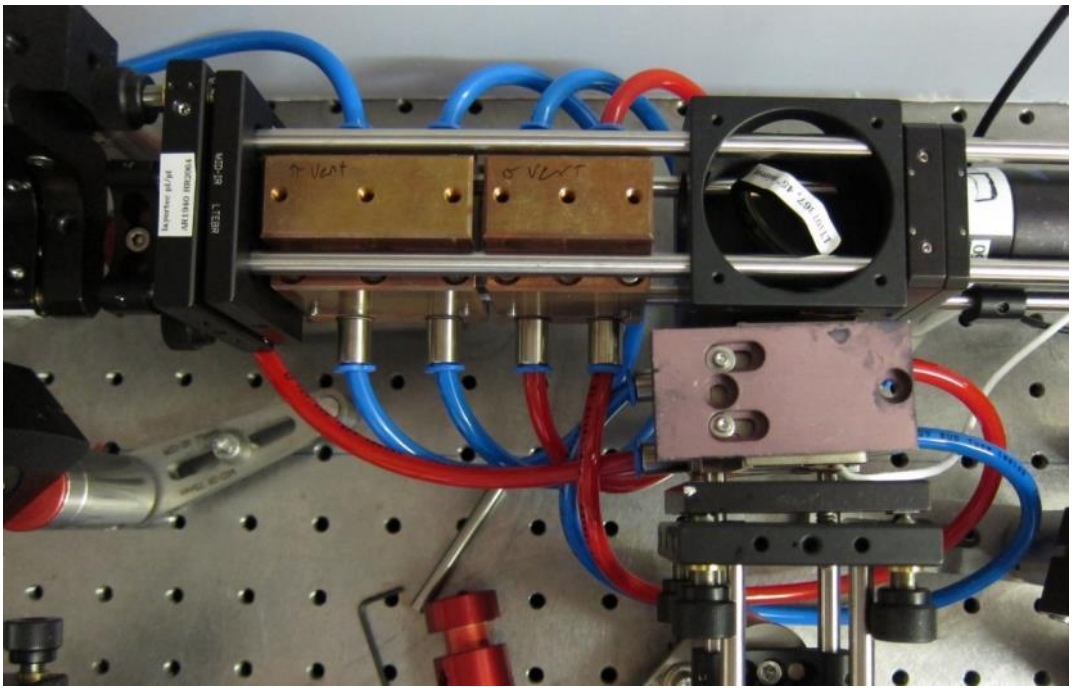

Figure 23: A top-view photo of the constructed Ho:YLF laser. The input coupler mirror is on the top left of the photo, followed by the two crystals in the water cooled copper mounts and the folding mirror. The AOM and output coupler mirror is shown bottom right.

At full pump power, the transmitted pump light was measured to be 7 W behind M_2, indicating pump absorption of nearly 92 %. Potentially, as this was less than 10 % of the total fibre laser power, this pump light could have been back-reflected through the laser crystal to improve the overall performance of the holmium laser even more, without risking feedback damage to the thulium fibre laser (Bollig et al. 2009).

Figure 25 (left) shows the laser beam intensity profile in the far field, as recorded with an *Ophir Spiricon Pyrocam III*. The laser's M^2 was measured to be better than 1.06 at full pump power, which is nearly diffraction limited. The laser wavelength was measured to be 2063 ± 3 nm using a *Jarrell Ash* monochromator and photodetector. When pulsing at a repetition frequency of 50 kHz at full power, laser pulse durations of between 46.2 and 49.2 ns (FWHM) long were measured.

Table 4: The Ho:YLF laser output parameters

parameter	measured performance
Max. output	45.1 W
Efficiency	53.3% optical to optical w.r.t. incident pump
Wavelength	2063±3 nm
Beam quality	$M^2 < 1.06$
Pulse width	46 to 49 ns at @ 50kHz PRF

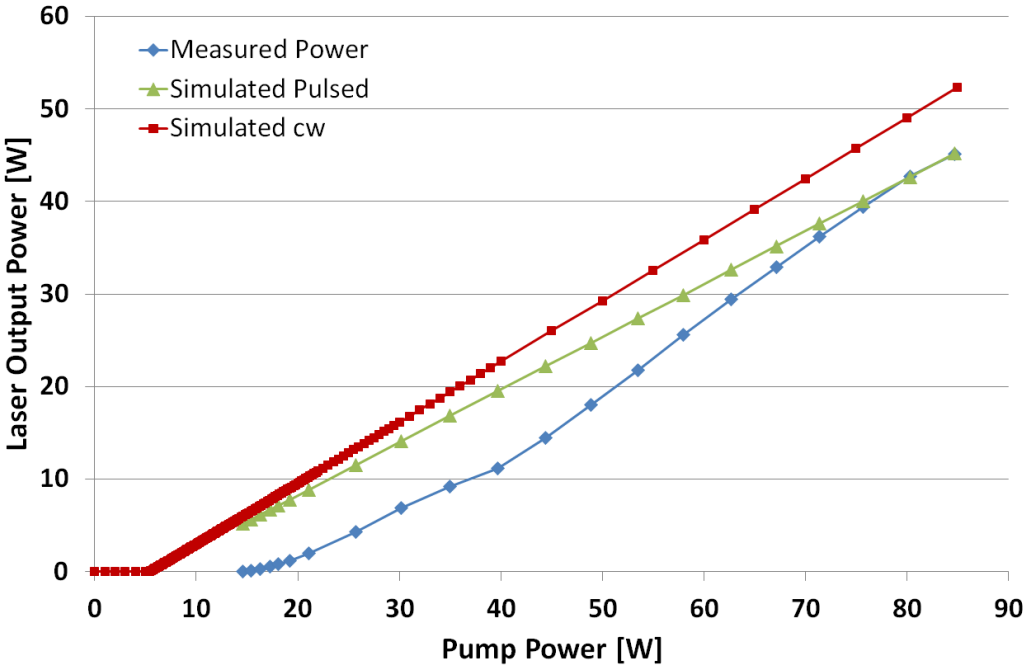

Figure 24: The Ho:YLF measured laser slope (cw) as a function of incident pump power. The simulated results are also shown. The difference between the simulated cw and Q-switched results can be attributed to AOM insertion losses (Jacobs 2013b).

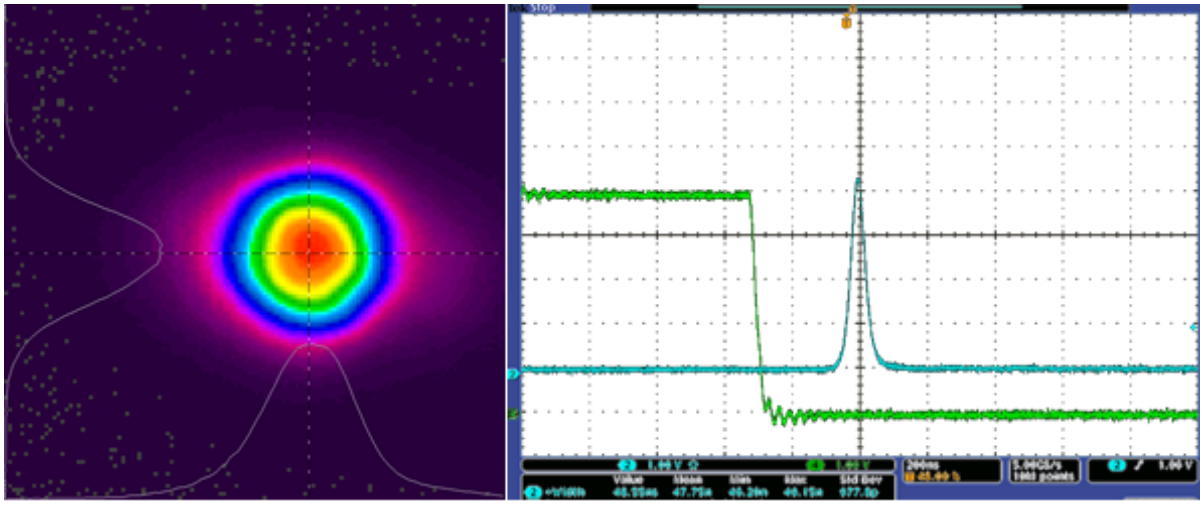

Figure 25: (left) Laser beam profile at full power and (right) the pulse trace of the laser when being Q-switched at a pulse repetition frequency of 50 kHz. The green trace is the AOM trigger while the cyan trace is the measured laser pulse.

3.4 Discussion

The experimental results are in good agreement with the simulations, as shown in Figure 24. The slightly lower output powers may be attributed to the limitations of the software which does not take into account the varying mode sizes under different pump powers (due to thermal lensing), and minor atmospheric absorption of the pump light. The variation of the pump light wavelength for different pump powers will also play a role.

Some key results from this experiment are compared with other published work in Table 5. To date, this is the highest power output obtained from a fibre-laser pumped Ho:YLF laser without any amplifier stage operating near room temperature. The power output as well as optical-to-optical efficiency of 53 % and 66 % slope efficiency compares very favourably with state of the art Ho:YAG lasers, which have the advantage of improved thermal conductivity as well as higher absorption and emission cross sections. This work shows, however, that the multiple crystal approach with the crystal axes perpendicular to each other can compensate for these drawbacks. While the extra crystal in the cavity does add some minor complexity to the system, the Ho:YLF

laser has one big advantage over Ho:YAG: Superior beam quality. The far stronger thermal lensing in Ho:YAG makes it very difficult to maintain good beam quality at even moderate output powers, while it has been shown in this work as well as several other publications that near-diffraction limited laser beams can be obtained with relative ease when using Ho:YLF as gain medium in a diverse number of operating regimes and configurations (Dergachev & Moulton 2003; Schellhorn 2011; W Koen et al. 2010; Koen et al. 2015; Dergachev et al. 2005; Kwiatkowski et al. 2015; Fonnum et al. 2013; Strauss et al. 2013; Bollig et al. 2009).

The laser pulse length under Q-switched operation in conjunction with the excellent beam quality and high average powers make this laser an ideal pump source for mid-infrared Optical Parametric Oscillators (OPO's), where a high pump peak fluence is required for efficient nonlinear conversion of the pump light (Schellhorn et al. 2007; Lippert, Fonnum & Stenersen 2010).

One improvement to this laser that would increase its output power would be the reuse of the transmitted pump light. This could be quite easily done with the addition of a pump mirror behind mirror M_2 in order to back reflect the remaining ~7 W of pump light. However, the existing pump absorption of 92 % is already excellent and the additional pump light will most likely not increase the laser output by more than 4 W, considering the existing efficiency.

Table 5: Comparison of efficient holmium YLF and YAG lasers

	similar Ho:YLF laser 1 (Dergachev et al. 2005)	**similar Ho:YLF laser 2** (Kwiatkowski, Zendzian, et al. 2014)	**this Ho:YLF laser**	**similar Ho:YAG laser 1** (Lippert, Fonnum & Stenersen 2010)	**similar Ho:YAG laser 2** (Elder 2009)	**similar Ho:YAG laser 3** (Kwiatkowski et al. 2012)
power	43 W	14.5 W	45.1 W	36.7 – 42 W	27.4 W	10.7 W
optical-to-optical efficiency (w.r.t. incident)	41 %	44.6 %	53 %	52 - 60 %	65 %	53.5%
slope efficiency	42 %	53.4 %	66 %	not published	71 %	55 %
beam quality	not published	M^2 1.05-1.09	M^2 1.06	$M^2 \approx 1.7$	M^2 1.4	$M^2 \approx 1.6$

3.5 Conclusion

A thulium fibre laser pumped Ho:YLF laser was demonstrated which delivered a maximum of 45.1 W of cw power at 2063 nm in a near diffraction-limited beam when pumped with 84.7 W of pump light. The optical-to-optical efficiency of 53 % surpassed all previously published Ho:YLF lasers of its type and compared favourably with similar Ho:YAG lasers reported upon in (Lippert, Fonnum & Stenersen 2010) and (Elder 2009) which had efficiencies of 51.3 - 60 % and 65 %, respectively. This high efficiency was achieved by pumping with a small diameter beam and having good absorption of the pump light by using two laser crystals whose c-axes were orientated orthogonally with respect to each other for optimal pump absorption.

4 Development of a 60 W Ho:YLF Oscillator-Amplifier System

A compact Ho:YLF oscillator–amplifier system pumped by two 54 W unpolarised Tm:fibre lasers, producing 60.2 W of output power at 2064 nm, has been developed. The seed laser delivered a maximum output of 24 W with an M^2 of 1.06. The two-crystal, single-pass amplifier provided a gain of 2.5, and M^2 of 1.09 at full power. The amplifier utilized the transmitted pump from the seed laser's single fibre laser in addition to a second fibre laser, resulting in an optical-to-optical efficiency of 55.5 %. Under Q-switched operation, laser pulse lengths of between 43 and 113 ns at repetition rates from 15 to 40 kHz were measured.

4.1 Introduction

In Chapter 3, an efficient Ho:YLF laser which delivered 45.1 W at 2063 nm when pumped with 84.7 W was demonstrated. The laser was end-pumped with a commercially available Tm:fibre laser at 1940 nm. The optical-to-optical efficiency of 53 % was obtained by pumping with a small diameter beam and obtaining good absorption of the pump light through the use of two a-cut laser crystals whose c-axes were orientated orthogonally with respect to each other for optimal pump absorption.

A novel master oscillator power amplifier (MOPA) scheme was also previously developed and demonstrated, where the unused Tm:fibre laser pump light transmitted by the Ho:YLF oscillator crystal was used to pump an amplifier crystal (W Koen et al. 2010). Improved absorption and

output power was obtained by having the c-axis of the laser crystal orientated by 90 degrees with respect to the amplifier crystal. The MOPA delivered 23.7 W at 2065 nm when pumped with 82 W at 1940 nm. The system had an optical-to-optical efficiency of 29 %. This approach, first implemented by our group in (Bollig et al. 2009) and (W Koen et al. 2010), has subsequently been successfully implemented by other research groups (Kwiatkowski et al. 2015), as discussed in Chapter 2.

The aim of the work reported on in this chapter was to demonstrate a compact Ho:YLF-based MOPA system that could deliver high average powers in a near-diffraction-limited beam, with very good optical-to-optical efficiencies near room temperature. To achieve this, the efficient oscillator design approach demonstrated in the previous chapter was combined with the compact and efficient oscillator-amplifier pumping scheme demonstrated in (W Koen et al. 2010). This entailed having a relatively small pump beam matched to a similarly small mode size in the oscillator crystal, as well as placing the oscillator and amplifier crystals “in series” in order that all the crystals could be end-pumped by two commercially available air-cooled Tm:fibre lasers. As described in the next section, this scheme would allow hard pumping of the oscillator crystal (for a low laser threshold), without being concerned that the transmitted pump light from the seed laser would damage the fibre lasers as it would be absorbed in the subsequent amplifier crystals.

In Section 4.2 of this chapter the experimental design and setup is presented, followed by the experimental results in Section 4.3. The results are discussed in Section 4.4 and compared to other reported MOPA systems. Finally, a conclusion is presented in Section 4.5.

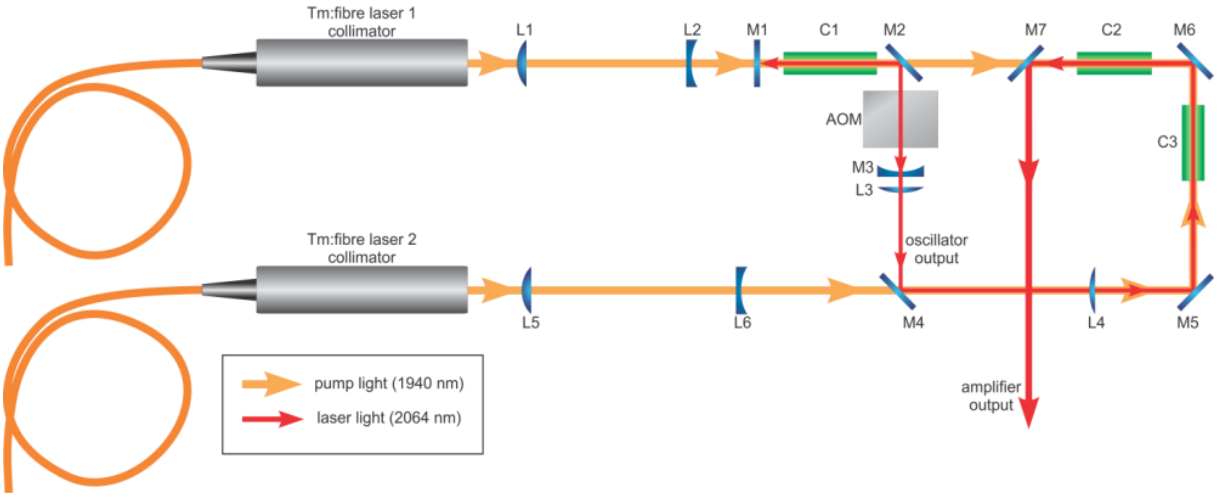

Figure 26: Schematic diagram of the Ho:YLF Master Oscillator Power Amplifier system.

4.2 Design and experimental setup of the Ho:YLF MOPA system

The schematic layout of the Ho:YLF oscillator and single-pass amplifier design is shown in Figure 26. The various components and design considerations are discussed in the respective subsections below. Section 4.2.1 describes the pump sources chosen as well as the pump design for the resonator. The selection of the Ho:YLF crystals is discussed in Section 4.2.2, while the design of the resonator and amplifier is presented in Sections 4.2.3 and 4.2.4 respectively.

4.2.1 Pump design

Two air-cooled thulium fibre lasers (Model number TLR-50-AC-Y12, from *IPG Photonics*) were selected as pump sources, each delivering up to 55 W of pump power in an unpolarised beam. These were the most powerful air-cooled Tm:fibre systems available on the market. The two fibre-lasers' wavelengths were selected to match the Ho:YLF absorption peak at 1940 nm and were subsequently measured to be 1939.5 and 1939.8 nm, respectively. Because the final MOPA system was to be enclosed in its own box, flushed with dry air, potential water absorption of the

Figure 27: The system control rack containing the two air-cooled Tm:fibre lasers and other electronic components

pump light did not pose a problem except during the initial setup. The lasers were mounted in a 19" rack, as shown in Figure 27 for increased portability. Both fibre lasers had a measured M^2 of ~1.06.

The collimated pump light from the first fibre laser ("Tm:fibre laser 1" in Figure 26) was transmitted through a telescope consisting of two lenses with respective focal lengths of 114 mm (L_1) and -23 mm (L_2), resulting in a pump beam radius of 280 µm in the oscillator crystal C_1. The full unpolarised pump beam from the first fibre laser was used to pump the oscillator crystal (C_1).

The design and setup of the second thulium pump laser optics is described in the amplifier design section (Section 4.2.4) as it was an integral part of the amplifier design, with shared optics shaping both the seed and amplifier beams.

4.2.2 Selection of the Ho:YLF laser crystals

While one crystal was used in the resonator, two crystals were used in the amplifier. All three crystals were 0.5 at. % doped, a-cut Ho:YLF crystal rods. The resonator crystal C_1 had a length of 50 mm, while the two amplifier crystals, C_2 and C_3 were both 40 mm long. The end surfaces of the crystals were coated to be anti-reflective for both the pump and the laser light (1.8-2.1 µm). The crystals in the setup were mounted in water cooled copper mounts in the same manner described in Chapter 3. The water temperature set-point was 18 °C.

4.2.3 Resonator design

The laser cavity design was aided by the *Psst! Laser Resonators* simulation package, a screenshot of which is shown in Figure 28 (Gillies et al. 2000). The optical length of the resonator was 115 mm with a flat input coupler mirror (M_1 in Figure 26), a flat folding mirror (M_2), an AOM, and a concave output coupler mirror (M_3). The input coupler mirror (M_1) had anti-reflective coatings for the pump light (1940 nm) and was highly reflective at the expected laser wavelength of 2064 nm. The output coupler mirror had a reflectivity of 82 % at 2064 nm. Neglecting thermal lensing, the calculated TEM_{00} beam radius in the YLF crystal C_1 was 310 µm.

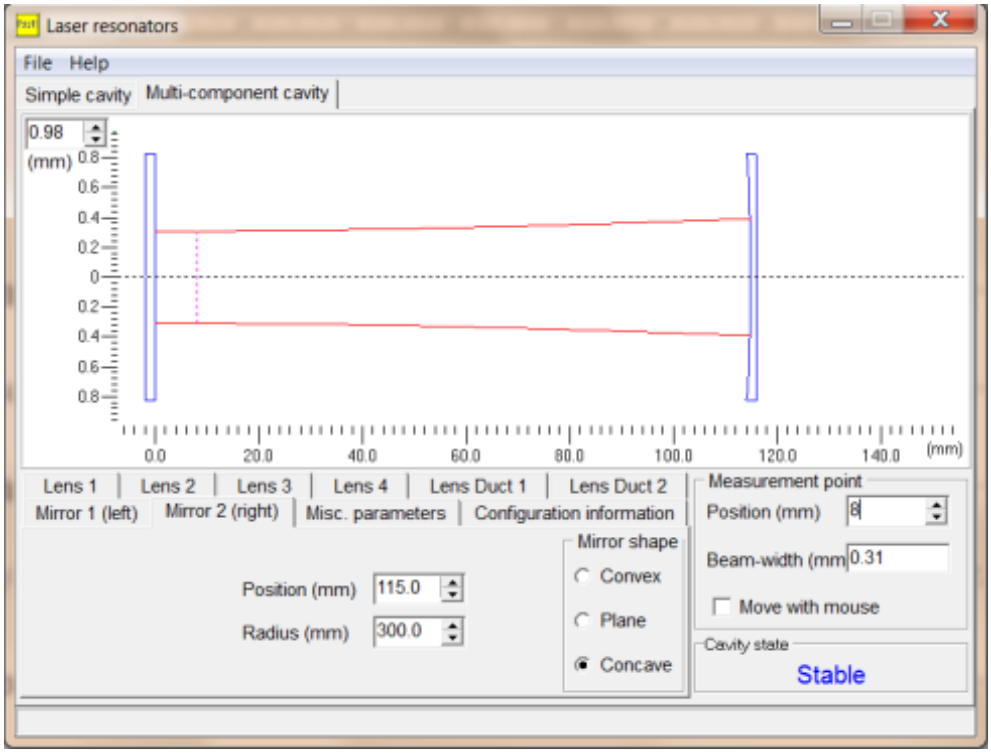

Figure 28: A screen shot of the Resonator design within *Psst!* software (Gillies et al. 2000). The optical components are shown in blue while the fundamental resonator mode is shown in red.

To keep the optical path of the pump light to the amplifier crystals (C_2 and C_3 in Figure 26) to a minimum, the resonator was folded using a 45° AOI dichroic mirror M_2 with high transmission for the pump light (s- and p-polarisation), high reflection for s-polarised laser light, and high transmission for p-polarised laser light. This polarisation-dependent folding mirror also forced the oscillator to operate vertically polarised. Having the c-axis of the crystal horizontal in combination with the polarisation dependent folding mirror, lasing was ensured on the σ-polarisation. This resulted in a good beam quality because of the weak thermal lensing. The pump light that was not absorbed by the oscillator's crystal (C_1) was transmitted through the 45° mirror into the amplifier crystal C_2.

A plane cut, AR coated crystalline quartz acousto-optic modulator (AOM) manufactured by *Gooch & Housego* (Model QS041-1.4C10V5-4-HC1) was inserted for Q-switched operation. The

AOM driver was set to a gate time of 2.1 µs at 15 W of RF power. This was the same AOM that was used in Chapter 3.

4.2.4 Design of the two-crystal amplifier

The amplifier design envisaged by the author was aided by in-house software *EXAG* developed by Cobus Jacobs, which is based on ABCD matrices for Gaussian beam propagation (Jacobs 2013a; Jacobs et al. 2009). The optimisation capabilities of this software package made it possible to develop an elegant and compact multiple crystal, multiple pump amplifier configuration where the incident pump and seed light could be shaped by the same lens (L_4) while propagating collinearly. The main interface of the software is shown in Figure 29.

The output from the software, depicting the resulting beam propagation, is shown in Figure 30. The Lenses L_3 and L_4 (with focal lengths of 172 mm and 344 mm, respectively) shaped the oscillator's output to a beam radius of 370 µm at the front face of amplifier crystal C_3 and 400 µm at the exit face of amplifier crystal C_2. The c-axis of C_2 was placed vertical, while that of C_3 was

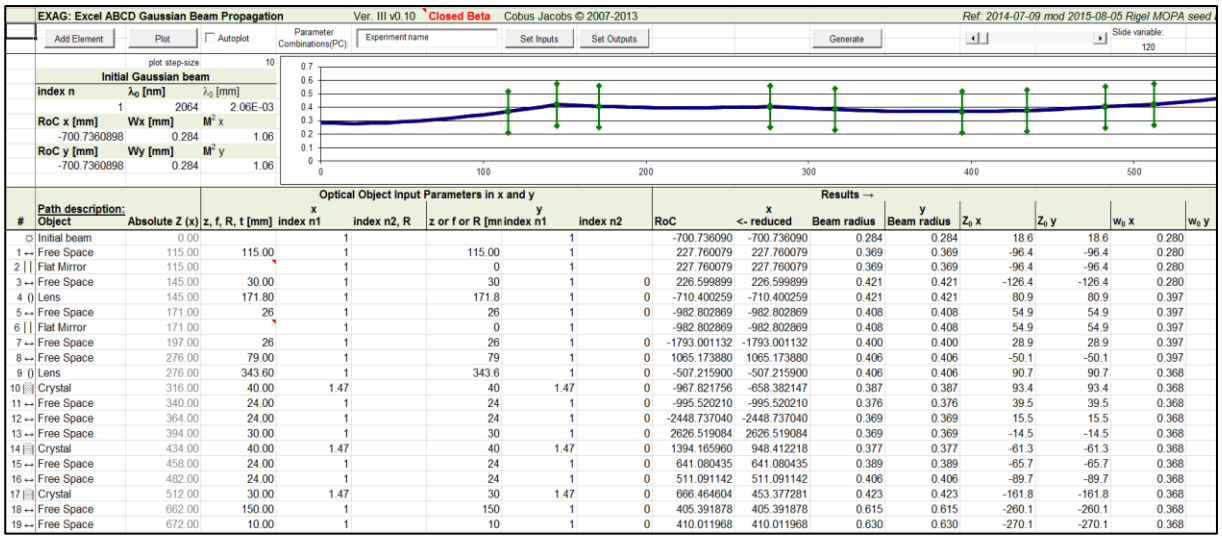

Figure 29: The input screen of the in-house developed beam propagation software, *EXAG*, used to design the Ho:YLF amplifier (Jacobs 2013a; Jacobs et al. 2009).

placed horizontal. With the seed beam being vertically polarised, it meant that C_2 amplified on its π-polarisation and C_3 on its σ-polarisation.

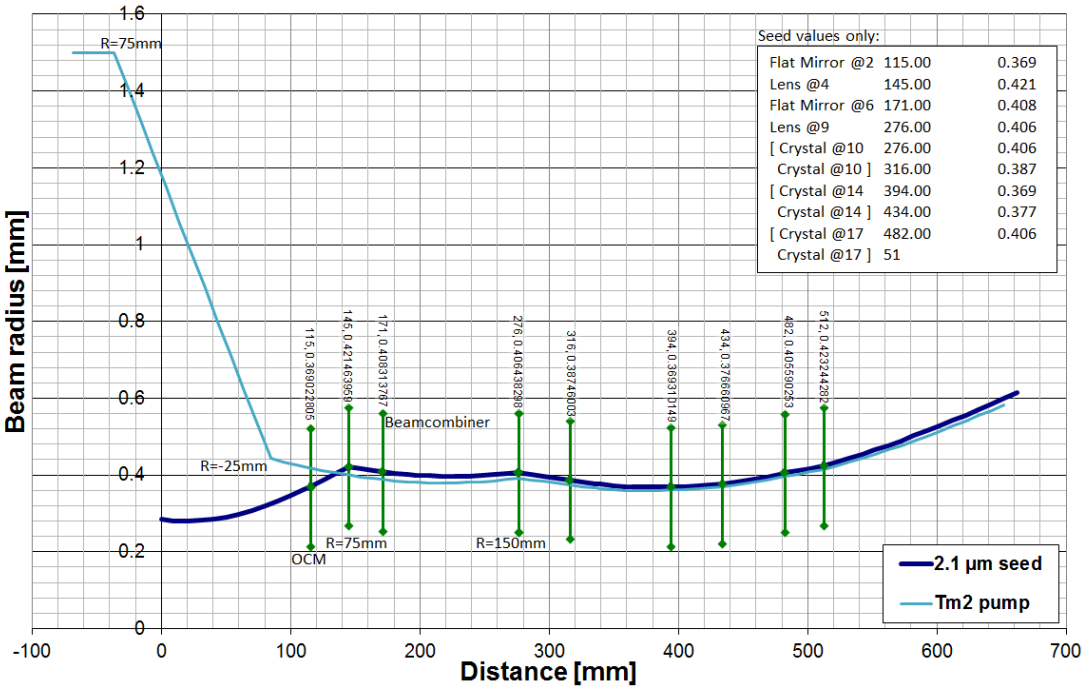

Figure 30: A screenshot from *EXAG* software depicting the amplifier seed beam (navy trace) and the second thulium fibre laser pump beam (cyan trace) design (Jacobs 2013a; Jacobs et al. 2009).

The pump beam from the second fibre laser was matched to the seed beam from the oscillator by using lenses L_5 (f = 172 mm), L_6 (f = -57 mm) and L_4 (f = 344 mm). Mirror M_4, which was highly transmissive at 1940 nm and highly reflective at 2064 nm, was used to combine the pump beam from the second fibre laser and the seed beam from the oscillator. From M_4 the second pump beam and the seed beam propagated collinearly through lens L_4, were reflected off the broadband mirror M_5, propagated through amplifier crystal C_3, reflected by mirror M_6, and then passed through crystal C_2 before being separated by the folding mirror M_7. M_7, which was highly transmissive at 1940 nm and highly reflective at 2064 nm, allowed any residual pump light from

the amplifier to enter the oscillator crystal, while reflecting the amplified laser beam to where it could be used.

4.3 Experimental results of the Ho:YLF MOPA system

A photo of the constructed MOPA before it was integrated into its box is shown in Figure 31. The fibre lasers were connected on the right (yellow delivery fibres). The pump light telescopes were temporarily enclosed in plastic and flushed with dry air to prevent interference caused by water vapour.

Figure 32 shows the same Ho:YLF MOPA system, but fully integrated into its portable box along with other optical components and devices such as a dynamic optical switching system and two optical parametric oscillators which are beyond the scope of this dissertation, but may be published at a later stage.

Figure 31: The Ho:YLF MOPA system prior to integration. The two thulium fibre lasers can be seen connected on the right. Their respective beam reducing telescopes are wrapped in plastic and flushed with dry air to prevent absorption of the laser light by water vapour from causing thermal blooming.

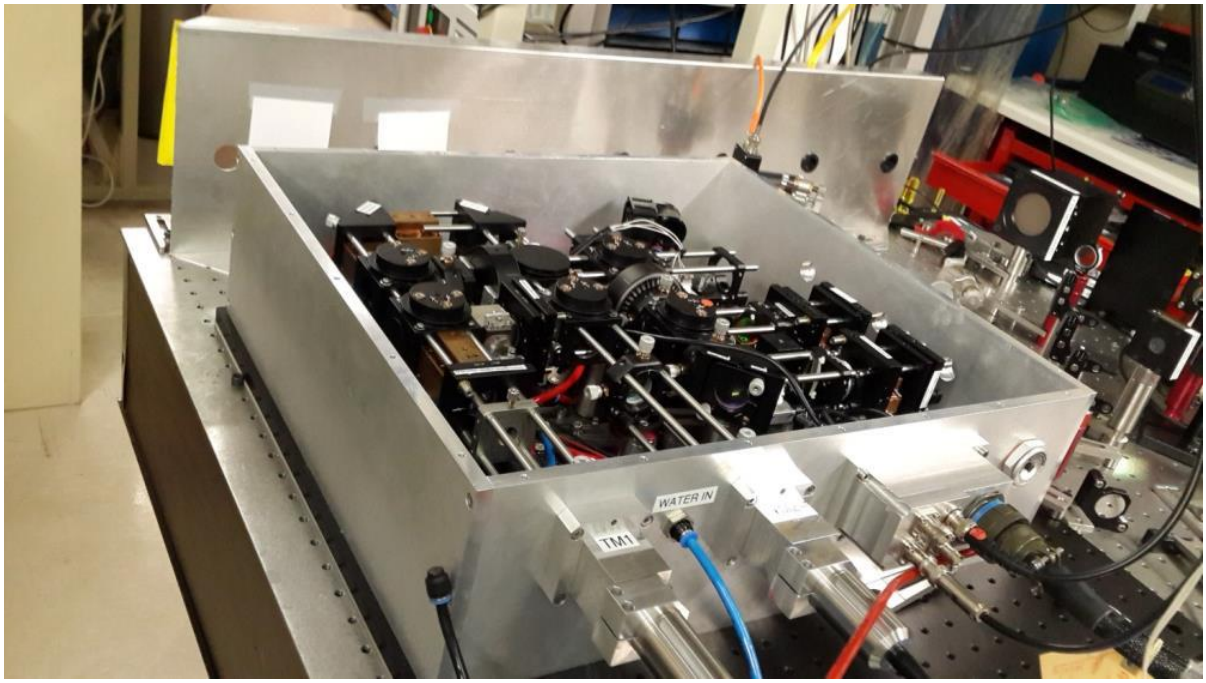

Figure 32: A photo of the Ho:YLF MOPA system integrated into its portable case. The MOPA occupied less than half of the box, with the rest occupied by a three-channel optical switching system and two optical parametric oscillators.

4.3.1 Oscillator results

The oscillator was first operated in cw mode with the AOM switched off. The cw output power as a function of the fibre laser pump light absorbed in the crystal is shown in Figure 33. The oscillator had a threshold of 4 W of incident pump power (2.7 W absorbed), with an overall slope efficiency of 50 % (75 % vs. absorbed power) when pumped with the first fibre laser. At full pump power (53.2 W) the oscillator output power was 24.6 W at a centre wavelength of 2064 nm. The output power was dependent on the pump laser's output power which in turn was dependent on the ambient temperature of the room (it appeared that the temperature of the air-cooled Tm:fibre lasers weren't actively controlled). The optical-to-optical efficiency of the oscillator with regards to incident pump power was 46 % (69 % vs. absorbed power). This far exceeded a similar system reported on previously by the author, whose oscillator had an overall slope efficiency of

25 % (47 % vs. absorbed power) and an optical-to-optical efficiency of 15 % (W Koen et al. 2010). It also compared well with the most powerful oscillator of this type reported on in Chapter 3 which gave an overall efficiency of 53 % (66 % vs. absorbed power), with a maximum of 45.1 W of output power (from 84.7W of pump power) (Koen et al. 2013). However, while the laser in Chapter 3 absorbed 92% of the incident pump power, the oscillator reported upon here only absorbed 66.5 % of the incident pump light, transmitting ~18 W into the amplifier crystals, thereby increasing the pump power available for the amplifier system. The oscillator beam quality at full power was excellent with a measured M^2 of 1.06. The beam profile of the MOPA, as taken by an *Ophir Spiricon Pyrocam III*, is shown in the insert of Figure 35.

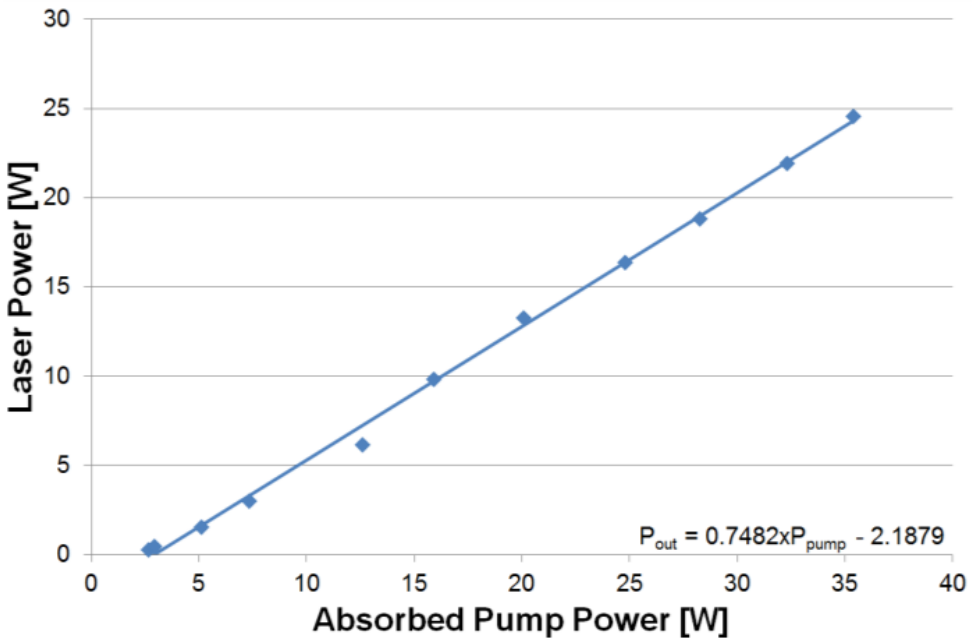

Figure 33: Oscillator output power versus absorbed fibre pump power under cw lasing conditions. The solid line is a linear fit of the measured data points, indicating a slope of 75 % with regards to absorbed pump power.

The oscillator was subsequently Q-switched with the acousto-optic modulator at the desired pulse repetition rates of between 15 and 40 kHz. The pulse energies of the oscillator and amplifier as

well as the FWHM pulse lengths at full pump power as a function of the repetition rate are shown in Figure 34. In this regime the laser pulse length responded nearly linearly to an increase in PRF, with the shortest measured pulse length of 44 ns at 15 kHz and the longest pulse of 116 ns at a PRF of 40 kHz. The highest calculated energy per pulse from the oscillator was 1.5 mJ at 15 kHz.

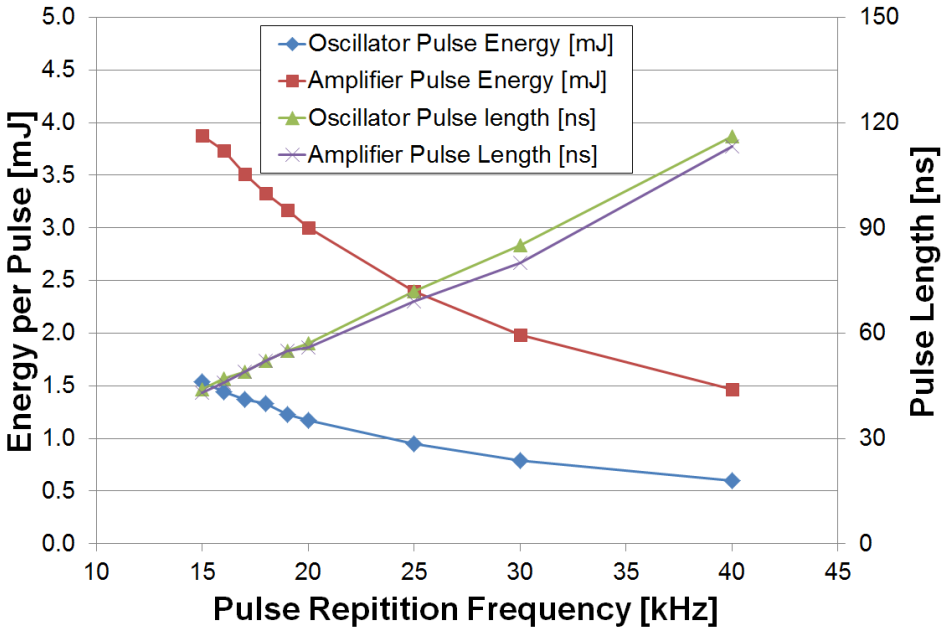

Figure 34: Oscillator and amplifier output energy (left axis) and FWHM pulse lengths (right axis) as a function of the pulse repetition rate at full pump power.

4.3.2 Amplifier Results

The MOPA system delivered up to 60.2 W of cw laser light when pumped with 108.5 W, with both thulium fibre pump lasers set to 100 %. This corresponded to an optical-to-optical efficiency of 55.5 % and an amplifier gain factor of 2.5. This MOPA exceeded the performance of a similar MOPA system which had an optical-to-optical efficiency of 29 % and a gain from the amplifier of

1.9 (W Koen et al. 2010). The temporal behaviour of the MOPA output as well as the spatial beam profile is shown in Figure 35. When seeded under Q-switched operation, the amplifier shortened the laser pulses slightly, delivering 43 ns at 15 kHz and 113 ns at 40 kHz, compared to 44 ns at 15 kHz and 116 ns at 40 kHz of the oscillator. The beam quality of the amplified beam at full power was measured to be better than an M^2 of 1.09, which was only slightly higher than that of the seed beam (M^2 = 1.06).

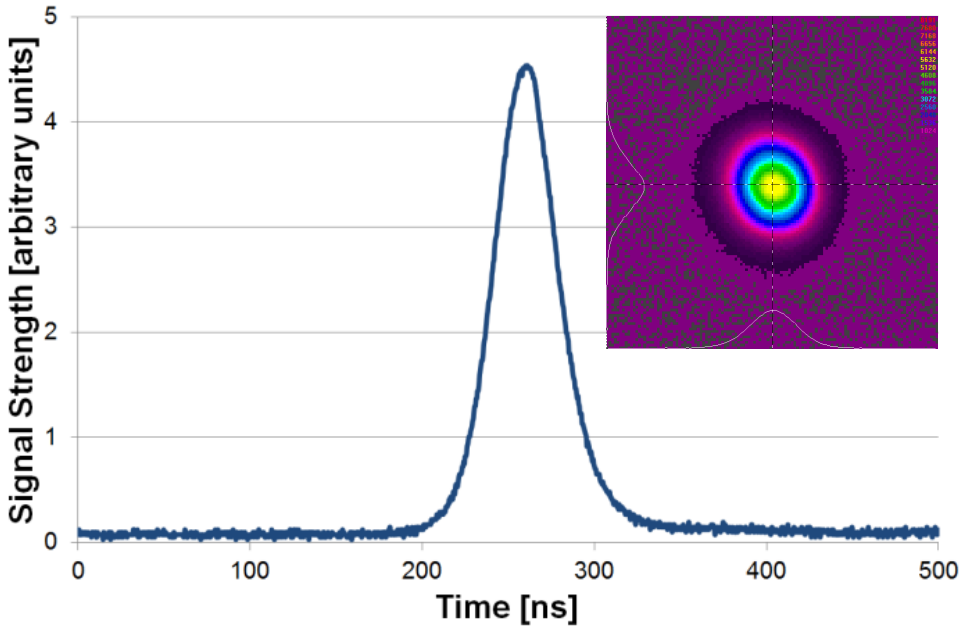

Figure 35: Temporal pulse trace of the MOPA output at a PRF of 15 kHz and full pump power. The FWHM pulse length was 43 ns. The spatial intensity profile of the MOPA output beam at full pump power, as measured by an *Ophir Spiricon Pyrocam III*, is shown in the inset.

4.4 Discussion

A direct comparison of this system with other reported work is difficult as nobody has simultaneously pumped an oscillator and amplifier using two unpolarised thulium fibre lasers in this manner before. One can, however, compare the basic output parameters and efficiencies. In this regard, the MOPA performed very well. For comparison this MOPA's output parameters are

summarized in Table 6 along with other published Ho:YLF MOPA systems. The total optical-to-optical efficiency of 55.5 % was excellent compared to other reported systems, as well as the total output power of over 60 W. The beam quality was near diffraction-limited at full power.

Should more than 60 W of laser power be required for an application, power scaling is possible by using this MOPA system to seed more amplifier stages in a similar fashion as described in (Dergachev et al. 2008) where an additional 2 amplifier stages increased their MOPA output of 39 W to a total of 115 W.

However, 60 W of average power from a Q-switched laser is already an ample amount of pump power for high-power OPO's. With the laser output of this MOPA at 2064 nm, this is a particularly attractive pump source for $ZnGeP_2$ based OPO's as well as other mid-infrared OPO's. Firstly, $ZnGeP_2$ is opaque at 1 µm and can therefore not be pumped with more readily available pump sources such as neodymium-based lasers; as indicated by the transmission spectra of $ZnGeP_2$ shown in Figure 36. Secondly, pumping a 3-5 µm OPO (a highly desirable region as it coincides with an atmospheric transmission window) with 2 µm light is far more efficient as both the signal and the idler wavelengths fall within the desired band. This is not the case for 3-5 µm OPO's pumped with 1 µm laser light ($\hbar\omega_{pump} = \hbar\omega_{seed} + \hbar\omega_{idler}$).

Table 6: Comparitive table of published Ho:YLF MOPA systems.

	this Ho:YLF MOPA (Koen et al. 2015)	(W Koen et al. 2010)	(Dergachev et al. 2008)	(Kwiatkowski et al. 2015)
Pump power	108.5 W	82 W	120 W	82.5 W
laser power	24.6 W	12.4 W	25 - 26 W	18 - 24.5 W
amplifier output	60.2 W	23.7 W	39 W	26.6 - 30.5 W
amplifier gain	2.5	1.9	up to 1.56	up to 1.75
MOPA optical-to-optical efficiency (w.r.t. incident)	55.5 %	29 %	32.5 %	up to 37 %
laser slope efficiency	69 %	25 %	na	25.5 - 35.4 %
amplifier M^2	1.09	<1.1	na	<1.1

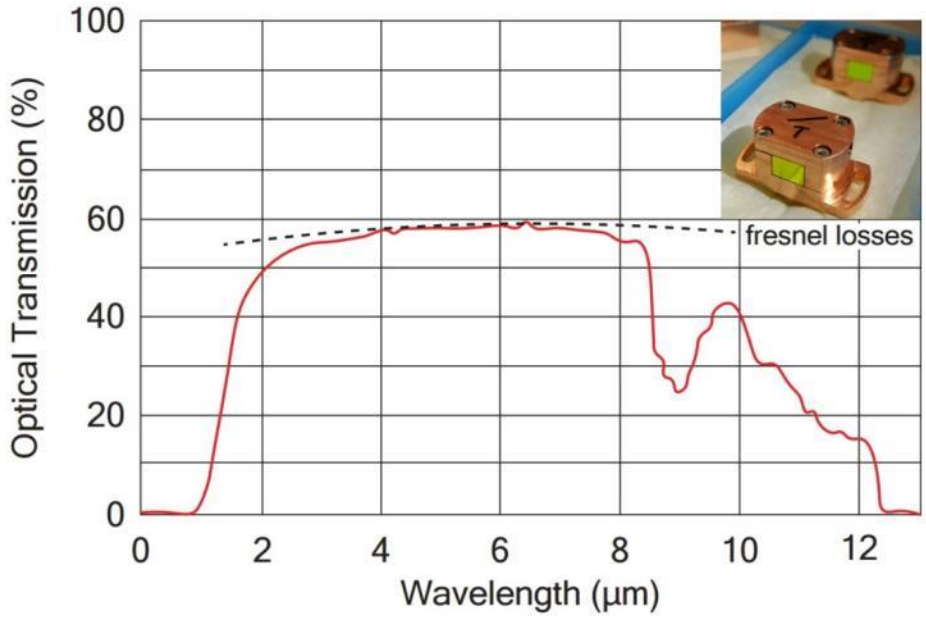

Figure 36: The optical transmission graph of uncoated zinc germanium phosphate crystals (Inrad 2015). A photo of AR coated ZGP crystals is shown in the insert.

4.5 Conclusion

An efficient oscillator–amplifier scheme was developed and successfully demonstrated, whereby two air-cooled unpolarised thulium fibre lasers were used to pump the oscillator and amplifier crystals in series. The system produced up to 60.2 W of laser light at 2064 nm in a near diffraction-limited beam. With an optical-to-optical conversion efficiency of 55 % with respect to incident pump power, this is to the author's knowledge the most efficient Ho:YLF MOPA system of its type. Under Q-switched operation, the system delivered 43 ns long laser pulses at 15 kHz and 113 ns pulses at 40 kHz. The properties of this system make it an ideal pump source for mid-infrared Optical Parametric Oscillators (OPO's) and amplifiers (OPA's). Further work may entail investigating passive cooling techniques of the MOPA components, further miniaturization and a more rugged design, as discussed in the conclusion of the dissertation (Chapter 9).

A single-frequency pulsed system at this wavelength is also an excellent coherent source for LIDAR and DIAL applications (Gibert et al. 2014). Additionally, such a narrow-band source can also be used to optically pump a molecular laser. For example, the single-frequency laser reported on in (Bollig et al. 2009) was successfully used to pump an HBr laser (Botha et al. 2009). In the subsequent chapter of this dissertation the author will describe how the laser reported on in (Bollig et al. 2009) was energy scaled to 330 mJ per pulse at a PRF of 50 Hz. The resulting high-energy laser light was then used to pump HBr molecular lasers as well as an HBr-based amplifier, as reported in Chapters 7 and 8.

.

5 Single-frequency Ho:YLF Slab Amplifier Pumped by a High-power Tm:YLF Slab Laser

A double-pass Ho:YLF slab amplifier which delivered 350 ns long single-frequency pulses of up to 330 mJ at 2064 nm, with a maximum M^2 of 1.5 at 50 Hz is presented. It was end-pumped with an in-house developed diode-pumped Tm:YLF slab laser and seeded with up to 50 mJ of single-frequency laser pulses from an injection seeded Ho:YLF ring-laser.

This chapter ***summarises*** work in which the author was closely involved in ***collaboration*** with his colleagues. The results of this ***collaborative*** work is included in the dissertation as the amplifier system presented here was used to pump the HBr systems presented in the subsequent chapters and thus illustrates how one may go from one domain of laser research to another (namely bulk solid-state to optically-pumped molecular lasers) in order to achieve a specific goal; in this case generation of laser light in the 3-5 µm region. Specific contributions by the author are indicated at the end of the chapter and reference is made to the relevant journal and conference papers based on this work, where appropriate.

5.1 Introduction

While the Ho:YLF laser systems presented in Chapters 3 and 4 were designed to deliver laser pulses at high repetition rates and high average powers which could be used to pump optical parametric oscillators emitting in the 3-5 µm region, one can follow a different design approach by utilizing Ho:YLF to generate high-energy single-frequency laser pulses to rather optically

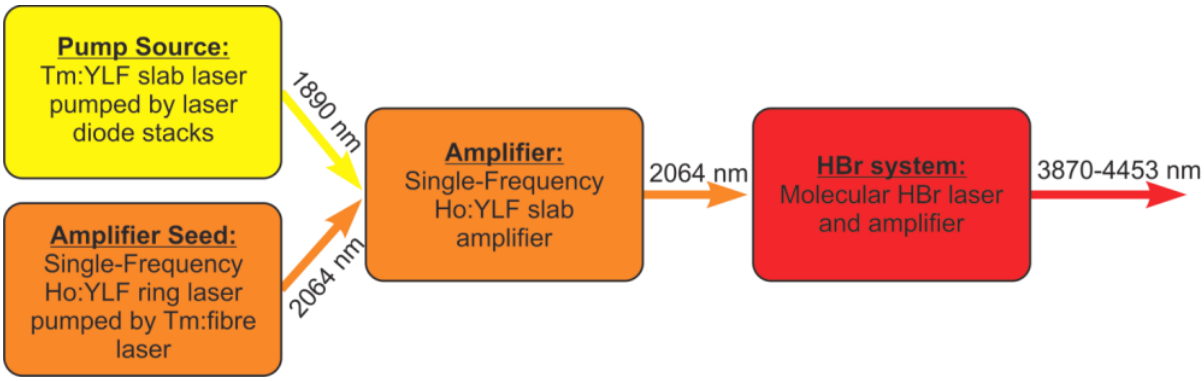

Figure 37: Schematic showing the inter-dependencies of the systems described in this as well as subsequent chapters. The Tm:YLF slab laser is described in Section 5.2 while the single-frequency Ho:YLF ring-laser is discussed in Section 5.3. The Ho:YLF slab amplifier, which is pumped by the thulium laser and seeded by the ring-laser, is presented in Section 5.4. Various configurations of the HBr system, which is optically pumped by the amplifier, are presented in Chapters 8 and 7.

pump a molecular laser based on HBr that also emits in the 3-5 µm region (See Figure 37). This is a promising alternative approach to OPO's, as shown by the author in the subsequent chapters of this dissertation.

Following this approach does present some challenges, however, one of which is the requirements the molecular laser imposes on the pump source. The narrow spectral linewidth of the various HBr absorption lines require that the pump laser be narrow-band in order for the pump light to be absorbed efficiently, but few narrow-band lasers are available, particularly emitting at 2064 nm which is one of the appropriate pump wavelengths for HBr (See Chapter 6 for a more in-depth discussion). As no appropriate laser was available, commercially or otherwise, our group developed a single-frequency Ho:YLF ring-laser with pre-amplifier that was locked to the P(9) HBr absorption line at 2064.12 nm (Bollig et al. 2009). This laser is briefly described in Section 5.3. This system was successfully used to pump a molecular HBr gas laser which delivered up to 2.5 mJ per pulse when pumped with 60 mJ of energy at a PRF of 50 Hz (Botha et al. 2009). The HBr laser emitted simultaneously at 4.17 and 4.19 µm. It was four times more

powerful than the previously reported optically-pumped HBr laser described in (Miller et al. 1994).

In order to obtain higher energy pulses from an HBr laser we needed to energy scale the single-frequency pump source's output further. This chapter describes how we achieved this through the development of a high-energy amplifier. It involved the design and development of a Ho:YLF slab amplifier which was pumped by a Tm:YLF slab laser which we also developed in-house. This scheme is depicted in Figure 37, with the different components discussed in the subsections of this chapter. Section 5.2 provides background on the development and properties of the Tm:YLF slab laser which was used as pump source for the Ho:YLF slab amplifier which is described in Section 5.4. Section 5.3 briefly describes the single-frequency ring-laser that was used to seed the amplifier. The amplifier's experimental results are given in Section 5.5, followed by the conclusions made in Section 5.6. The author's contributions to this body of work are listed in Section 5.7.

5.2 Development of a Tm:YLF slab laser as pump source for a Ho:YLF slab amplifier

The Ho:YLF laser and amplifier systems described in Chapters 3 and 4 were pumped by commercially sourced 1.9 µm Tm:fibre lasers. Unfortunately these commercial lasers are currently limited to a maximum of 120 W of cw output power for the water-cooled systems and 50 W per laser for the air-cooled models (IPG 2015). Scaling Ho:YLF output to higher powers and/or energies would therefore require several of these lasers as demonstrated in Chapter 4, where the author used two 50 W air-cooled fibre lasers, as well as by (Dergachev et al. 2008) who

used three 120 W water-cooled systems. While these fibre lasers exhibit several desirable properties such as excellent beam quality (M^2<1.1), stability and compactness, as well as acceptable wall plug efficiencies; this approach can prove to be quite a costly exercise as there is currently only a single supplier (*IPG*) capable of supplying reliable Tm:fibre laser systems at these power levels (It would be naïve to think that cost does not influence design choices made in applied laser research, as is the case in so many other fields of research).

An attractive alternative for generating 1.9 µm laser light to pump holmium-doped systems with are Tm:YLF lasers. These lasers had limited output powers though, held back by the low fracture limit of the host material. YLF does have several beneficial properties, however, such as low thermal lensing, and a natural birefringence which can aid laser design.

Fortunately successful power scaling was demonstrated using an end-pumped slab laser geometry, delivering up to 148 W of laser power at 1912 nm (Schellhorn et al. 2009) from a 2.0 % at. doped Tm:YLF slab laser. This was a significant improvement over the previous record power of 68 W

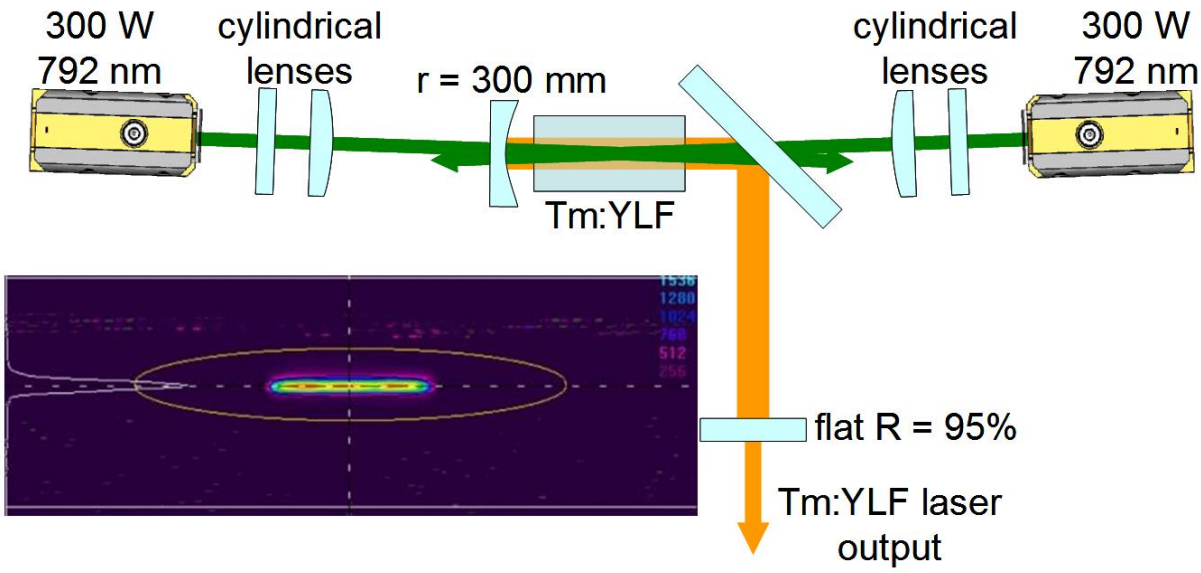

Figure 38: A schematic of the initial Tm:YLF slab laser setup. The beam intensity profile of the laser is shown in the insert, bottom left (W. Koen, H. J. Strauss, et al. 2010b).

from a Tm slab laser (So et al. 2006). The laser slab geometry proved a particularly successful power scaling strategy for Tm:YLF as it allowed for efficient cooling from both the top and bottom of the crystal. Additionally the elongated shape of the crystal is well suited for end pumping by laser diode stacks whose beams are usually highly astigmatic.

Subsequently our group developed a Tm:YLF slab laser with the aim of using it as a pump source for Ho:YLF crystals (Esser 2010). It consisted of a 2.5 % at. doped a-cut Tm:YLF crystal slab (11 mm wide, 19 mm long, and 1.5 mm thick, with its c-axis horizontally orientated, orthogonal to the optical axis of the laser) end-pumped pumped by two 300 W laser diode stacks emitting at 792 nm (model NL-VSA-05-300-792-F900D manufactured by *nLight*). A schematic of this laser is shown in Figure 38. The crystal was mounted in a custom water cooled copper mount which

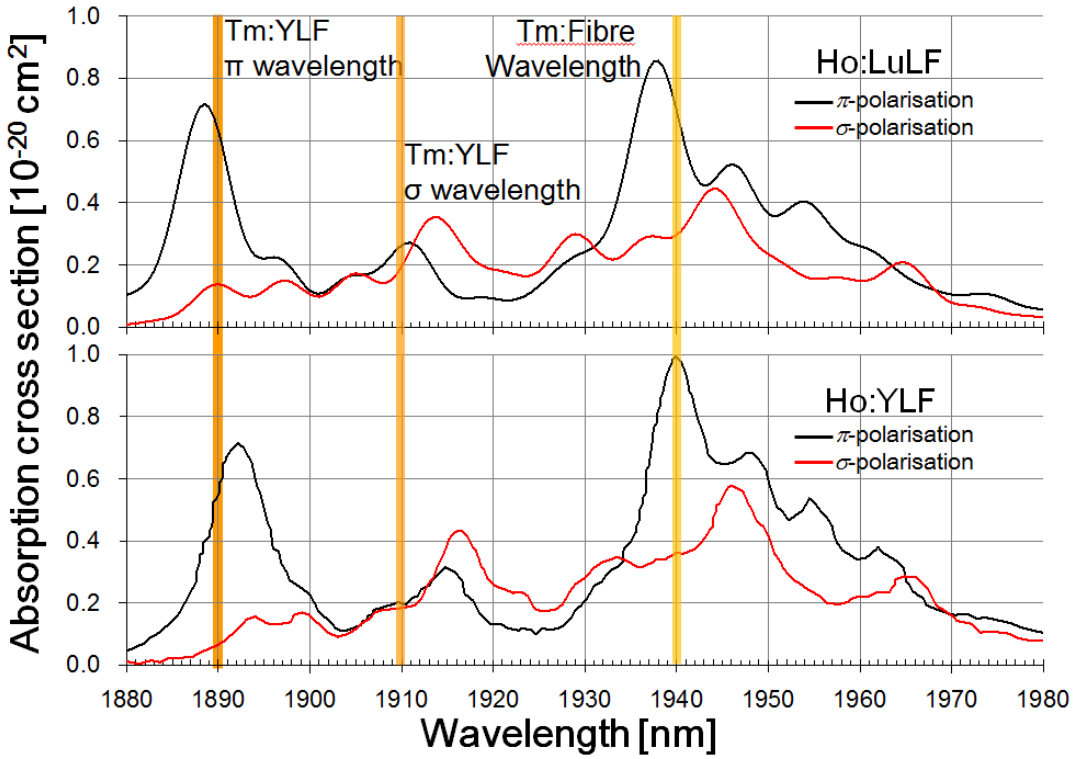

Figure 39: Ho:YLF and Ho:LuLF absorption spectra on the σ- and π-polarisation. Laser wavelengths of the Tm:YLF slab laser (σ- and π-polarisation) as well as a typical Tm:fibre laser output wavelength is also shown (as used in Chapters 3 and 4), indicating which of these sources are appropriate for pumping these crystals. (Reproduced from (W. Koen, H. J. Strauss, et al. 2010b))

was developed in-house. The pump light from each laser diode stack was focussed inside the crystal to a beam width of approximately 10 mm wide and 0.9 mm high. The resonator cavity consisted of a 300 mm ROC concave dichroic input coupler mirror on the one side of the crystal, a 45º flat dichroic folding mirror on the other side and a flat output coupler mirror. An output coupler reflectivity of 90 % resulted in the highest output power of 225 W at 1909 nm, with the laser operating on the σ-polarisation of the crystal. This wavelength, however, is undesirable for use with Ho:YLF as its absorption cross-section is less than 0.2×10^{-20} cm^2 at 1909 nm, as indicated in Figure 39. This would result in low absorption of the pump light in the planned Ho:YLF amplifier. It was also an inappropriate wavelength with which to pump Ho:LuLF crystals which we also had available for use. An approach was therefore needed to force the laser to operate at a more appropriate wavelength.

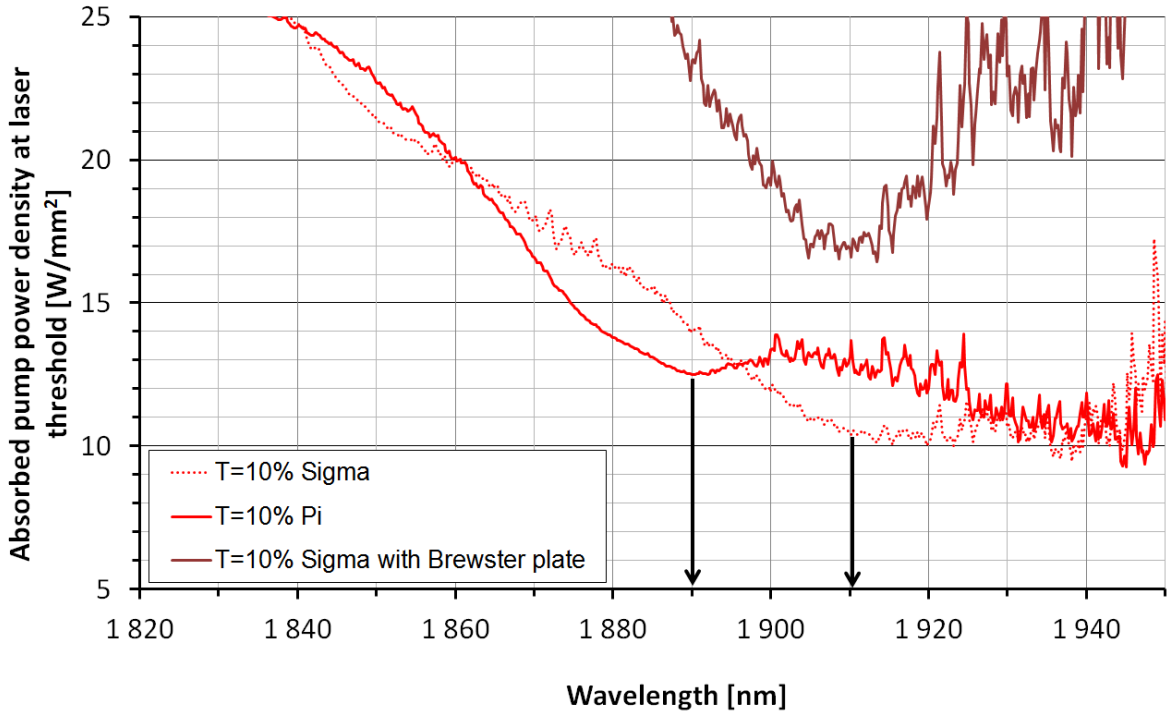

Figure 40: The calculated laser threshold pump power density (absorbed) of the Tm:YLF laser for a 10 % output coupler, with and without a Brewster plate inducing loss on only the sigma polarisation. This work was based on an approach developed by (Fan & Byer 1987) and subsequently expanded on by (Stoneman & Esterowitz 1995). Spectroscopic data from (Walsh et al. 1998) was used in the calculations.

Laser threshold analysis indicated that the thulium laser would naturally lase on the σ-polarisation in the region of 1910 nm for the given resonator losses and output coupling, as is shown in Figure 40. This work was based on an approach developed by (Fan & Byer 1987) and subsequently expanded on by (Stoneman & Esterowitz 1995) (Refer to Chapter 4 of (Esser 2010) as well as (Esser et al. 2009) for a more comprehensive description on laser threshold and wavelength analysis and its benefits to laser design).

However, if one were to induce sufficient losses in the cavity for the σ-polarisation while keeping the losses for the π-polarisation unchanged, the laser would rather operate on π, emitting laser light in the region of 1890 nm instead. This could be done by insertion of a Brewster plate which would induce loss for the σ-polarisation, but not for the π-polarisation. However, as discussed in previous chapters, the π-polarisation in YLF crystals exhibits a stronger negative thermal lens

than the σ-polarisation. A new resonator design therefore had to be implemented to accommodate this stronger negative thermal lens in order that the laser cavity remains stable under high-power operation where the thermal lensing is strongest.

Based on these results, the author jointly redesigned the laser cavity so that the slab laser would rather operate on the π-polarisation in order to have an output wavelength of 1890 nm instead of 1909 nm. With the absorption cross-section of Ho:YLF being ~0.6 x 10^{-20} cm^2 at 1890 nm (for π-polarisation), far better absorption would be obtained in the planned Ho:YLF amplifier system (Walsh et al. 1998).

A schematic and photo of the resulting optical layout for the Tm:YLF slab laser is shown in Figure 41. To ensure that the resonator remained stable for lasing on the π-polarisation, the flat output coupler mirror was replaced with a concave mirror with a 200 mm radius of curvature in order to accommodate the stronger negative thermal lens. A CaF_2 Brewster plate was inserted between the folding mirror and the output coupler as to induce sufficient losses for the σ-

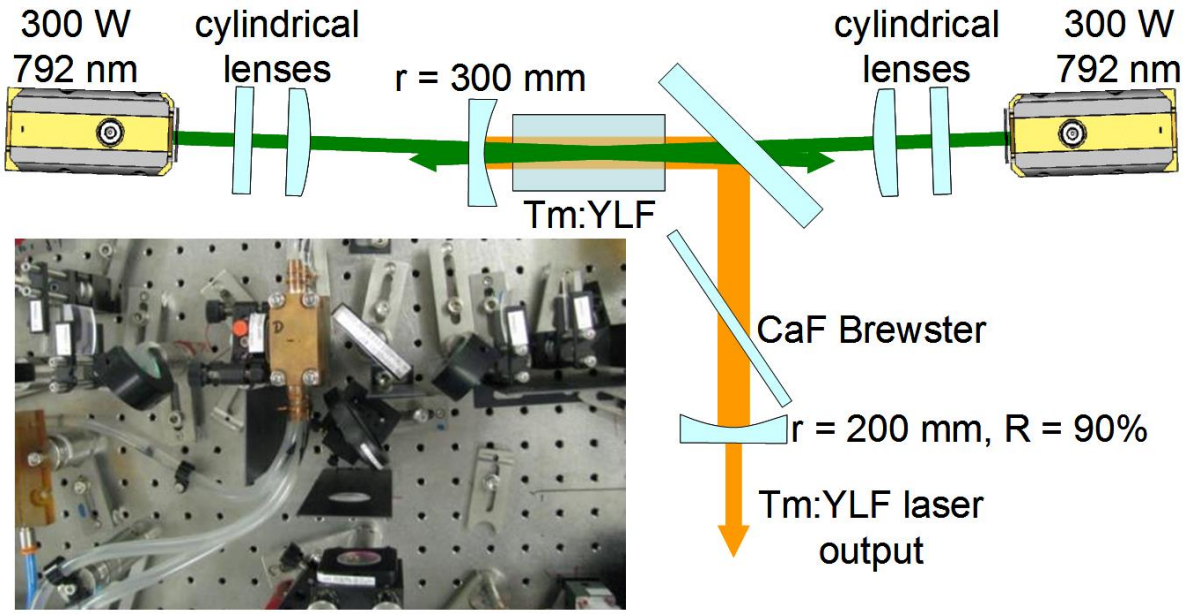

Figure 41: Schematic of the redesigned Tm:YLF slab laser. A top-view photo of the laser layout is shown in the insert, bottom left (W. Koen, H. J. Strauss, et al. 2010b).

polarisation, ensuring laser operation on only the π-polarisation.

The resulting wavelength was measured to be in the region of 1890 nm for all output powers. The laser output as a function of incident laser diode pump power is shown in Figure 42. The beam intensity profile of the laser at full power is shown in the insert. The curved input coupler in conjunction with the stronger negative thermal lens resulted in a more divergent laser beam. This was collimated by placing an f = 100 mm positive plano-convex lens right next to the output coupler mirror outside the resonator.

A maximum output power of 189 W was obtained from the laser with a slope efficiency of 38 % with regard to incident pump power and an optical-to-optical efficiency of 34 %. At full power, the beam quality factor (M^2) was measured to be 3.8 in the vertical axis and 440 in the horizontal.

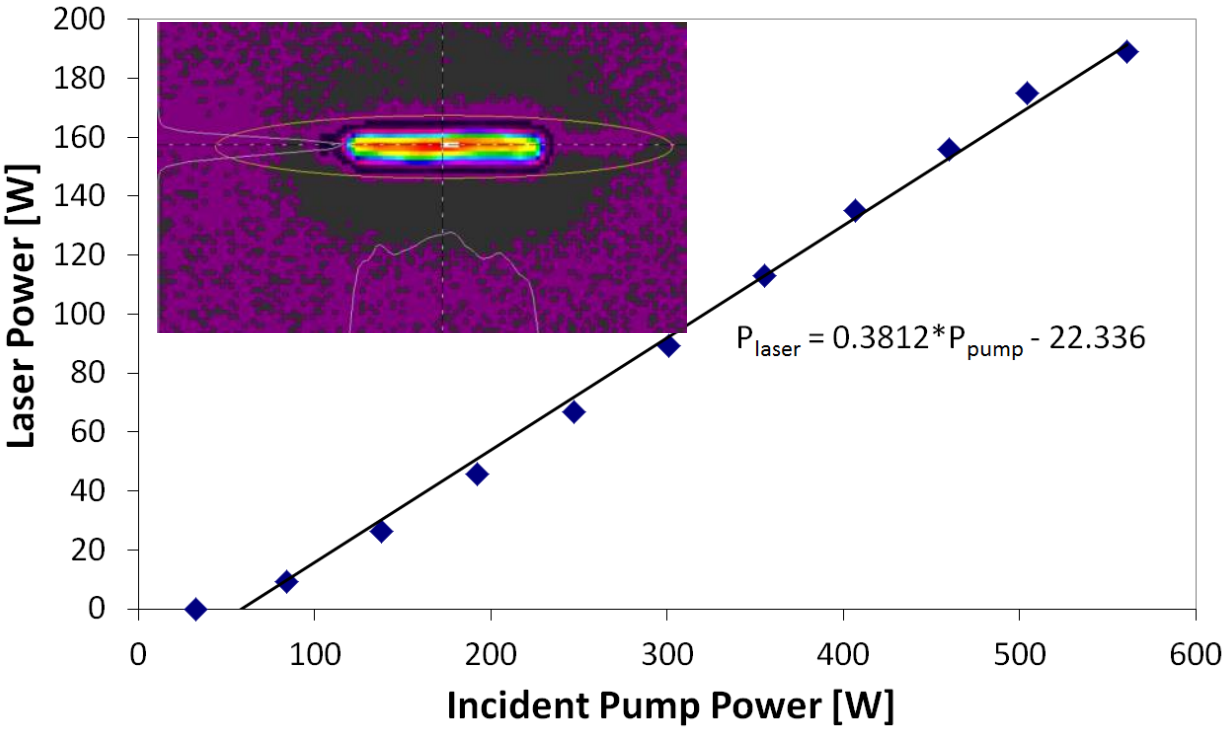

Figure 42: The modified Tm:YLF lab laser output power as a function of incident pump power. The laser's beam intensity profile at full power is shown in the insert.

The Tm:YLF slab laser was subsequently used in this configuration to pump the Ho:YLF amplifier, as discussed in the subsequent sections of this chapter.

5.3 The single-frequency Ho:YLF seed laser

As seed laser for the Ho:YLF slab amplifier we used a single-frequency, injection-seeded Ho:YLF ring-laser that was previously developed by our group as a pump source for HBr lasers

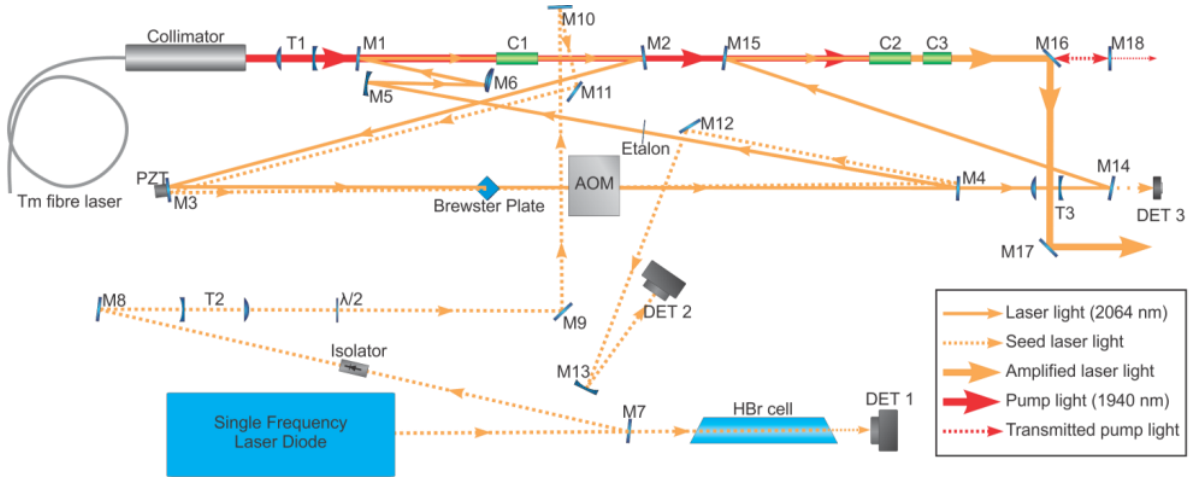

Figure 43: Schematic of the optical layout of the injection-seeded, single-frequency Ho:YLF ring laser and its pre-amplifier.

(Botha et al. 2009; Bollig et al. 2009). A diagram of the laser's layout is shown Figure 43. (As this laser system was developed during the author's studies for his Master's degree, only the parameters relevant to this dissertation are provided. A full description of the resonator and pre-amplifier design can be found in (Bollig et al. 2009)). The system delivered up to 72 mJ of energy per pulse at a pulse repetition frequency (PRF) of 50 Hz in a near-diffraction limited beam at 2064 nm. The laser's full width at half maximum (FWHM) pulse length varied with PRF from ~320 ns at 10 Hz to 600 ns at 350 Hz.

5.4 The double-pass Ho:YLF slab amplifier design and setup

We previously demonstrated 210 mJ single-frequency 2 µm pulses by using a two crystal Ho:YLF & Ho:LuLF slab amplifier (Strauss et al. 2011). Subsequent simulations, based on a space-resolved rate-equation model, done by Oliver Collett indicated that using longer gain

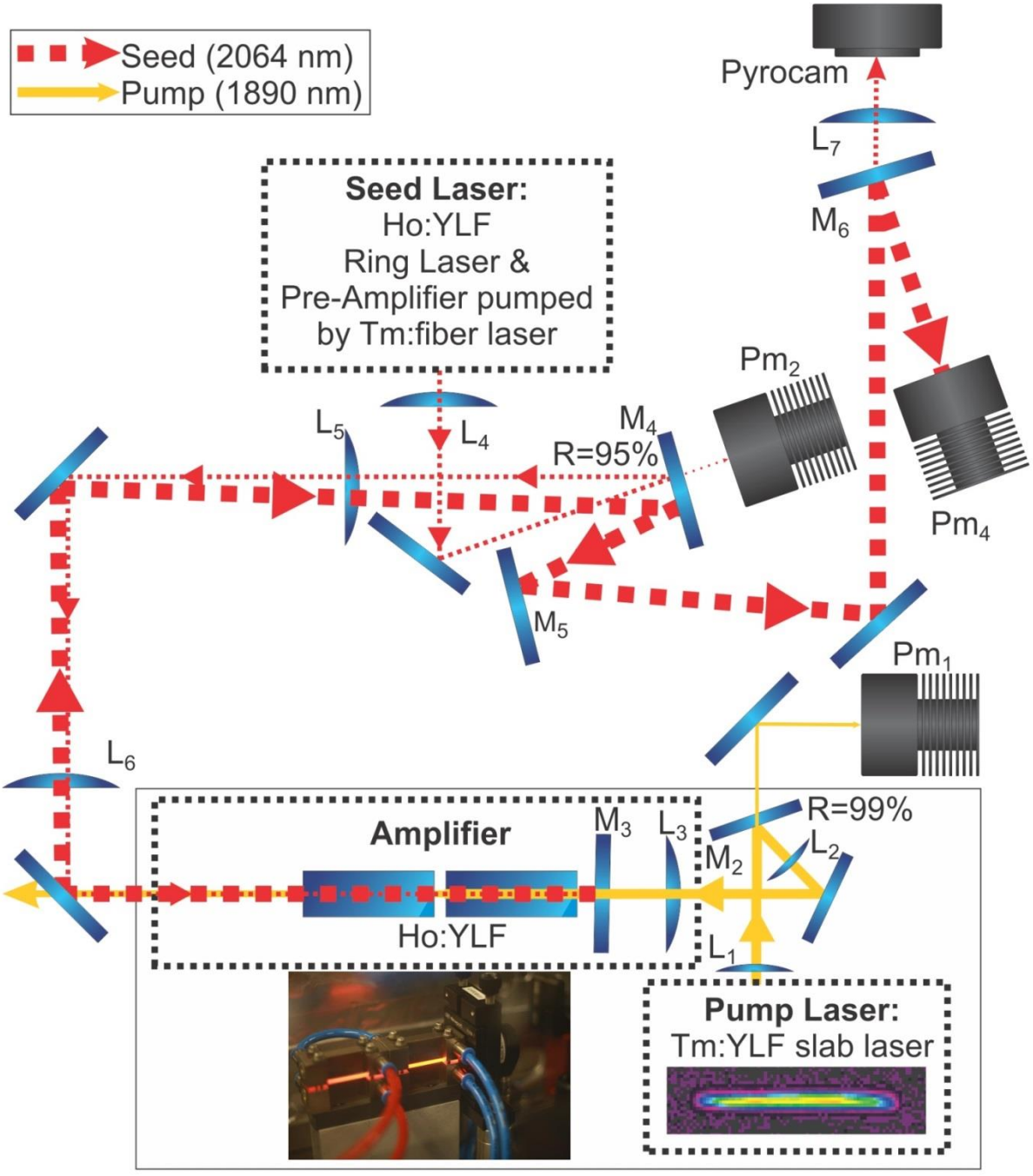

Figure 44: Schematic of the experimental setup for the double-pass Ho:YLF slab amplifier. A photo of the mounted slab crystals is shown in the insert.

crystals and double passing the seed beam would lead to a significant increase in gain and thus more output energy (Collett 2013).

Based on the simulation results we subsequently used two 0.5 % at. doped Ho:YLF slabs in series. Both crystals, which were supplied by *VLOC*, were 10 mm wide, 2 mm thick and 50 mm long and were a-cut with their c-axis horizontal. The crystal slabs were mounted with indium foil as thermal interface material, clamped from top and bottom between two in-house designed water-cooled mounts, with a water temperature set point of 22 ºC. This experimental setup is illustrated in Figure 44. The slabs were placed in series to provide a total of 200 mm in gain length when double passed.

As pump source we used the Tm:YLF slab laser described in Section 5.2. The polarisation was kept horizontal so that the pump light was absorbed by the stronger absorbing π-polarisation of Ho:YLF crystals as discussed in Section 5.2. The Tm:YLF laser's output power was monitored with a power meter which was placed behind an R = 99% mirror (M_2). The pump beam was steered into the Ho:YLF amplifier crystals using a mirror that was highly-reflective at 1.9 µm. To shape the pump beam it was first collimated with an f = 100 mm plano-convex spherical lens (L_1) placed very close to the output coupler mirror, and focussed into the Ho:YLF slabs with an f = 60 mm spherical lens (L_3). An f = 250 mm cylindrical lens (L_2) was used to match the horizontal focus position after L_3 to that of the vertical waist. The Ho:YLF crystals were placed so that the pump focus was positioned in the gap between them. The 1890 nm pump beam radii were measured with a pyro-electric camera (Pyrocam III from *Spiricon*) as 3.5 × 0.4 mm on the inner facing surfaces of the crystals and 4.5 × 0.45 mm ($w_x \times w_y$) on the outer surfaces. The amplifier and Tm:YLF pump laser were both enclosed in a dry air box to avoid temporal spiking in the

Tm:YLF laser output caused by water absorption. The relative humidity was kept below 20 % for all measurements by flushing the enclosure with dry air.

The seed laser for the amplifier was the injection-seeded, single-frequency Ho:YLF ring-laser with pre-amplifier which was pumped by a commercial 80 W 1940 nm Tm:fibre laser, as described in Section 5.3. It delivered diffraction-limited output with energies of up to 70 mJ per pulse at 50 Hz, and had a pulse-duration of 370 ns.

The seed laser power was monitored by power meter Pm_2 which was placed behind an R = 95 % partial reflector (M_4). The seed beam was then steered into the Ho:YLF amplifier crystals using various high reflectors at 2 µm. In the vertical axis, two plano-convex cylindrical lenses L_4, (f_y = 774 mm) and L_5, (f_y = 504 mm) were used to shape the seed beam in the Ho:YLF crystals, with a beam waist position on to the normal incidence mirror which was highly reflective for 2064 nm and highly-transmissive for the 1890 nm pump light (M_3). This mirror reflected the seed beam back for a second pass at a slight horizontal angle relative to the incident beam direction. The vertical component of the beam radii of the seed beam in the crystals were 0.38 mm on the first crystal surface it encountered and 0.34 mm on the crystal surface closest to M_3, with similar beam sizes on the return path (not taking thermal lensing or gain into account). In the horizontal plane a single cylindrical lens L_6 (f_x = 2133 mm) was used to collimate the seed beam to a radius of 3.3 mm. The second pass of the amplified beam was almost spatially symmetrical to the incident beam and passed through cylindrical lenses L_6 & L_5 before being separated by mirror M_5 from the seed laser beam. The seed polarisation was kept vertical (perpendicular to the crystal c-axis) so that it was amplified on the σ-polarisation of the Ho:YLF slabs, which has an intrinsic weak thermal lens, at the cost of lower gain due to its lower emission cross section when compared to the π-polarisation. Optical feedback into the master ring oscillator was prevented by

inserting an optical isolator (IO-4-2050-HP from *OFR*) between the oscillator and its pre-amplifier. This reduced the available seed energy incident on the amplifier to ~50 mJ at 50 Hz.

Various high-reflectors and a partial-reflector mirror at 2 µm (M_6) reflected the amplified beam onto power meter Pm_4 which measured the average amplified power. The beam contained a continuous wave (cw) component which originated from the injection seeding of the Ho:YLF ring laser which was also amplified. This component had a maximum value of 340 mW and was characterized at various Tm laser pump powers. These were then deducted from the total measured average powers of the amplified pulses.

5.5 Performance of the Tm:YLF slab laser pumped Ho:YLF slab amplifier system

We first optimised the alignment of the amplifier at a PRF of 350 Hz and at full pump power, where the risk of optical damage was the lowest, and then gradually reduced the PRF to 40 Hz. The resulting output energy and average amplified power as a function of the repetition rate is shown in Figure 45.

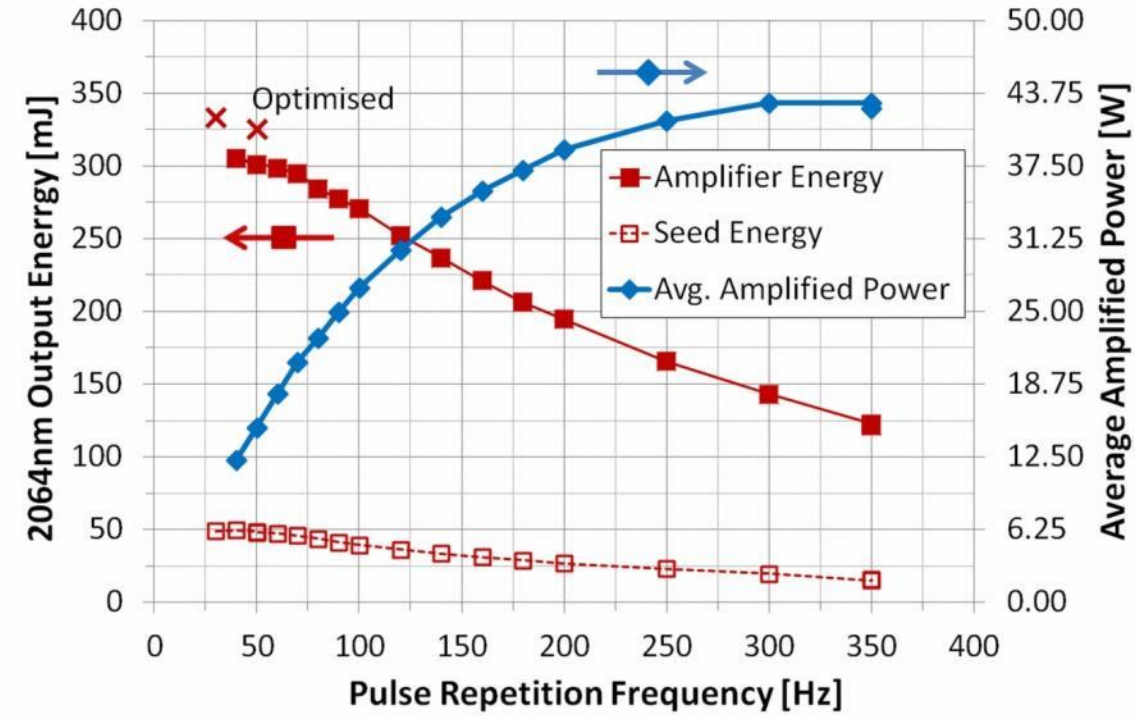

Figure 45: Seed and Amplified 2064 nm output energy (left axis) and the average power of the amplified pulses (right axis) as functions of Pulse Repetition Frequency.

The limit where the average power does not increase with PRF was found to be at PRFs above 300 Hz and was 43 W. For lower PRFs the average output power decreased to ~12 W at 40 Hz. When decreasing the PRF, the pulse energy increased from 122 mJ at 350 Hz to above 300 mJ at PRFs below 50 Hz.

No optical damage was observed throughout these experiments. The amplifier was then optimised at low PRFs with respect to seed and pump alignment. A maximum pulse energy of 333 mJ was obtained at the minimum PRF of 30 Hz. An output energy of 325 mJ was measured at the desired PRF of 50 Hz. All subsequent measurements were performed at a PRF of 50 Hz.

We subsequently characterized the optimised amplifier with respect to the Tm:YLF pump power incident on the amplifier. The results are shown in Figure 46. It was estimated that up to 96% of the 1890 nm power was absorbed in the amplifier crystals, dropping to 83% at maximum pump

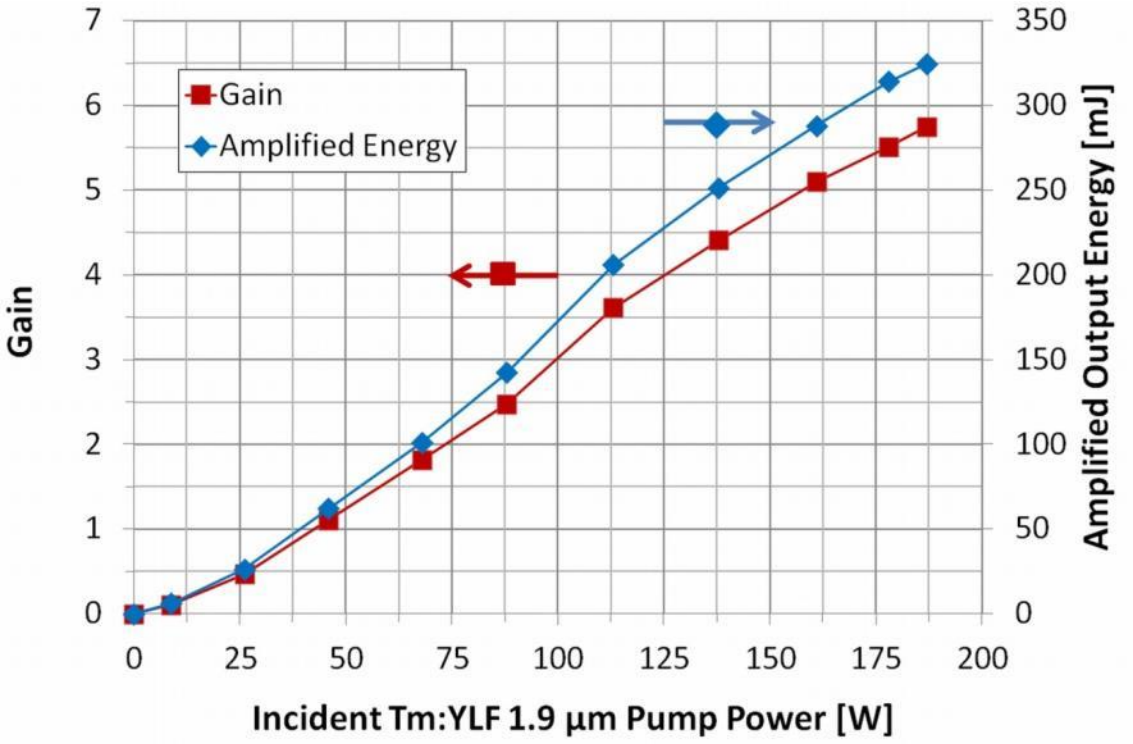

Figure 46: The amplified output energy (right axis) and gain (left axis) as functions of incident 1890 nm Tm:YLF pump power.

power. This indicated that the total effect of the Ho:YLF pump saturation was minimal due to the long combined length of the slab crystals. The output energy increased nearly linearly from low levels and slightly rolled over to the maximum output energy of 325 mJ. The roll-over could be attributed to the slight increase in beam diameter of the 1890 nm pump beam with power, which was caused by strong negative thermal lensing in the Tm:YLF slab crystal.

From the gain curve shown in Figure 46 it can be seen that the crystals only reached transparency (gain = 1, in other words no seed light is absorbed) at ~41 W of pump power for 50 mJ of seed energy. At full pump power the gain increased to 5.7.

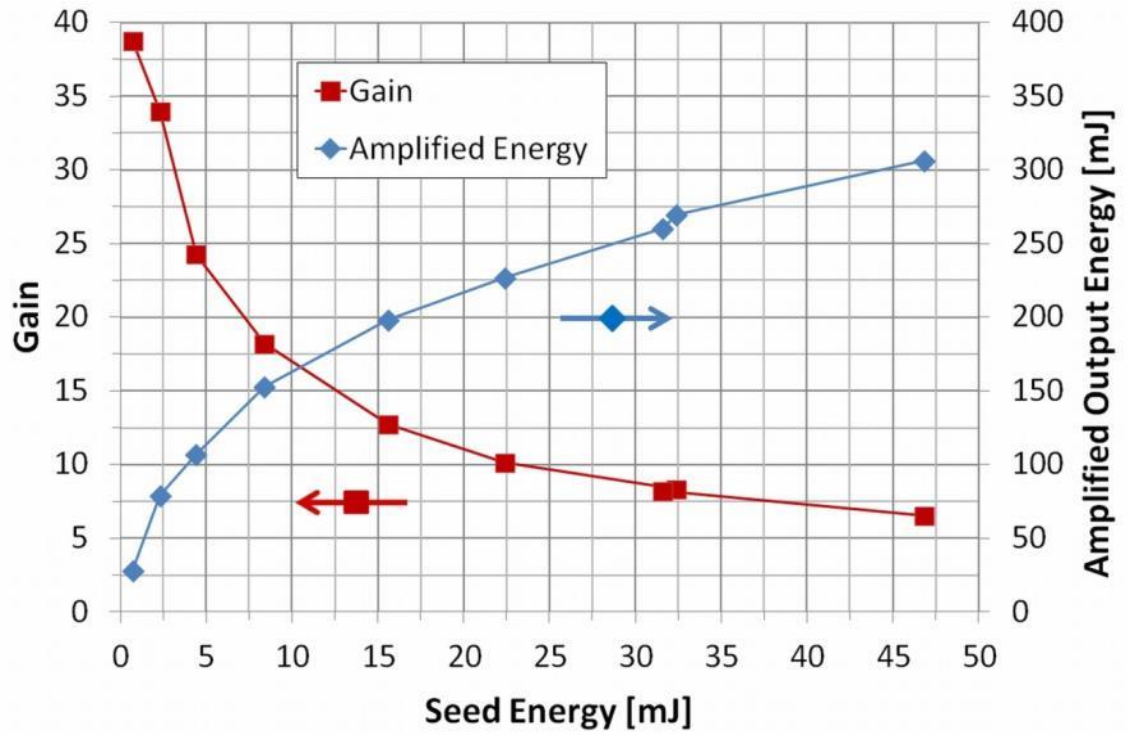

Figure 47: The amplified output energy (right axis) and gain (left axis) as functions of seed energy at a PRF of 50 Hz.

The amplifier performance as a function of the seed energy at full pump power is shown in Figure 47. The seed energy was varied by attenuating the seed beam with various partial reflectors. The gain at low seed energies (~1 mJ) was nearly 40, implying that the small-signal gain was in excess of 40.

The amplified beam's spatial intensity profile in the far field is shown in Figure 48 (a). The observed astigmatism was due to the fact that the amplified beam was not shaped with L_4 to be circular symmetric, as well as the astigmatic thermal lens associated with the Ho:YLF amplifier crystals. It can be seen that there was a slight degradation in horizontal beam quality. This was also reflected in an increased horizontal beam quality factor (M_x^2) of 1.5 and was possibly due to the variation in the horizontal intensity profile of the pump beam, which had a large M^2 value in

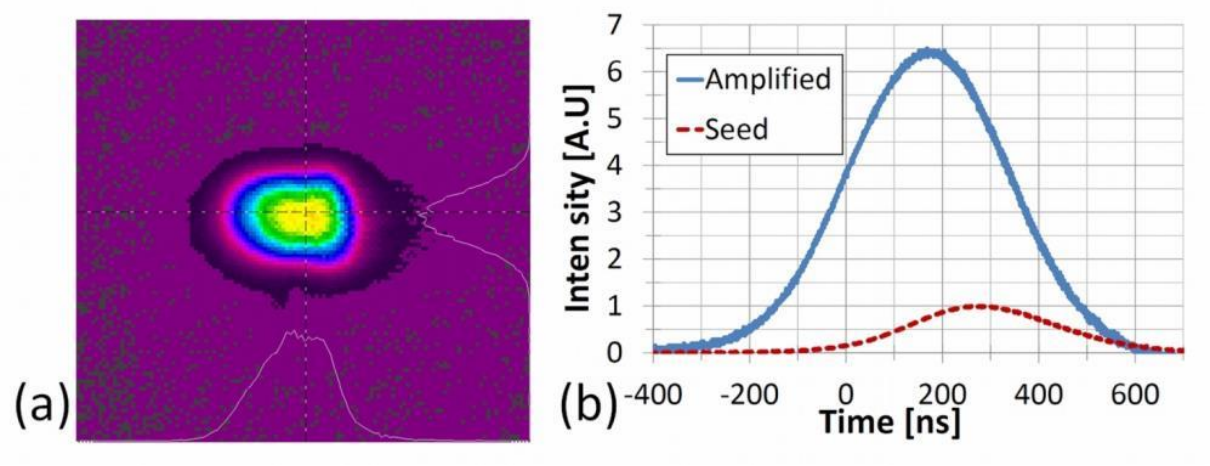

Figure 48: Amplified beam profile in the far field at full power (a) and the seed and amplified pulses at maximum output and a PRF of 50 Hz (b).

this direction. In the vertical direction the beam stayed near-diffraction limited with an M_y^2 of less than 1.1.

The temporal pulse trace of the amplifier's output beam is shown in Figure 48 (b). The amplified pulse length at full pump power was measured to be ~350 ns at a PRF of 50Hz. The pulse to pulse energy variation was measured to be less than 5 %. The amplified 2 µm beam was subsequently used to pump an HBr molecular gas laser/amplifier system, as presented in the subsequent chapters.

5.6 Conclusion

In conclusion, we have demonstrated a 2064 nm, single-frequency, Ho:YLF slab amplifier, emitting a good quality beam with output energies of up to 333 mJ per pulse. The horizontal beam quality factor (M_x^2) was 1.5 while the vertical (M_y^2) was less than 1.1. This work shows that

Ho:YLF amplifiers pumped with Tm:YLF slabs provide an effective way to obtain high energies at 2 µm which could be scaled even further using the same architecture.

The output energy of this amplifier system can still be significantly scaled. The maximum fluence in the system was calculated to be 10.9 J/cm^2 which was still below the optical damage threshold of good quality coatings (>20 J/cm^2, as considered by (Dergachev et al. 2008)). The same architecture can therefore be used to scale the energy at least 2 times higher by simply adding more amplifier modules. However, slight modifications to the system in its current form can also lead to improvement. Higher gain is expected if the unabsorbed 1890 nm pump power is reflected back into the amplifier crystals. Amplification on the stronger gain, π-polarisation would also be possible if thicker slab crystals were to be used. It was not possible to implement it in this setup because of clipping of the amplified beam due to the relatively strong thermal lensing associated with the π-polarisation of YLF.

5.7 Contributions

This chapter presented the development of a large yet cohesive ensemble of lasers and amplifiers which would not have been possible were it not for the concerted ***collaborative*** efforts of the research group team members who were involved. The contributions made by the author to this work are listed below:

Tm:YLF slab laser

- Jointly designed the 1890 nm Tm:YLF slab laser resonator cavity.
- Implemented the new 1890 nm Tm:YLF slab laser experimental configuration.

- Jointly analysed the 1890 nm Tm:YLF slab laser performance.

Ho:YLF single-frequency ring-laser

- Characterised the single-frequency diode laser used as injection seed.
- Designed and implemented the multi-pass HBr reference absorption cell setup.

Ho:YLF slab amplifier

- Jointly implemented the pump setup.
- Jointly characterised the amplifier performance.
- Jointly prepared results and schematics for publication (Strauss et al. 2013).

6 Introduction to Mid-infrared Optically Pumped Molecular Lasers Based on HBr Gas

In this chapter the concept of optically pumped molecular lasers is introduced. The pump and laser transitions of HBr gas relevant for optical pumping at 2 µm is presented and discussed. A summary of optically pumped molecular HBr lasers reported upon in literature is provided, illustrating the different design approaches followed previously. Conclusions are made with regard to the HBr laser and amplifier design considerations taken into account in the subsequent two chapters of this dissertation.

6.1 Optically pumped HBr lasers as mid-infrared laser sources

Laser output in the mid-infrared region can be generated with optical parametric oscillators (OPO) pumped by 2 µm laser sources such as the holmium-doped lasers reported in (Schellhorn et al. 2007) and (Lippert, Fonnum, Arisholm, et al. 2010). The Ho:YLF lasers and amplifiers presented in Chapters 3 and 4 are also prime examples of such pump sources. This all-solid-state approach can lead to efficient, compact and robust systems. However, optical damage of the nonlinear materials used, e.g. $ZnGeP_2$, can limit scaling the energy output (Schellhorn et al. 2007).

Optically pumped molecular lasers are an attractive alternative to OPO's due to the gas's resilience to high pump energies. Specifically, HBr lasers have the potential to efficiently oscillate in the 4 µm region making it an alternative to mid-IR OPOs (Ratanavis et al. 2009; Kletecka et al. 2004; Miller et al. 1994).

The first HBr laser was a longitudinal *electrical discharge activated* laser reported in 1967 which used a gas mixture of H_2 and Br_2 (Deutsch 1967). This laser was *chemically pumped* by the following reaction:

$$H + Br_2 \rightarrow Br + HBr(v), (v = 1 \text{ to } 5, \text{indicating the vibrational levels excited})$$

Lasing would then occur on the P-branch, emitting in the 4-4.5 µm range (Rutt 1979). Subsequently, transverse discharge HBr lasers were also demonstrated (Chang & Wood 1972), with some systems delivering up to 550 mJ laser pulses at 1 Hz (Rutt 1979). However, these systems proved to be large and inefficient.

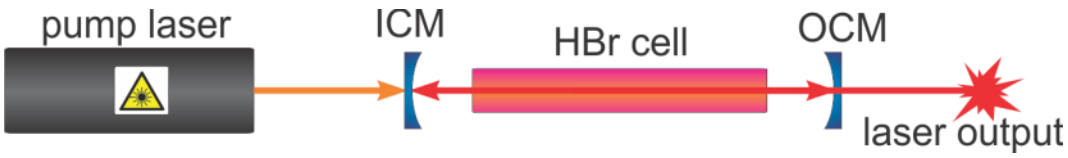

Figure 49: A schematic diagram of an optically pumped HBr laser.

In *optically pumped* HBr lasers, the HBr gas is excited to the higher vibrational levels with a laser source (as depicted in Figure 49). This has the potential to be both compact (Miller et al. 1994) and efficient (Ratanavis et al. 2009). In this chapter the properties of HBr relating to the optically pumped HBr systems in this dissertation is presented (Section 6.2). Previously reported work done on optically pumped HBr lasers is presented in Section 6.3 and the various design approaches considered discussed in Section 6.4, followed by the conclusion of this chapter in Section 6.5.

6.2 Properties of HBr gas as an optically pumped laser medium

Understanding the vibrational-rotational energy level structure and transitions of HBr allow us to determine in which manner we may utilise these properties to design and develop OPML systems. An energy level diagram showing the pumping and lasing transitions of a 2 µm pumped HBr laser is shown in Figure 50. The HBr systems reported in this dissertation were optically pumped by exciting the molecule from the ground vibrational level v=0 to the v=2 vibrational level, as depicted by the orange line in Figure 50. Lasing can occur on various P branch (J=J'+1) and R branch (J=J'-1) transitions from v=2 to v=1, depicted by the blue and red lines (J' and J are the upper and lower level rotational quantum numbers, respectively). After lasing, the remaining excited vibrational levels eventually relax back to v=0 through vibration-to-translation (V-T) processes, releasing heat into the gas.

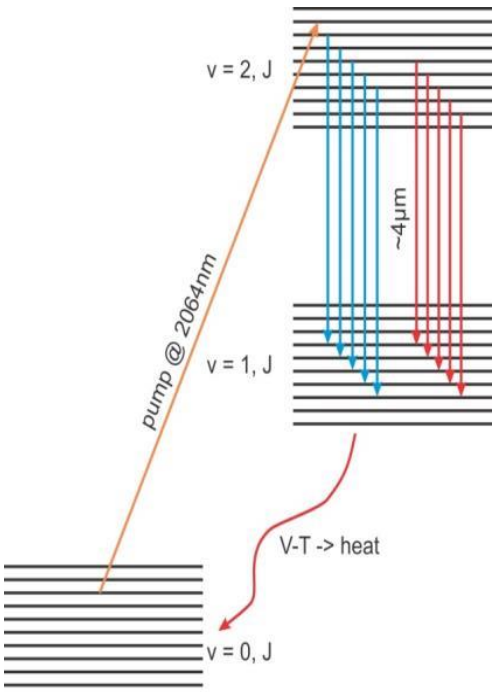

Figure 50: Schematic depicting pumping and lasing transitions of a 2 µm pumped HBr laser. Pumping is from the ground vibrational level v=0 to the v=2 vibrational level. Lasing can occur on various P branch (J=J'+1) and R branch (J=J'-1) transitions from v=2 to v=1. After lasing, the remaining excited vibrational levels eventually relax back to v=0 through vibration-to-translation (V-T) processes, releasing heat into the gas. J' and J are the upper and lower level rotational quantum numbers respectively.

6.2.1 Pumping transitions

The *v*=0 to *v*=2 band transition wavelengths and A-coefficients, as calculated by (Miller et al. 1994) are given in Table 7 for P(1) to P(10) and R(0) to R(10). The transition wavelengths and their individual line strengths are of interest when designing an optically pumped HBr system, since they determine which pump wavelength would be most appropriate. These transitions range from 1.943 µm to 2.074 µm, so that several solid-state laser sources can be considered as pump lasers. These can be Tm:fibre lasers which can operate readily from 1.910 µm to 2.045 µm, potentially pumping on the R or P branch, or Ho:YLF lasers which can operate from 2.050 µm to 2.065 µm, which can pump on the P(8) or P(9) transitions.

Matters are complicated, however, by the narrow linewidths of these transitions. The literature is unclear on the exact linewidth values, ranging from 205 MHz for Doppler broadening in (Miller et al. 1994), to 400 MHz reported in (Nicholson & Neumann 2001). Previously Dr. Lourens Botha calculated, based on experimental and simulation results, that a value of 430 MHz for Doppler broadening and 10.7 MHz per millibar for pressure broadening is more likely (Botha et al. 2009)). Regardless of the precise values, the narrow linewidth imposes an extra criterion on the pump source's spectral properties - one that can be challenging to meet.

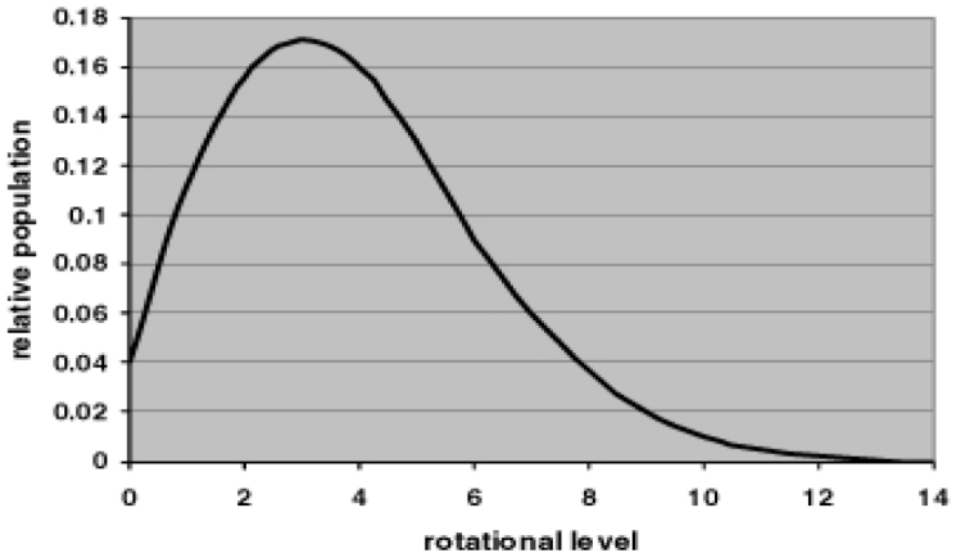

Figure 51: The calculated rotational (J) partition function of the vibrational ground state (*v*=0) at 300 K, reproduced from (Botha et al. 2009).

The rotational levels (J = 0, 1, 2, ..) of the individual vibrational levels are populated according to Boltzmann statistics. As the energy difference between the different vibrational levels (v = 0, 1, 2, ..) are large, the upper vibrational levels have very low populations at room temperature (Miller et al. 1994) with essentially only the ground vibrational state occupied. For the ground vibrational state (v = 0) the maximum population is found in J = 3 at 300 K, as shown in Figure 51.

Table 7: HBr v=0 to v=2 band transition wavelengths and A-coefficients (Miller et al. 1994).

Transition v=0 to v=2	Wavelength [µm]	Einstein A-coefficient [sec^{-1}]	Transition v=0 to v=2	Wavelength [µm]	Einstein A-coefficient [sec^{-1}]
			R(0)	1.98299	0.1087
P(1)	1.99584	0.3150	R(1)	1.97717	0.1296
P(2)	2.00288	0.2051	R(2)	1.97175	0.1382
P(3)	2.01033	0.1805	R(3)	1.96673	0.1428
P(4)	2.01821	0.1685	R(4)	1.96210	0.1459
P(5)	2.02651	0.1609	R(5)	1.95787	0.1482
P(6)	2.03535	0.1554	R(6)	1.95403	0.1288
P(7)	2.04442	0.1297	R(7)	1.95058	0.1523
P(8)	2.05404	0.1479	R(8)	1.94753	0.137
P(9)	2.06412	0.1286	R(9)	1.94486	0.1556
P(10)	2.07467	0.1433	R(10)	1.94259	0.1586

Table 8: HBr v=2 to v=1 band transition wavelengths and A-coefficients (Miller et al. 1994).

Transition v=2 to v=1	Wavelength [µm]	Einstein A-coefficient [sec^{-1}]	Transition v=2 to v=1	Wavelength [µm]	Einstein A-coefficient [sec^{-1}]
			R(0)	4.02559	4.262
P(1)	4.07813	13.032	R(1)	4.00094	5.056
P(2)	4.10607	8.756	R(2)	3.97735	5.350
P(3)	4.13515	7.933	R(3)	3.95479	5.473
P(4)	4.16539	7.597	R(4)	3.93326	5.514
P(5)	4.19682	7.419	R(5)	3.91274	5.508
P(6)	4.22948	7.309	R(6)	3.89321	4.691
P(7)	4.26339	6.198	R(7)	3.87466	5.416
P(8)	4.29857	7.171	R(8)	3.85709	4.749
P(9)	4.33508	6.328	R(9)	3.84047	5.256
P(10)	4.37295	7.070	R(10)	3.82481	5.159

6.2.2 Laser transitions

Table 8 lists the v=2 to v=1 band transition wavelengths and A-coefficients provided in (Miller et al. 1994) which is relevant to the HBr laser's output wavelengths. From this one can calculate the cross sections of the individual lines using

$$\sigma(v) = \frac{\lambda^2 A}{8\pi} g(v)$$

where A is the A-coefficient, $g(v)$ is a normalised lineshape factor, and λ is the transition wavelength (Ratanavis et al. 2009). The calculated gain cross sections, as shown in Figure 52, are provided to aid the discussion that follows. From this figure one can see that lasing can potentially occur on the P branch from P(1) emitting at 4.08 µm to P(10) at 4.37 µm. Lasing on R branch from 3.82 to 4.02 µm has not been observed previously, until the work reported in this dissertation.

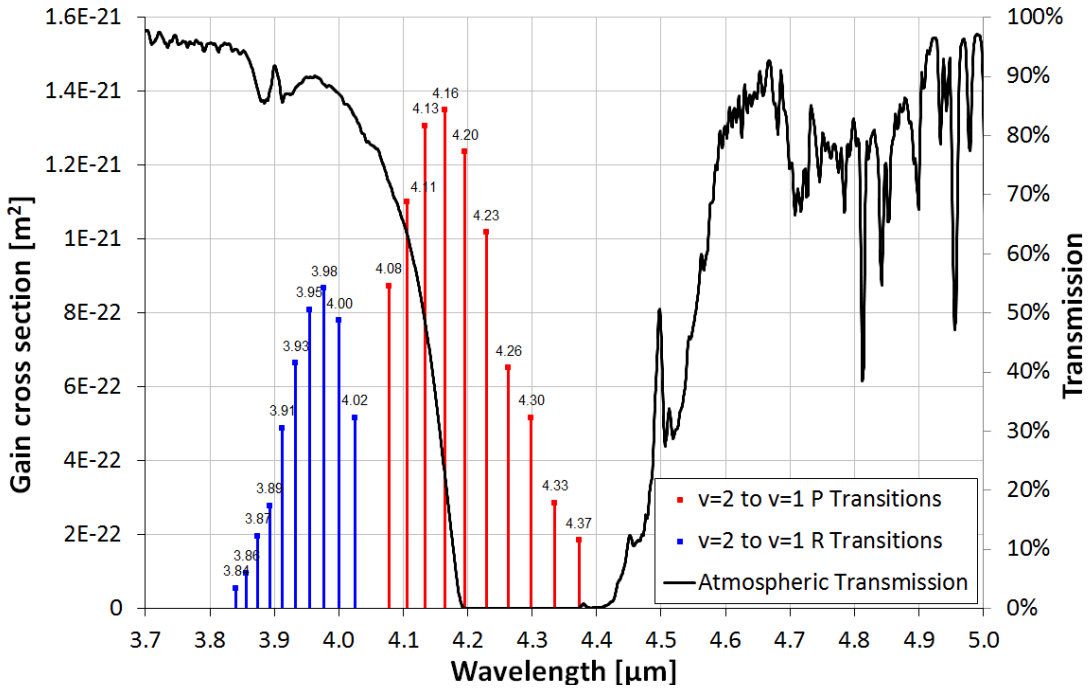

Figure 52: Atmospheric transmission in the 3.7 µm to 5 µm region (from space to ground at an altitude of 4.2 km) using the program IRTRANS4 (UKIRT 2013) with the gain cross sections of HBr superimposed upon it (Miller et al. 1994).

6.3 Optically pumped HBr molecular lasers in literature

This section provides a historical overview of optically pumped HBr lasers, as reported in the literature. Unfortunately the list of these lasers is short - especially when considering that the wavelength range that these lasers can potentially cover (3.8 to 4.5 µm) is serviced by very few other types of lasers.

A molecular HBr laser optically pumped by a laser system was first reported on in 1994 by (Miller et al. 1994) (Figure 53). The pump source was a commercially sourced laser system consisting of an injection-seeded narrow-linewidth Nd:YAG laser pumping a tuneable optical parametric oscillator. The OPO was capable of generating 5-10 ns long pulses with wavelengths ranging from 1.5 to 4.0 µm. It was set to pump the P(3) line of HBr at 2.01 µm (from v=0 to v=2). The HBr oscillator consisted of a concave input coupler mirror (ROC = 5 m), a 21 cm long HBr

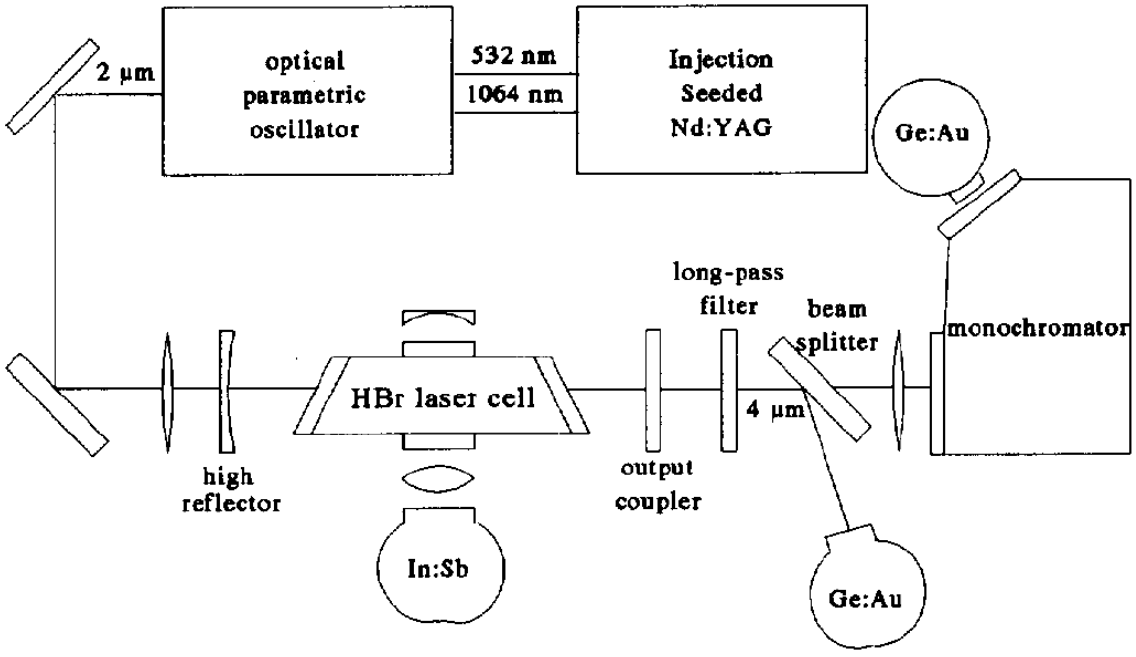

Figure 53: Schematic of the optically pumped HBr laser reported by (Miller et al. 1994).

cell, and a flat output coupler mirror with a reflectivity of 80 % at 4 µm. The resonator length was set to 23 cm, resulting in a fundamental mode diameter of approximately 3 mm.

With this setup, a maximum output energy of up to 0.84 mJ per pulse at 4 µm was obtained from 3.47 mJ of absorbed pump energy. This equated to an efficiency of 24 % with regards to absorbed pump light.

In 2004 an HBr pumping and lasing scheme where the second overtone of HBr was excited by a Nd:YAG laser (v=0 to v=3) was implemtented by Kletecka et al. A schematic of the system is shown in Figure 54. As pump source a temperature-tuned, injection-seeded, frequency-stabilised Q-switched Nd:YAG laser operating at 1.34 µm with ~400 ns long pulses was used (Kletecka et al. 2004). The pump laser delivered 15 mJ of energy per pulse. The pulse repetition rate was not

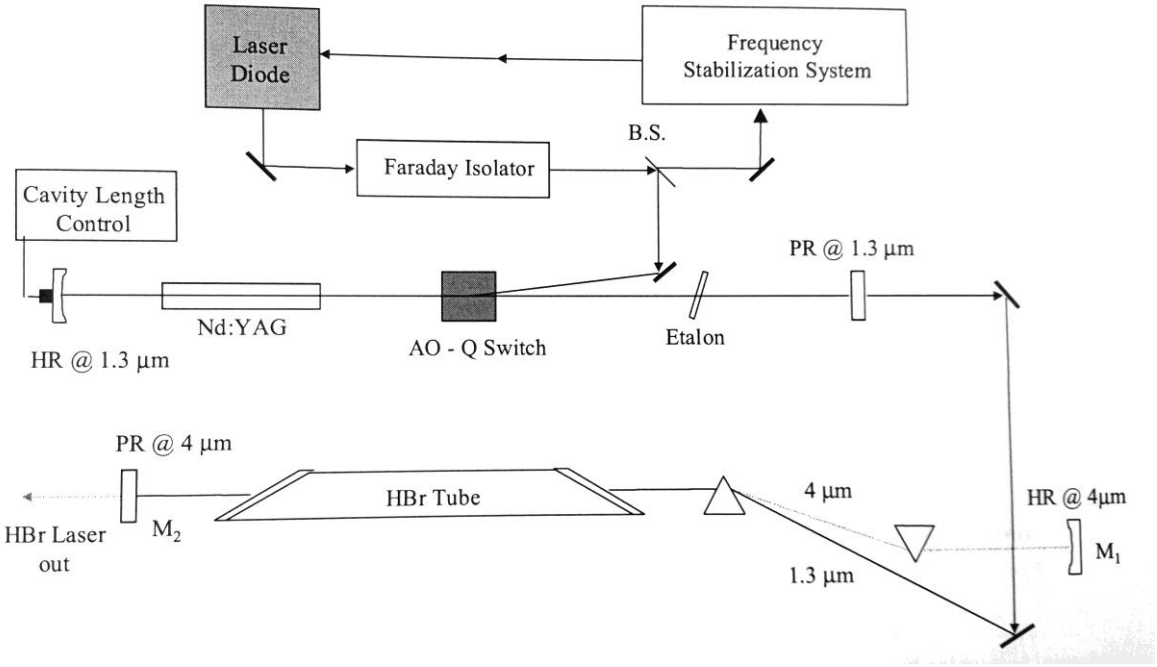

Figure 54: Experimental setup of the HBr laser reported by Kletecka et al. which was optically pumped by a 1.3 µm Nd:YAG laser (Kletecka et al. 2004).

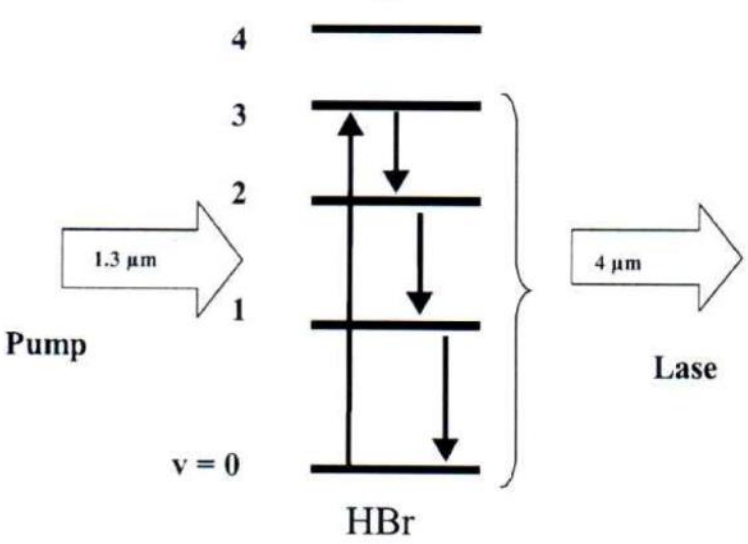

Figure 55: The HBr pumping and lasing scheme implemented by Kletecka et al. in 2004. The second overtone of HBr (*v*=0 to *v*=3) was excited by pumping with a temperature-tuned, frequency-stabilised Q-switched Nd:YAG laser operating at 1.3 µm. Cascade lasing was observed from the *v*=3 to *v*=2 and *v*=2 to *v*=1 vibrational levels (Kletecka et al. 2004).

reported. The pump laser populated the *J*=5 rotational level of the *v*=3 vibrational level (See Figure 55). Two HBr cavities were implemented. For both laser cavities a 75 cm long HBr gas cell was used. The first resonator design used a 5 m ROC concave backreflector, a prism, and flat output coupler (R=60 %), with the pump light coupled into the cavity using a second CaF_2 prism (See Figure 54). The pump light was double passed through the HBr cell, reflecting off the output coupler which was highly reflective at 1.3 µm. Total pump absoption for this setup was 15 %. In the second resonator setup, the two prisms were replaced by a dichroic mirror allowing collinear double-pass pumping while relying on a Faraday optical isolator to prevent feedback to the pump laser. Cascade lasing was observed from the *v*=3 to *v*=2 and *v*=2 to *v*=1 vibrational levels on various transitions of the P branch. The output energy and efficiency of the HBr lasers were not reported, however.

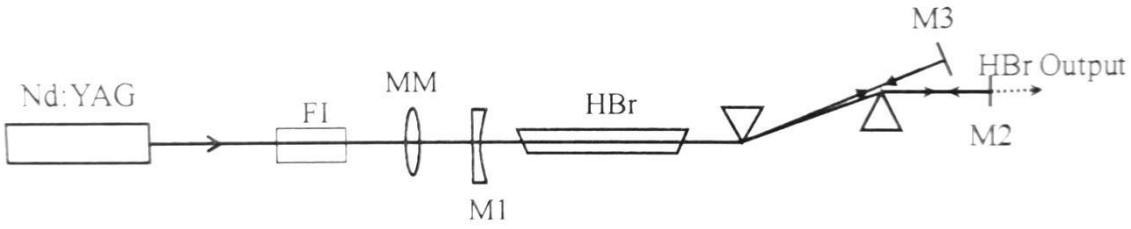

Figure 56: Schematic layout of the HBr laser reported on by (Ratanavis et al. 2008). The HBr laser was optically pumped by a temperature-tuned, frequency-stabilised, injection-seeded 1.34 µm Nd:YAG laser from the *v*=0 to *v*=3 overtone of HBr.

A commercial DF-laser was also used to successfully pump an HBr laser in 2005 (Burtsev et al. 2005). This was the first time an HBr laser was successfully pumped on the R branch at 3.836 µm, with the HBr laser operating from 4.017 to 4.215 µm. The quoted efficiency varied between 2 and 5 %.

In 2008 Ratanavis et al. investigated an optically pumped HBr laser both experimentally and theoretically (Ratanavis et al. 2008). The HBr laser was optically pumped by a temperature-tuned, frequency-stabilised, injection-seeded 1.34 µm Nd:YAG laser on the *v*=0 to *v*=3 overtone transition of HBr. Exact specifications of the HBr resonator were not reported except that the cavity contained a 1 m long gas cell with HBr at a pressure of 33 mbar and that the pump light was double passed through the cell in a manner similar to that reported in (Kletecka et al. 2002) which was described earlier in this section. When the HBr laser was pumped with 60 mJ, 200 ns long pulses, lasing was observed on several transitions from the *v*=3 to *v*=2 manifold as well as the *v*=2 to *v*=1 manifold, emitting laser light from 4.16-4.40 µm. While no mention was made with regard to the output energies of the experimental HBr laser, simulation results reported by them indicated that efficiencies of between 38 and 51 % are theoretically obtainable when pumping HBr on the second overtone (*v*=0 to *v*=3) with up to 1 mJ of laser pump light.

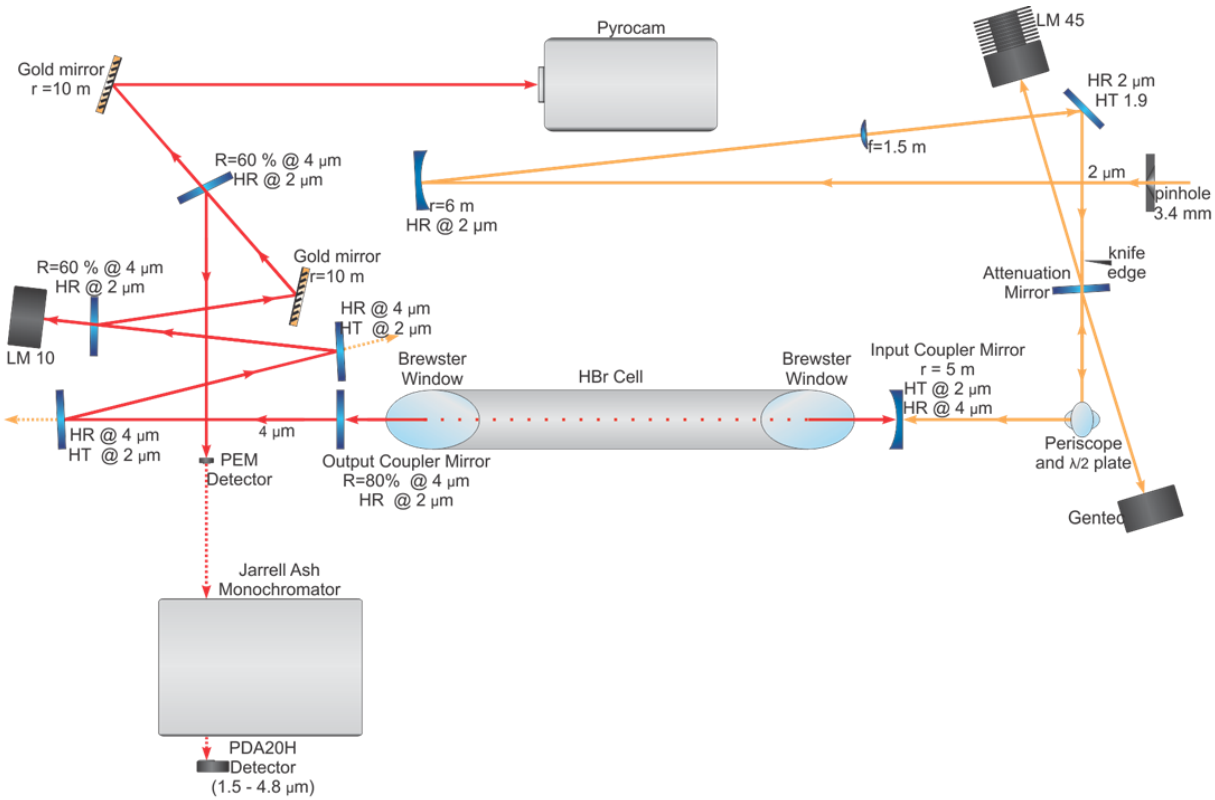

Figure 57: Schematic layout of the Ho:YLF pumped HBr laser system reported by our group in 2009 (Botha et al. 2009).

Until the work reported in this dissertation, the highest reported output energy from an optically pumped HBr laser was 2.5 mJ in a 132 ns long pulse, as was reported by our group in (Botha et al. 2009) (a schematic of the experimental setup is shown in Figure 57). An in-house developed injection-seeded, single-frequency Ho:YLF ring-laser was used as pump source. This ring-laser is briefly described in Chapter 5 as it was also later used as the seed laser of the amplifier reported on in Chapter 5. This system in turn acted as the pump source for the optically pumped HBr systems in Chapters 7 and 8. The Ho:YLF ring-laser was locked to the P(9) (v=0 to v=2) HBr absorption line at 2064.12 nm using a reference absorption cell with a Pound-Drever-Hall feedback loop (Bollig et al. 2009). The pump laser delivered energies of up to 72 mJ in ~350 ns long pulses at a pulse repetition rate of 50 Hz. The HBr laser consisted of a concave dichroic input

coupler mirror (ROC = 10 m), a 940 mm long HBr cell and a flat output coupler mirror which was highly reflective for the 2 µm pump light and had a 80 % reflectivity at 4 µm. The HBr laser emitted simultaneously on the P(4) and P(5) lines (4.17 and 4.20 µm). A maximum efficiency of 12 % with regard to absorbed pump energy was reported, with the modelling results indicating that an efficiency of up to 20 % should be obtainable from a fully optimised system.

6.4 Discussion

It is possible to formulate a design approach for an optically pumped HBr system by taking the properties of HBr presented in Section 6.2 and the published work discussed in Section 6.3 into account. This involves the development of an appropriate pump source, the HBr resonator design, and the consideration of energy scaling though the use of HBr amplifiers, if needed.

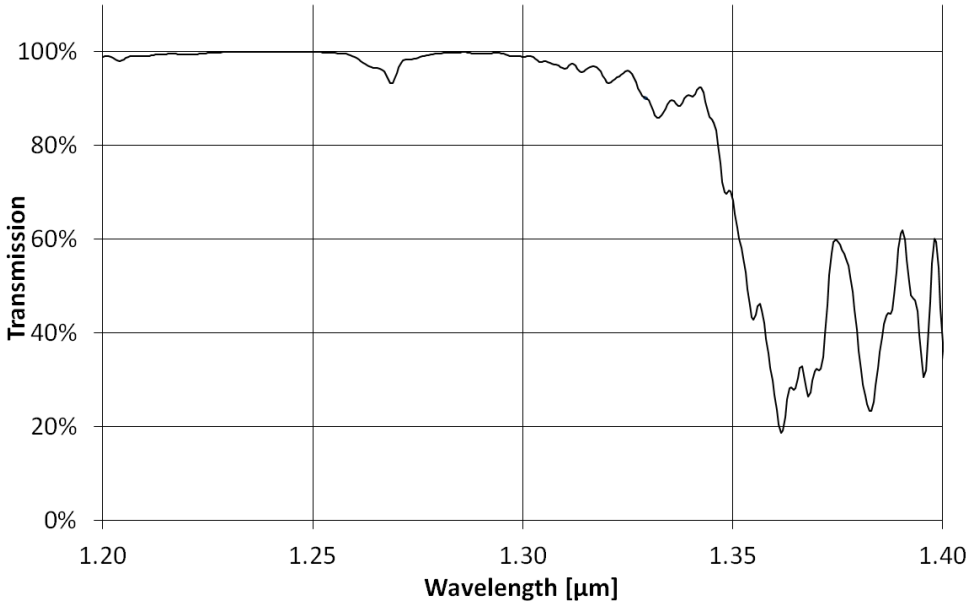

Figure 58: Atmospheric transmission of light through air in the 1.2 to 1.4 µm region, showing the sharp drop in transmission from 1.3 µm onwards (4.2 km propagation from space to ground) (UKIRT 2013).

Firstly, choosing which HBr overtone to pump (v=0 to v=1 or v=2 or v=3 etc.) is restricted by the availability of suitable pump sources. The narrow linewidths of these pump transitions require that the pump laser emit narrow-band laser light. This generally requires special single-mode, frequency-locked, injection-seeded laser systems, as is evident from literature (with the exception of the DF-laser pumped system mentioned in Section 6.3).

Several successful experiments used temperature-tuned Nd:YAG lasers emitting at 1.34 µm to pump HBr on the second overtone band (v=0 to 3). This approach resulted in cascade lasing from the v=3 to v=2 and v=2 to v=1 band. One disadvantage of having a pump laser emitting at 1.34 µm is that the pump laser itself cannot efficiently be used for free space propagation as the atmospheric transmission window in that region cuts off from 1.3 µm, as shown in Figure 58.

Another option is to pump HBr on the first overtone with ~2 µm laser light (Miller et al. 1994; Botha et al. 2009). This has the advantage of the pump laser output wavelength coinciding with an atmospheric transmission window which is of particular interest for directed infrared countermeasure (DIRCM) applications. The available options here are predominantly thulium and holmium based systems. Relatively high-energy (though not single-frequency) thulium fibre lasers, however, have only been gaining attention fairly recently, but very promising work has already been reported (Kieleck et al. 2015). Holmium based systems, however, have a proven record of being able to deliver high pulse energies at varying repetition rates, as shown by the work presented earlier in this dissertation and work published by other groups (See Chapters 2 through 5). Our group reported that it is possible to pump HBr on the P(9) transition at 2064.12 nm using a high-energy, single-frequency Ho:YLF laser (Botha et al. 2009). It is, however, not clear whether pumping HBr on the P(9) line at 2064.12 nm would result in the same

efficiency as compared to pumping from one of the lines that have a higher relative population (for example using the P(3) transition at 2010 nm instead (see Figure 51)) as no such comparative experiment has been done before. Effective pumping and lasing would depend on the fast repopulation of the v=0, J=9 from the other rotational states of the manifold and the redistribution from the excited v=2, J=8 rotational state to other states in the v=2 manifold. For an HBr gas pressure of around 27 mbar near room temperature this rotational relaxation towards a Boltzmann distribution has been stated to take between 5 ns (Kletecka et al. 2002) and 15 ns (Ratanavis et al. 2009). It does, however, suggest that longer pump pulses could result in better absorption, allowing sufficient time for the pumped line to be repopulated from the adjacent ones while being pumped.

Reported experimental and simulation results suggest that double passing the pump light through the HBr cell is the best approach to obtain sufficient absorption, if feedback to the pump system can be prevented. Reported HBr lasers had cell lengths between 20 and 100 cm, with gas pressures varying between 10 and 100 mBar. With regards to resonator design, a good spatial overlap between the pump beam and the fundamental mode is desirable for efficient operation. In the case of an amplifier, good spatial overlap of the seed and pump beam is important.

6.5 Conclusion

The main conclusion that can be drawn from this chapter is that optically pumped molecular HBr lasers are a promising source of laser light in the 4 µm region. It is also possible to pump HBr lasers efficiently with solid-state lasers, although the spectral properties of the HBr pump transitions impose exacting specifications on these pump sources.

In the subsequent two chapters optically pumped HBr laser systems are taken even further. With the 330 mJ, 2 µm single-frequency amplifier reported on in Chapter 5 used as pump source, an HBr laser could be pumped with more energy than ever before, as demonstrated in Chapter 7. Scaling of HBr output energies with the use of an optically pumped HBr amplifier, a world first, is also reported upon in Chapter 7. In Chapter 8 the first tuneable, optically pumped HBr laser is developed and demonstrated.

7 Development of an Optically Pumped HBr Master Oscillator Power Amplifier

An optically end-pumped HBr MOPA has been demonstrated for the first time. It produced a record output energy of up to 10.3 mJ at 4.20 and 4.34 μm when pumped with a single-frequency Ho:YLF slab amplifier. Wavelength selection with the use of an intra-cavity CO_2 absorption cell was also demonstrated, forcing the oscillator to emit at 3.89, 4.13 and 4.16 μm simultaneously, with a maximum output energy of 6.5 mJ per pulse after amplification.

7.1 Introduction

Laser output in the mid-infrared region can be generated by starting from a diode-pumped thulium-doped bulk solid-state or fibre laser at 1.9 μm, pumping a holmium-doped system emitting at 2.1 μm to subsequently pump a non-linear device such as an optical parametric oscillator based on ZGP (Lippert, Fonnum, Arisholm, et al. 2010; Schellhorn et al. 2007). Second harmonic generation by pumping a nonlinear crystal with a CO_2 laser is also a feasible approach (Ratanavis 2011). For high-energy operation, optically pumped molecular lasers can be an attractive alternative due to the potential to scale to very high pump energies without optical damage to the gain medium. One such an example is an optically pumped HBr laser, which has the potential to be highly efficient (Ratanavis et al. 2009). The highest reported output energy for such a laser was 2.5 mJ in a 132 ns pulse at a pulse repetition rate of 50 Hz when pumped with a narrow-band Ho:YLF laser (Botha et al. 2009).

HBr lasers do pose some challenges, however. Scaling the HBr laser for high-energy operation is limited by the availability of a suitable narrow-band, high-energy pump laser stabilised to an HBr absorption line. Secondly, corrosion in addition to optical damage of the HBr resonator optics and components may cause further difficulties (Rutt 1979). To address the first issue we developed a Ho:YLF slab amplifier discussed in Chapter 5 (which in turn was pumped by an in-house developed 1890 nm Tm:YLF slab laser (W. Koen, H. J. Strauss, et al. 2010)) to amplify the 70 mJ output of our single-longitudinal mode 2064 nm Ho:YLF ring-oscillator (Bollig et al. 2009) to 330 mJ per pulse at a 50 Hz pulse repetition rate.

To avoid optical damage while successfully demonstrating energy scaling, an optically pumped HBr master oscillator power amplifier (MOPA) which was pumped by the single-frequency Ho:YLF oscillator and amplifier system described in Chapter 5 was developed and demonstrated for the first time, as reported in this chapter.

Section 7.2 of this chapter discusses various design considerations that were taken into account with regard to the 2 µm pump light, the HBr resonator, and the HBr amplifier. The experimental setup is then designed based on these factors. In Section 7.3 the author presents the experimental results obtained from the system, including pump light absorption measurements, the oscillator performance, as well as the amplifier results. These results and their implications are discussed in Section 7.4 after which conclusions are drawn in Section 7.5.

7.2 Experimental design and setup

In order to illustrate the scale of the overall system a photo of the HBr MOPA system is shown in Figure 59 (right) alongside the single-frequency Ho:YLF oscillator and amplifier system


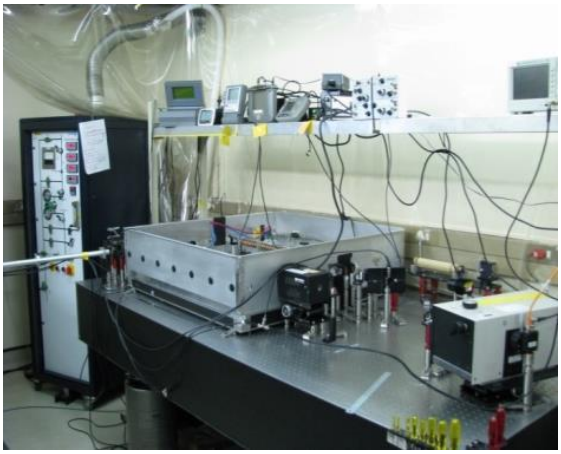

Figure 59: The single-frequency ring-laser and amplifier system used as pump source (left) and the HBr MOPA setup with the gas handling system (right).

described in Chapter 5 which was used as a pump source. A schematic of the experimental setup of the HBr MOPA is shown in Figure 60. The various components of the setup are discussed in the subsections below, with a list of components provided in Table 9. Section 7.2.1 describes the pump design and setup, including an elegant method of preventing optical feedback into the pump laser when using a double-pass pump configuration. The resonator design and setup are discussed in Section 7.2.2 while the single-pass amplifier is described in Section 7.2.3.

7.2.1 Pump design and setup

The oscillator and amplifier were optically end-pumped on the P(9) (2.06412 µm) line of HBr. This specific wavelength was chosen as Ho:YLF lasers could readily operate at this wavelength in addition to having good atmospheric transmission at 2064 nm. It is, however, not clear whether pumping HBr on the P(9) line at 2064 nm would result in the same efficiency as pumping on one of the lines that has a higher relative population, for example using the P(3) transition at 2010 nm instead, as no such comparative experiment has been done before (most likely due to the lack of a suitable high-energy, single-frequency pump source operating at 2010 nm) (Botha et al. 2009).

The linearly polarised laser pulses from the 2 µm single-frequency oscillator previously developed by our group (Bollig et al. 2009) were amplified by the 2 µm amplifier reported upon in Chapter 5. The amplifier delivered up to 330 mJ in ~350 ns long pulses at a pulse repetition frequency (PRF) of 50 Hz where the Ho:YLF laser output energy was highest. The amplified 2 µm beam from the slab amplifier was shaped to be approximately circular symmetric using cylindrical lenses before being steered into the HBr MOPA setup (See Figure 60, Figure 64 & Figure 65).

The incident 2 µm pump light was split between the oscillator and the amplifier with a variable beam splitter consisting of a λ/2-wave plate (WP1, Figure 60) and a polarisation dependant 45° mirror (M1) that was highly transmissive for the horizontal polarisation (HTp) and highly reflective for the vertical polarisation (HRs). By varying the angle of the λ/2-wave plate the relative pump energies between the oscillator and amplifier could be adjusted to any ratio.

The 2 µm pump beam was double passed through the oscillator tube by using an output coupler mirror for the HBr oscillator (M4) that was also highly reflective (HR) at 2 µm.

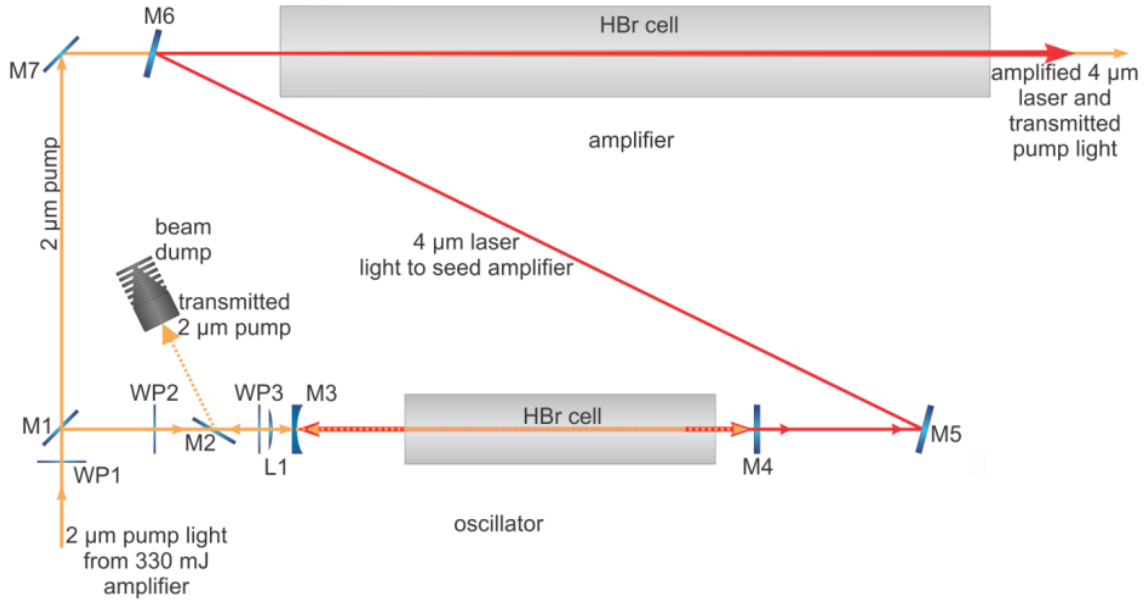

Figure 60: Schematic layout of the HBr oscillator and amplifier.

To avoid back reflections into the 2 µm pump system, a polarisation-based optical isolation setup was implemented. This consisted of a Brewster-type thin film polariser (M2) and a λ/4-wave plate (WP3) placed just before the oscillator cavity. On the forward path, the horizontally polarised 2 µm pump was transmitted by the plate polariser and then converted into circularly polarised light by the λ/4-wave plate before entering the HBr oscillator. The beam then passed twice through the oscillator HBr cell, by being back reflected off the output coupler mirror M4. On the backward path, the unabsorbed circularly pump light was converted to vertically polarised light by the λ/4-wave plate WP3, and then reflected off the plate polariser M2. The transmitted pump light could then be measured with a power meter or dumped on to a heat sink.

Table 9: HBr MOPA component list as labelled in Figure 60.

Component/Parameter	Specification
Mirror M1	Flat, HRs 2064 nm, HTp 2064 nm, 45º AOI
Mirror M2	Flat Brewster-type thin film polariser, HRs 2064 nm, ARp 2064 nm
Mirror M3	Input Coupler, ROC = 5 m concave, HT 2064 nm, HR 4 µm
Mirror M4	Output Coupler, flat, R = 80 % at 4 µm, HR @ 2064 nm
Mirror M5	Flat, HR 4 µm
Mirror M6	Flat, HR 4 µm, HT 2064 nm
Mirror M7	Flat, HR 2064 nm, 45º AOI
Wave plate WP1	Half-wave plate, AR 2064 nm
Lens L1	f = 2 m plano convex lens
Wave plate WP2	Half-wave plate, AR 2064 nm
Wave plate WP3	Quarter-wave plate, AR 2064 nm
HBr Cell - Oscillator	510 mm long electro-polished Stainless Steel tube, with AR 2064 nm, AR 4 µm coated laser windows
HBr Cell - Amplifier	760 mm long electro-polished Stainless Steel tube, with AR 2064 nm, AR 4 µm coated laser windows

7.2.2 Resonator design and setup

The resonator design was aided by design software developed by the *University of St Andrews*, called *PSST!*. The resonator design took into account the pump beam size obtained from the 330 mJ 2 µm Ho:YLF amplifier, the HBr cell length, as well as the laser optics which were available for the experiment. The resulting HBr resonator consisted of a concave input coupler mirror (M3, 5 m radius of curvature), and a flat output coupler mirror (M4) placed 580 mm apart. This cavity length and mirror combination resulted in the fundamental mode matching of the pump beam size and allowed sufficient space between the mirror mounts and the HBr cell to access the optics.

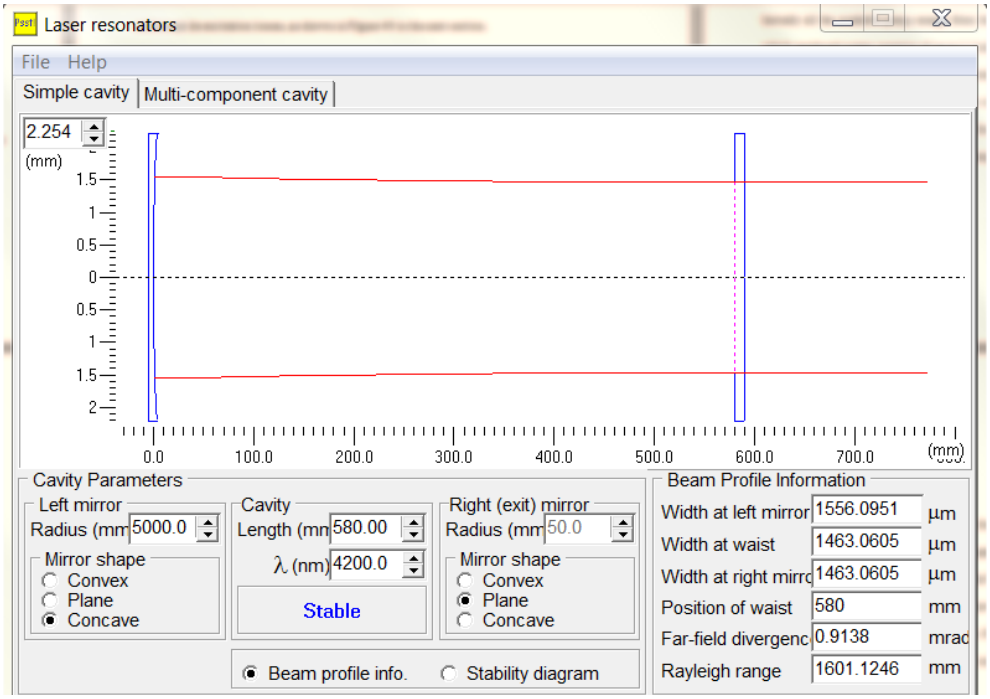

Figure 61: Screen grab of *PSST!* laser resonator software displaying the calculated fundamental resonator mode of the HBr oscillator. The software allows one to design oscillator cavities by specifying various mirror curvatures, intra-cavity lenses, propagation distances and laser wavelengths. The resulting fundamental mode of the cavity is shown in red, while the optics are shown in blue.

The input coupler mirror was highly reflective at 4 µm and highly transmissive for 2 µm, while the output coupler mirror reflected 80% of the 4 µm light while being highly reflective for the 2 µm pump light. A 510 mm long HBr gas cell, the length of which was determined by previous results and simulations (Botha et al. 2009), was placed 26 mm away from the output coupler mirror. The cell windows were made from Cleartran® (which has good transparency in the 2 to 5 µm region and is not birefringent) with anti-reflective coatings for both 2 and 4 µm light. The gas cell, which was made from electro-polished stainless steel, was wrapped in copper piping in order to water cool the cell walls and maintain a set temperature (this was also the case for the HBr amplifier cell). The 2 µm pump beam was fairly well collimated over the length of the tube and had an average radius of 1.5 mm, which was matched by the fundamental resonator mode, as calculated by *PSST!* (shown in Figure 61).

One concern with the system was that the initial output wavelengths of 4.20 and 4.34 µm fell within a CO_2 absorption band, severely limiting free space propagation of the laser light. A very

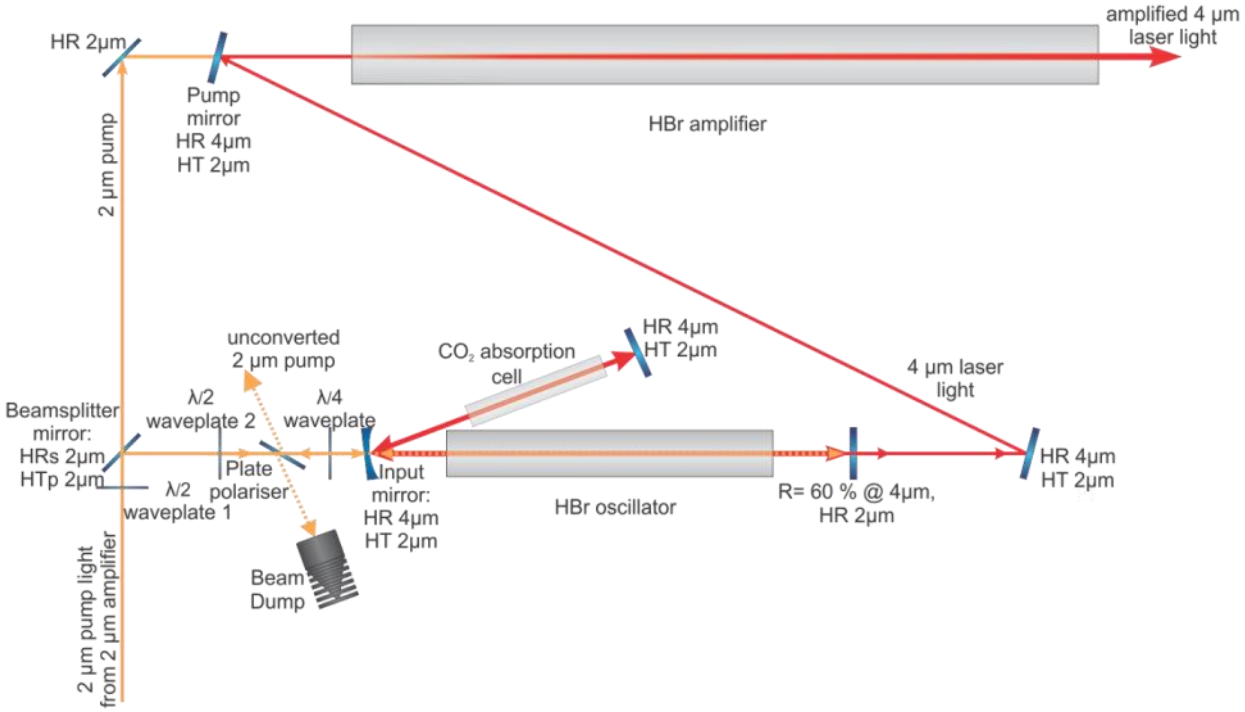

Figure 62: Experimental layout of the HBr oscillator with a CO_2 absorption cell.

successful way of avoiding this was the implementation of a tuneable HBr laser, as demonstrated in Chapter 8, which was done subsequent to the work reported on in this chapter.

Another way to force the HBr output wavelength to the atmospheric transmission window is to insert a CO_2 absorption cell into the cavity as intra-cavity CO_2 may prevent the oscillator from lasing on the undesired transitions which overlap with those of CO_2 (Kletecka et al. 2004). This uses the gas that is responsible for the near opacity over long distances beyond 4.2 µm to force the laser onto wavelengths where the CO_2 does not absorb the radiation by increasing the intra-cavity losses for all the undesired wavelengths. This approach has subsequently been implemented and demonstrated successfully by the author, as briefly described below:

A 30 cm long cell was constructed in-house with available components and subsequently filled with laser quality CO_2 gas (with no buffer gas) near atmospheric pressure. The cell was then inserted into a simple folded cavity as shown in Figure 62. Figure 63 is a photo of the CO_2 absorption cell in the oscillator with the optical path also illustrated in the photo. While most of the measurements in this chapter were done using the unmodified oscillator, mention will be made with regard to the results obtained with the CO_2 cell in place, where appropriate.

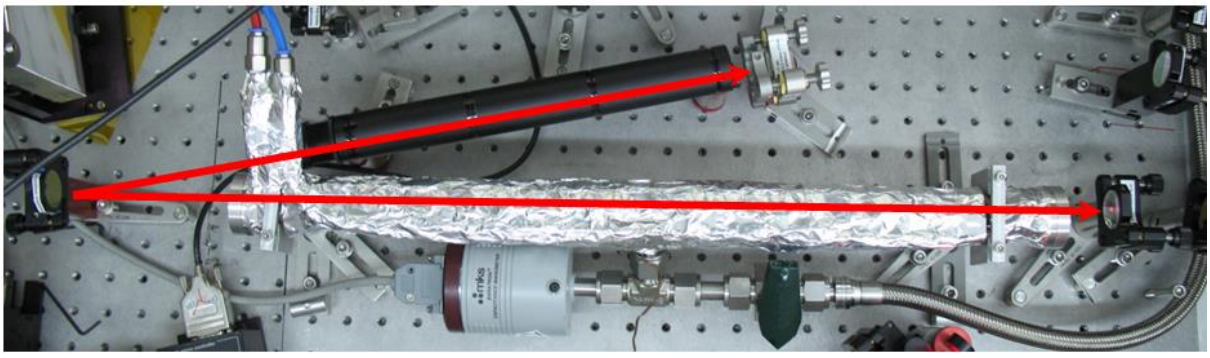

Figure 63: Photo of the modified HBr oscillator containing an absorption cell (black tube) filled with CO_2 gas at ambient pressure.

7.2.3 Amplifier design and setup

This section discusses the HBr amplifier design and the resulting experimental arrangement. The amplifier pump beam shaping design was done by Cobus Jacobs using his in-house developed software *EXAG* which was previously presented in Chapter 4, after which the author implemented and characterised the proposed solution. The proposed pump design is shown in Figure 64, but will not be discussed for the sake of brevity, except to mention that the target 2 µm pump beam radius for the HBr MOPA was 1.4 mm.

The pump light incident on the amplifier from mirror M7 (refer to Figure 60) propagated through a beam combiner M6 (HR 4 µm, HT 2 µm) and into the amplifier tube. The seed beam from the 4 µm oscillator was reflected off a HR 4 µm mirror M5 onto the beam combiner M6. These two mirrors were then used to co-align the 4 µm seed to the 2 µm pump beam inside the 760 mm long HBr amplifier cell. The HBr amplifier cell length was chosen based on previous results and

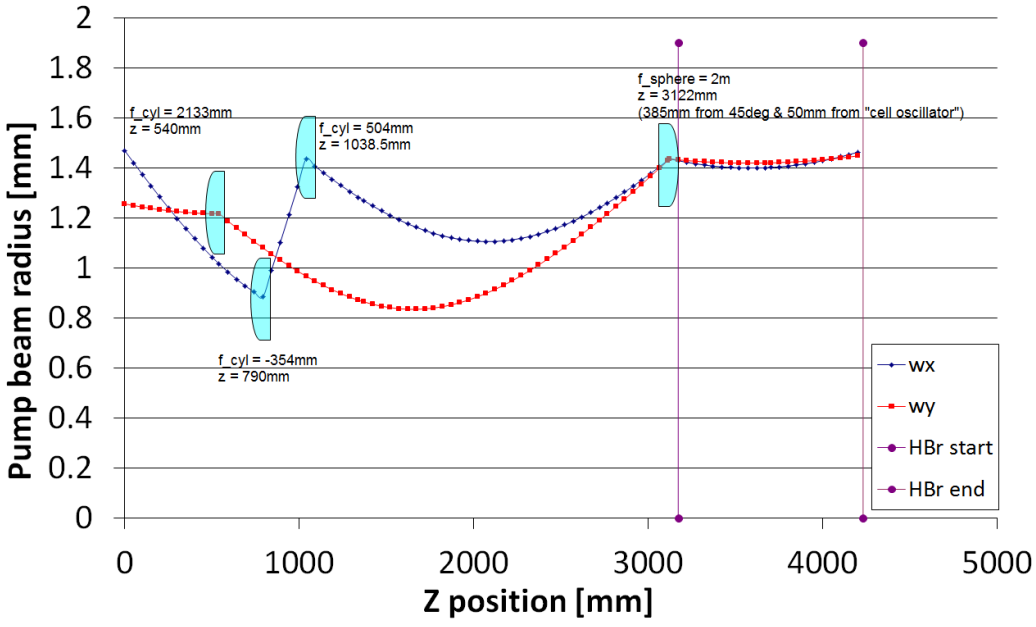

Figure 64: Proposed 2 µm seed beam shaping design as generated by *EXAG* software (Jacobs 2013a). The x-axis indicates the distance from the Ho:YLF amplifier while the two purple lines indicate the region of interest for the HBr system. The vertical and horizontal pump beam radii are shown in red and blue respectively.

simulations (Botha et al. 2009).

The amplifier was used in a single-pass pump configuration, as single-pass absorption of the pump light was already significant, as later discussed in Section 7.3.1. Double-passing the pump light could further improve absorption and efficiency but increased the risk of optical damage to components due to the resulting increase in pump fluence (~6 J/cm^2 for single pass vs. ~12 mJ/cm^2 for double pass for 200 mJ pump in 2.9 mm beam), and one would therefore have to increase the beam size. The measured beam diameters of the seed and amplifier beams inside the HBr amplifier cell is shown in Figure 65. Both the seed and pump beams diverged slightly along the length of the tube with the seed beam diameter increasing from 4 to 5 mm. The amplifier pump beam was astigmatic at the tube's entrance with a beam diameter near the cell entrance of 2.9 mm in the x-axis and 3.8 mm in the y-axis. As it diverged, the pump beam became circular near the exit side of the amplifier tube measuring 4.3 mm in both axes, 750 mm away from the

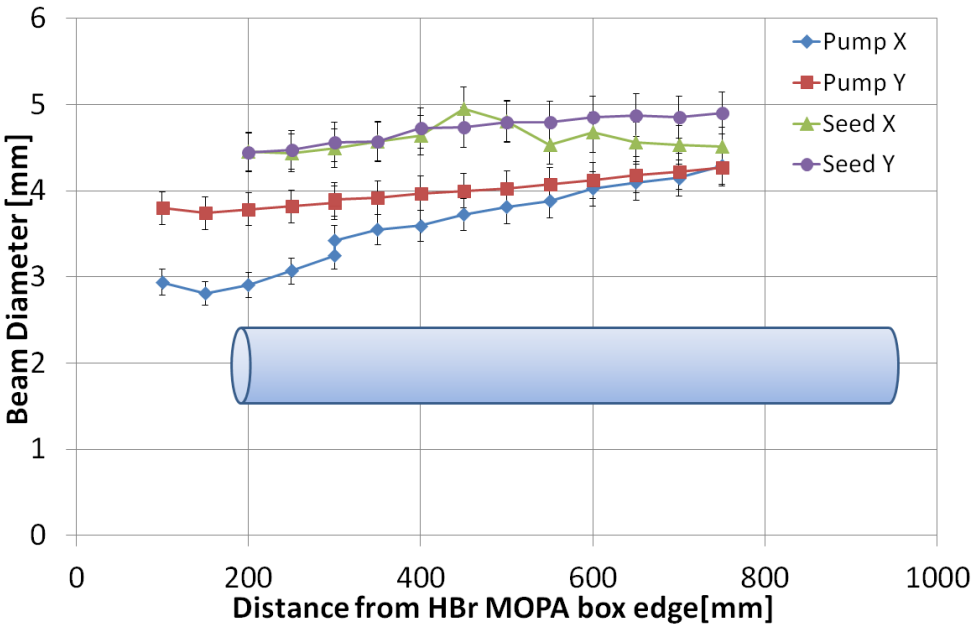

Figure 65: The amplifier pump and seed beam diameters, as measured by an *Ophir Spiricon PyroCam III* (90/10 knife edge calculation). The HBr amplifier cell position is depicted by the blue cylinder.

HBr cell's front end. The pump beam diameter was larger than the original design shown in Figure 64, but this was a rather challenging pump design to implement successfully and the resulting setup was deemed fit for purpose.

7.3 Experimental results

A photo of the experimental setup of the HBr oscillator and amplifier is shown in Figure 66. The HBr cell of the oscillator and the longer HBr amplifier cell are clearly visible. Various parameters such as the incident pump energy, HBr gas pressure, and seed energy could be varied

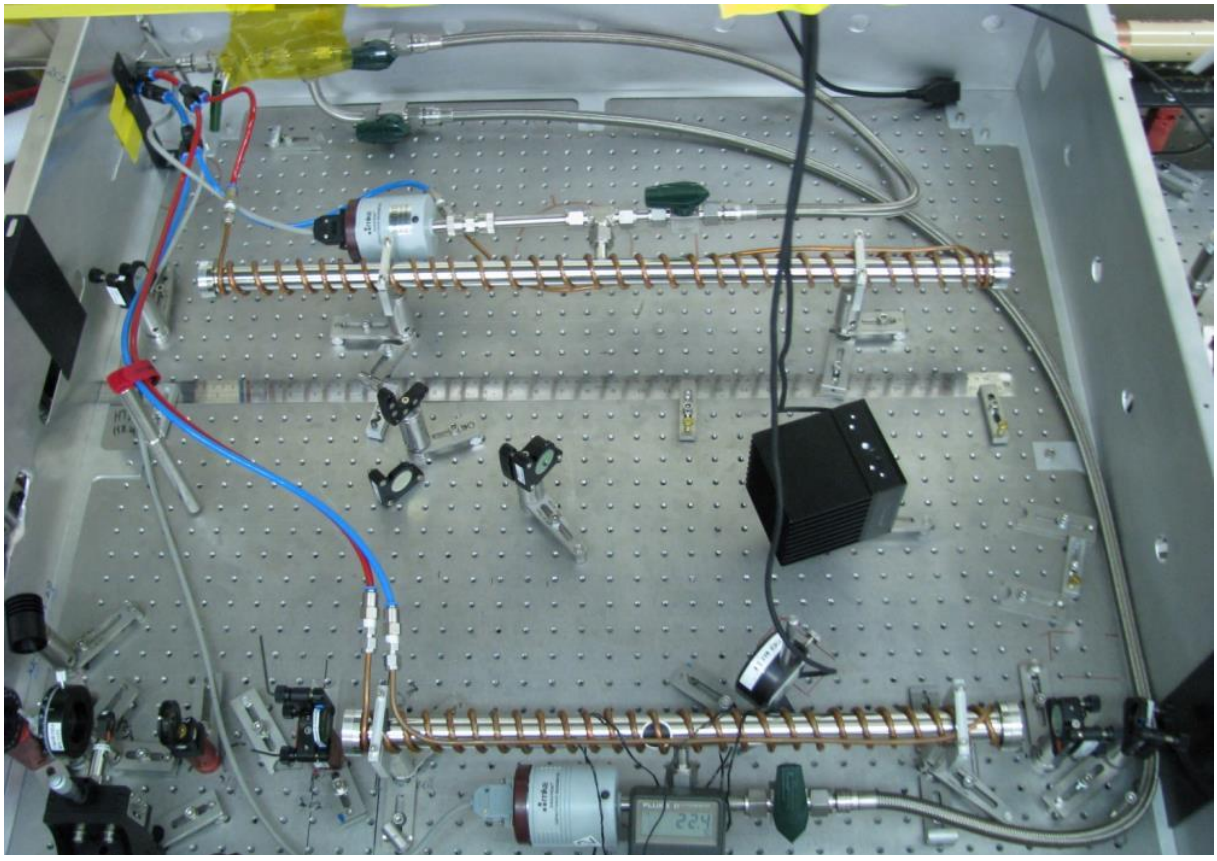

Figure 66: A photo of the HBr MOPA system. The oscillator is shown at the bottom of the photo while the amplifier is shown at the top.

in order to study the effects they had on the HBr laser and amplifier performance. The resulting pump absorption measurements for the oscillator and amplifier are presented in Section 7.3.1. The oscillator performance and amplifier results are presented in Sections 7.3.2 and 7.3.3 respectively.

7.3.1 Absorption measurements

The HBr MOPA system's pump light absorption was characterized with regards to HBr pressure. Figure 67 shows the absorption coefficients of the 2 µm pump light in a single pass through the HBr oscillator cell for an incident pump energy of 43 mJ at different HBr gas pressures. Also shown are the measured absorption coefficients for the seeded amplifier (with 200 mJ of pump energy incident on the HBr amplifier cell) and the oscillator under lasing conditions, which corresponded well between 50 and 95 mBar, where measurements had been taken for both.

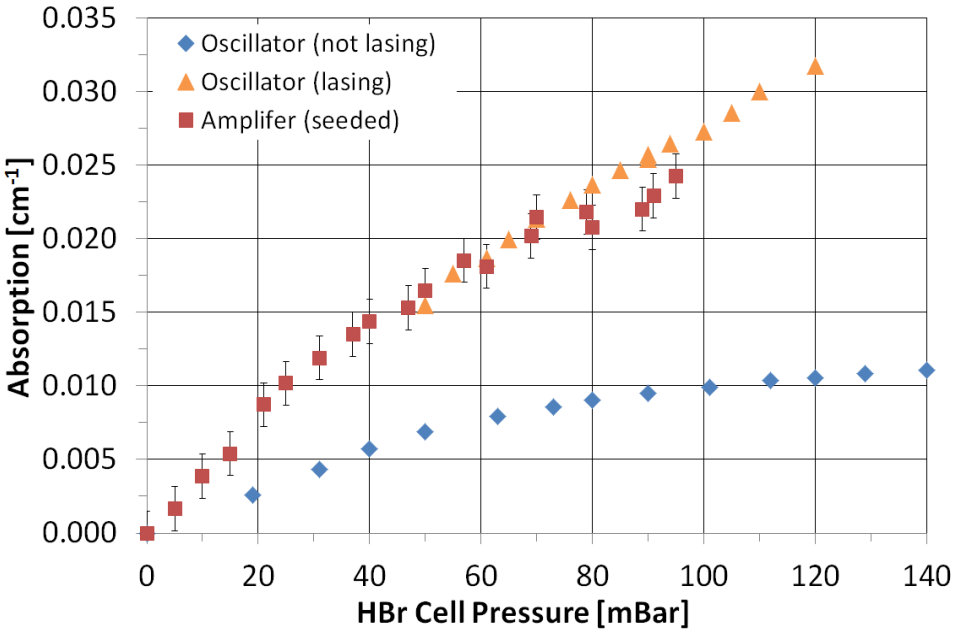

Figure 67: Comparison of the single-pass absorption of the HBr amplifier (seeded) and the HBr oscillator (lasing and non-lasing) as a function of HBr pressure. The pump energy was kept fixed at 43 mJ for the HBr oscillator cell, and 200mJ for the HBr amplifier cell.

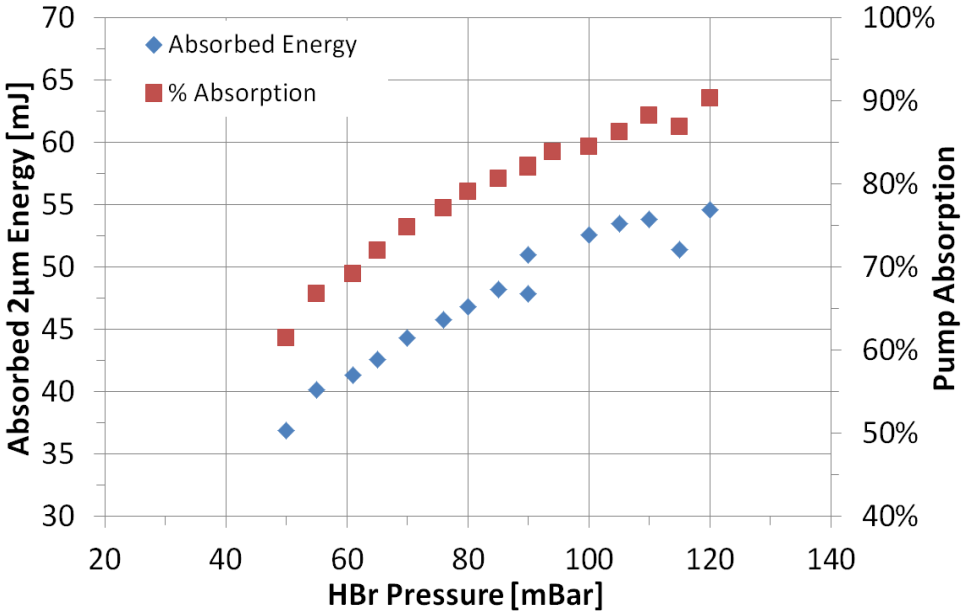

Figure 68: Double-pass absorbed 2 µm pump energy (left axis) in the HBr oscillator cell and total absorption (right axis) as a function of HBr pressure at a fixed pump energy of 43 mJ.

The higher absorption under seeded and lasing conditions is due to the lower laser level being repopulated from the upper lasing level after stimulated emission. Under non-lasing conditions, the upper laser level is populated for a longer time, reducing the population of the ground state and therefore decreasing the pump absorption. The flattening out of the absorption curves at higher pressures is attributed to pressure broadening of the HBr lines. It was previously found that a pressure broadening value of 10.7 MHz/mBar fit both experimental and simulation work best (Botha et al. 2009).

Figure 68 shows the pump absorption as a function of HBr pressure in the oscillator cell where the circularly polarised pump light is double passed. Measurements provided in both figures indicate good pump absorption by the HBr, increasing with increasing gas pressures with up to 90 % of pump light being absorbed in the double-pass configuration of the HBr oscillator cell at 120 mBar

of HBr pressure under lasing conditions. However, optimal HBr laser performance does not coincide with maximum pump light absorption, as shown in Figure 69 in the next section.

7.3.2 Oscillator performance

The HBr oscillator performance as a function of gas pressure is shown in Figure 69. It was found that the oscillator was most efficient at an HBr pressure range of 85 to 90 mBar when pumped with 50 mJ of 2 µm pump energy at a PRF of 50 Hz. Approximately 80% of the incident 2 µm pump light was absorbed when the HBr pressure was 85 mBar (see Figure 68).

Initially all the available pump energy from the Ho:YLF amplifier was coupled into the HBr oscillator which produced output energies of up to 5.4 mJ per pulse for 206 mJ of incident 2 µm pump energy, at which point optical damage of the HBr oscillator cell's front window was observed due to the high intensity of the pump light in the double-pass configuration (slope shown

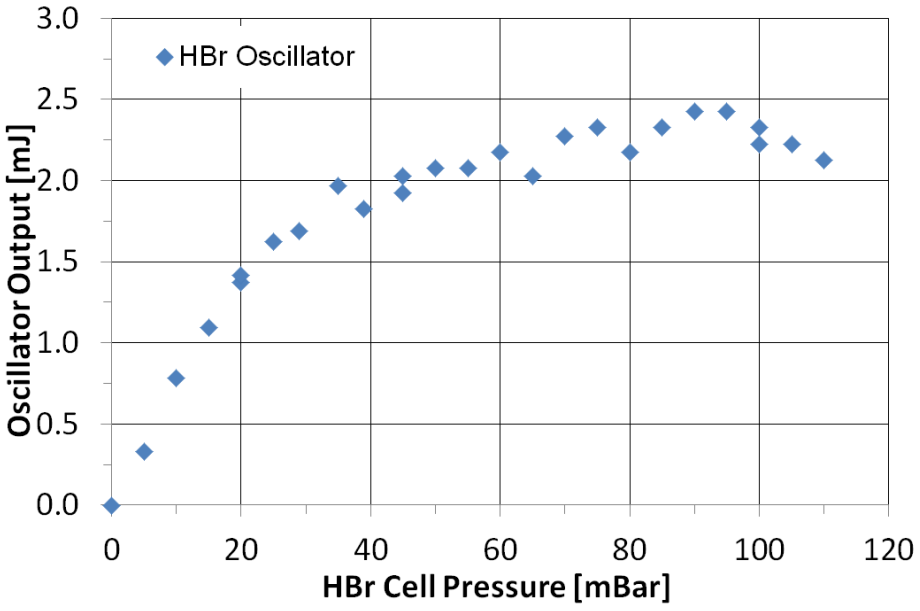

Figure 69: The 4 µm laser output energy as a function of HBr pressure for an incident 2 µm pump energy of 50 mJ.

in Figure 70). Before damage occurred the laser had a 2.3 % slope with regards to incident pump energy, and a laser threshold at 4 mJ of pump energy. The oscillator was subsequently operated at a reduced input energy of 50 to 60 mJ at the point where the HBr laser was most efficient with respect to incident energy (Figure 71), leaving the remaining pump energy for use in the amplifier.

Keeping the HBr pressure at 85 to 90 mBar the 4 µm output of the HBr oscillator was re-measured as a function of the incident pump energy, as shown in Figure 71. It can be seen from Figure 71 that the HBr oscillator output energy increased nearly linearly with incident pump energy, as was the case in previously reported work (Botha et al. 2009). The oscillator's temporal behaviour matched closely to that of the amplifier and is discussed in the subsequent section.

Using a *Jarrell Ash* monochromator and photodetector, it was observed that the oscillator emitted simultaneously at 4.20 and 4.34 µm. These wavelengths reside in an undesirable region of the

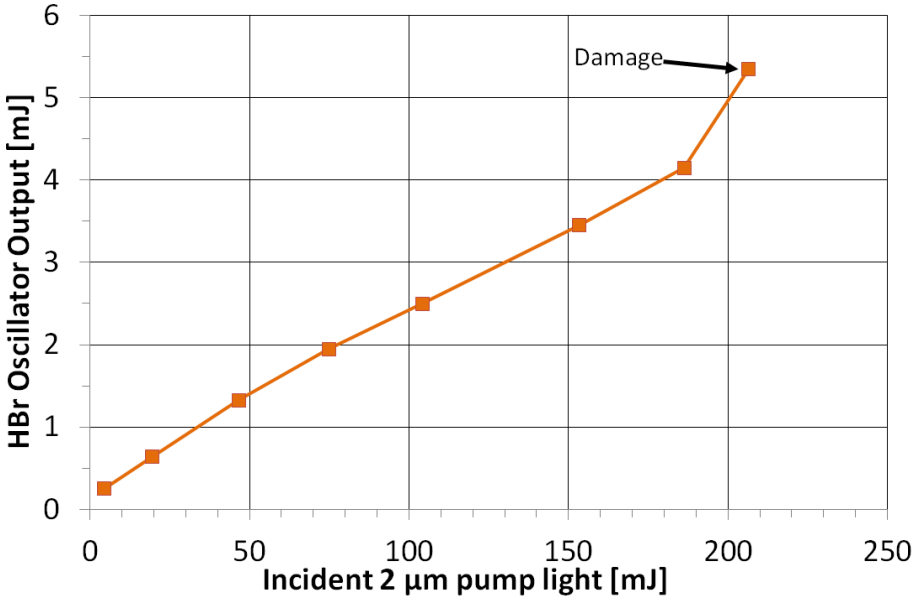

Figure 70: HBr Oscillator output energy as a function of incident 2 µm energy. The laser had a slope efficiency of 2.3 % with regards to incident pump energy. Optical damage of the HBr cell's front window occurred during the experiment where indicated.

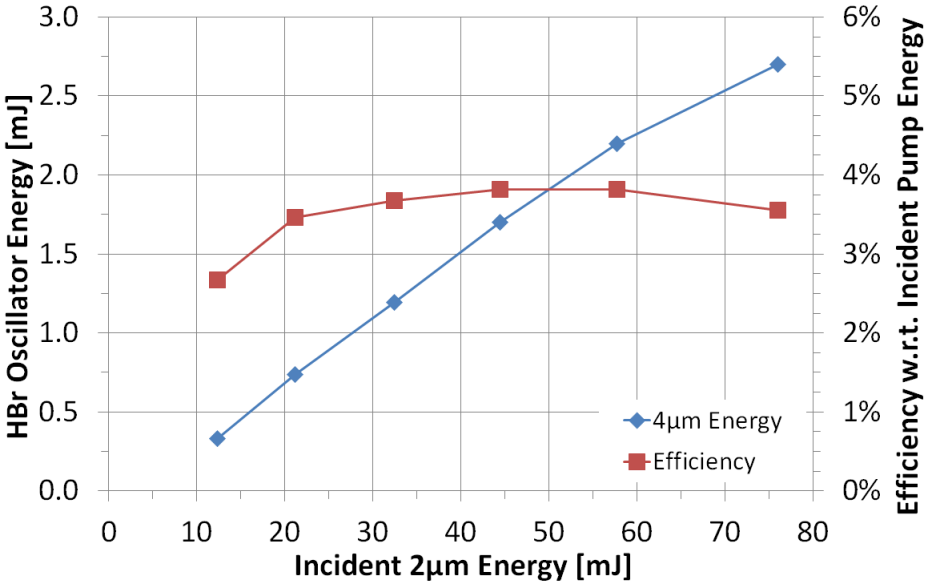

Figure 71: The 4 µm oscillator output energy and efficiency as a function of incident pump energy.

spectrum for free space propagation as it falls within a strong CO_2 absorption band. The laser emission lines of the HBr resonator containing the intra-cavity CO_2 absorption cell were subsequently measured and are shown together with the atmospheric transmission spectrum in Figure 72. The HBr laser oscillated on three lines simultaneously (3.89, 4.13, and 4.16 µm). The relative strengths of these three laser lines could not be measured accurately with the given monochromator. As can be seen, all the newly obtained laser emission lines were within the atmospheric transmission band. A maximum output energy of 2 mJ was measured from the HBr oscillator when the intra-cavity CO_2 cell was present.

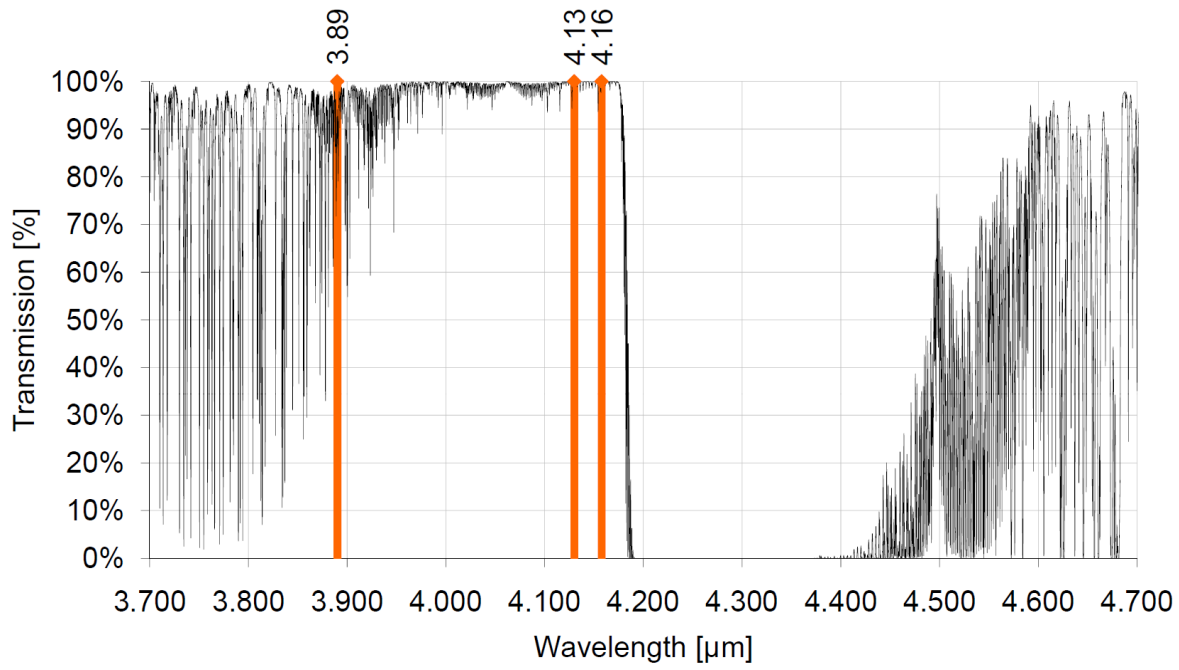

Figure 72: Emission lines of HBr obtained with a CO_2 absorption cell placed in the resonator as well as the atmospheric absorption spectrum shown in black (for a propagation distance of 2 km, 1 atm. pressure, 296 K, USA tropics model (UKIRT 2013)).

A typical beam intensity profile of the oscillator is shown in Figure 73. The beam profile remained similar for different pump intensities and HBr cell pressures. An M^2 measurement was not taken but it can be assumed that the laser operated on the TEM_{00} mode as one could easily obtain individual operation on TEM_{10}, TEM_{20}, etc., as well as TEM_{01}, TEM_{02}, etc. by misaligning the input coupler in either the horizontal or vertical direction. This view is further supported by the fact that the calculated fundamental Gaussian resonator mode size was well matched to the pump beam radius in the gain medium, not providing gain to higher order modes that are larger.

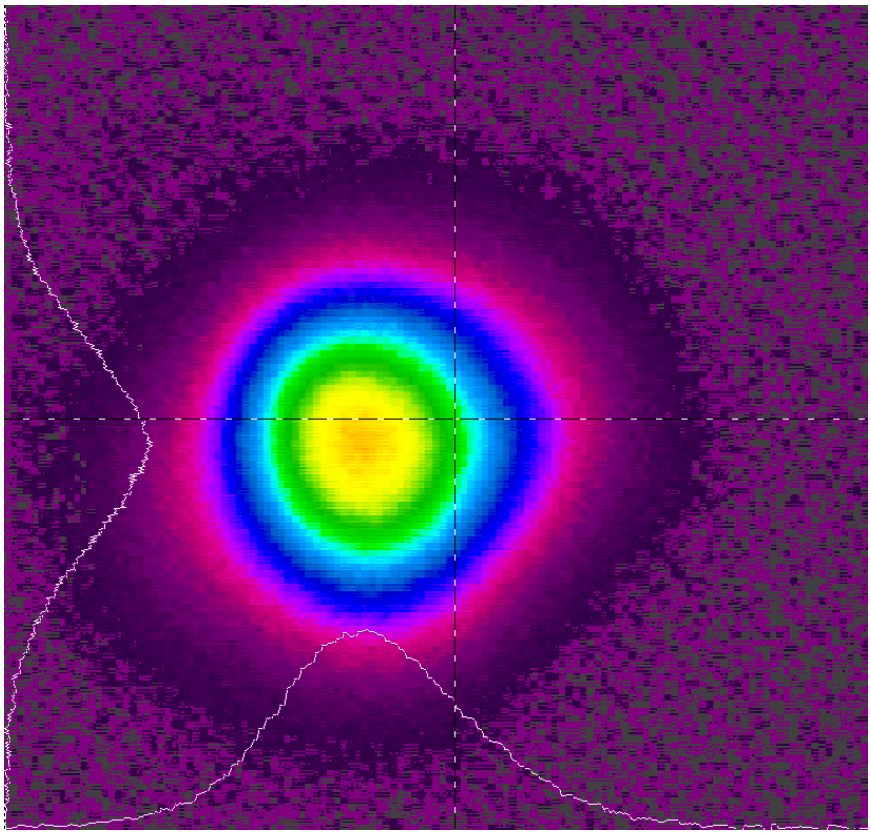

Figure 73: The 4 µm oscillator beam intensity profile at 50 mJ of pump power and an HBr pressure of 40 mBar, as recorded by an *Ophir Spiricon Pyrocam III*.

7.3.3 Amplifier performance

To determine the optimal gas pressure for the amplifier cell, the HBr pressure was varied while recording the single-pass 2 µm pump absorption and the amplified 4 µm output energy for a fixed incident pump energy of 200 mJ at a 50 Hz PRF. For these measurements the oscillator output which seeded the amplifier was between 2.0 and 2.5 mJ. The results are shown in Figure 74. The amplifier output energy and gain increased almost linearly with pressure up to 30 mBar after which it flattened out to a maximum energy of 9.3 mJ and gain of 4 at 57 mBar (for a seed energy of 2.3 mJ). Increasing the pressure beyond 60 mBar led to a decrease in performance.

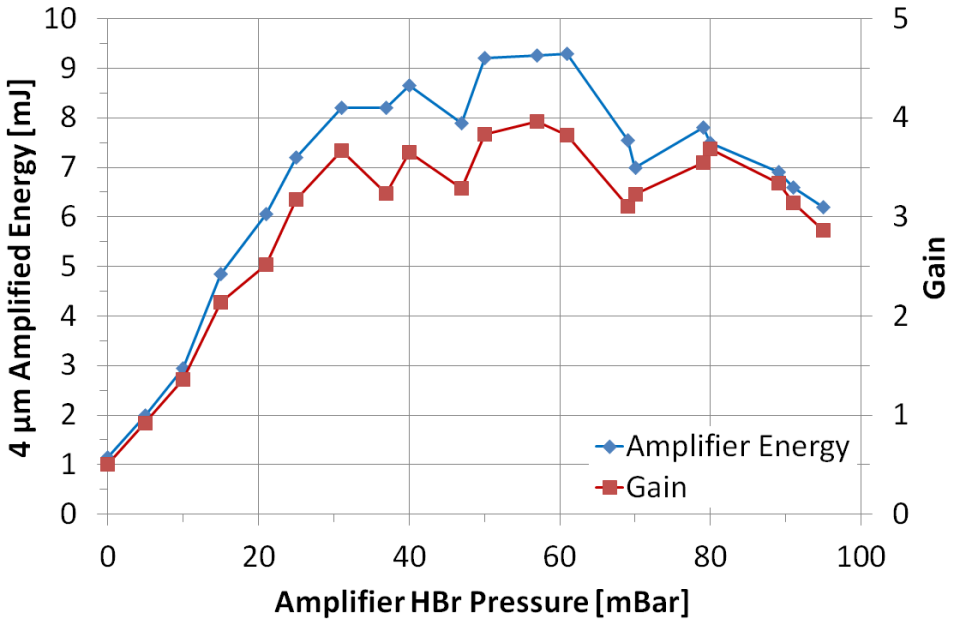

Figure 74: Amplified energy and gain as functions of the HBr pressure in the amplifier cell.

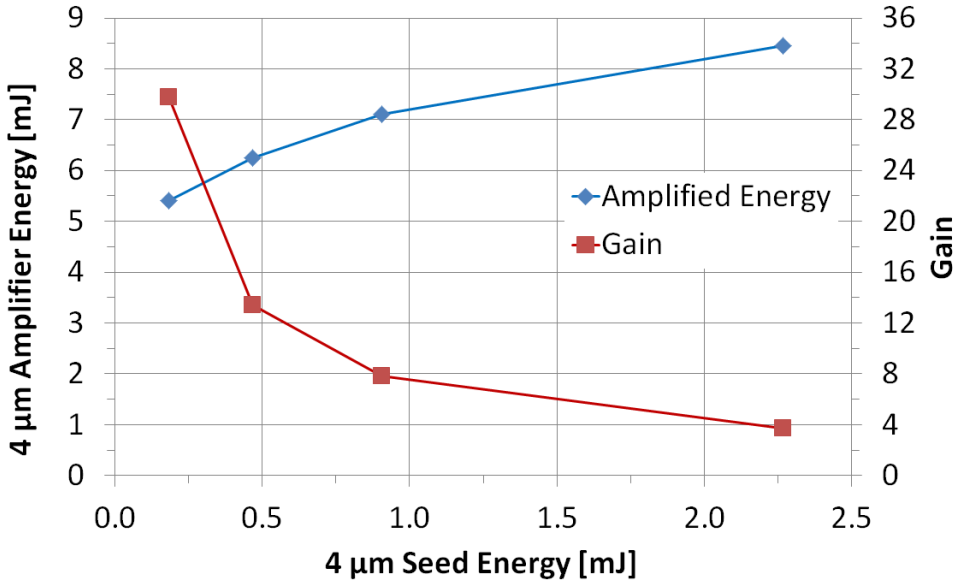

Figure 75: Amplified 4 µm energy and gain as functions of the seed energy from the 4µm oscillator.

The amplifier performance was also characterized with regards to the incident seed energy as well as the incident 2 µm pump light at a constant optimal HBr cell pressure of 60 mBar. The amplified energy and the amplifier's gain as a function of the seed energy are shown in Figure 75. The seed energy was varied by temporarily attenuating the incident seed beam with partial reflectors placed between mirrors M5 and M6 (refer to Figure 60). A gain of nearly 30 was achieved when the amplifier was seeded with 0.2 mJ. When all of the seed energy was used (2.3 mJ), a gain of nearly 4 was measured. This indicates good saturation of the amplifier.

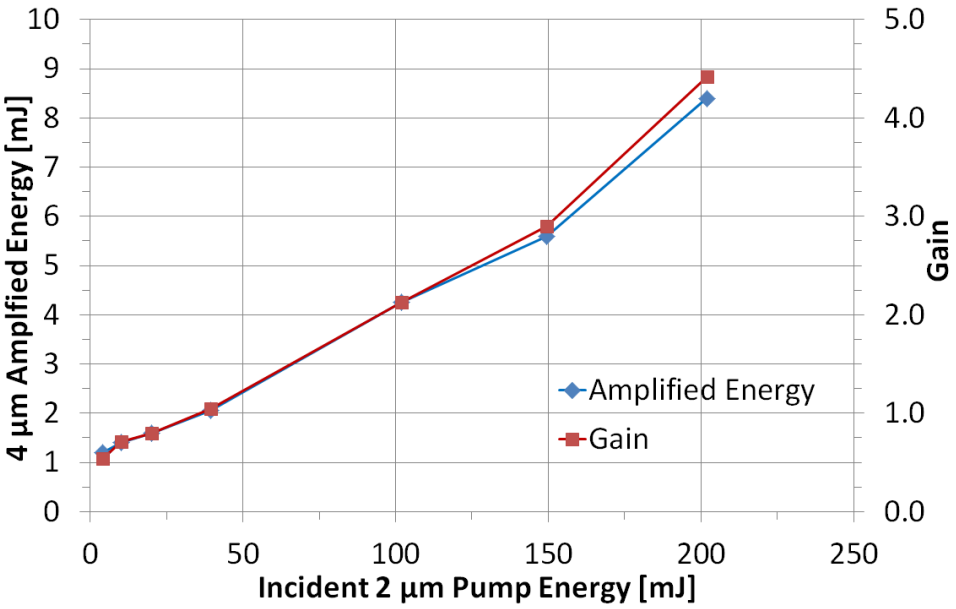

Figure 76: Amplified energy and gain as functions of incident 2 µm pump energy to the HBr amplifier.

The HBr amplifier's output energy and gain as a function of the incident 2 µm pump energy for a fixed seed energy (~2 mJ) is shown in Figure 76. The incident pump light was varied from 4 mJ to 200 mJ for the amplifier (by temporarily placing attenuation mirrors between M1 and M7, with reference to Figure 60) while keeping the pump energy of the HBr oscillator constant. The HBr amplifier output energy and the amplifier gain exhibited a roughly linear dependence on the incident pump light. For these measurements the single pass amplifier gain was over 4 at the highest incident pump energy of 200 mJ.

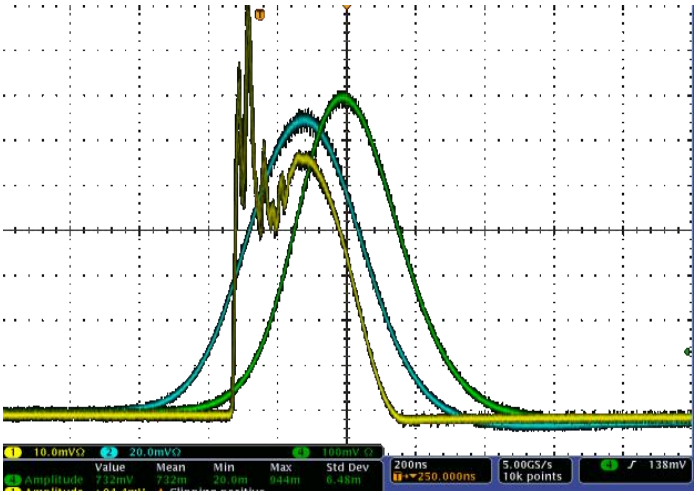

Figure 77: The temporal pulse shape of the 4 µm amplifier output is shown in yellow. The 2 µm pump pulse is shown in blue and the pulse from the single-frequency 2 µm laser before amplification shown in green. All trace amplitudes are arbitrary and not relative to one another.

The yellow trace in Figure 77 shows the temporal pulse shape from the 4 µm amplifier at an incident pump energy of 184 mJ, an HBr pressure of 58 mBar and a 4 µm amplified energy of 10.3 mJ from a seed energy of 2.04 mJ (gain of 5). This was the highest output energy obtained from the system but could not be repeated, probably due to the gradual degradation of the optical components which were exposed to HBr. The temporal profile looks very similar to that of the

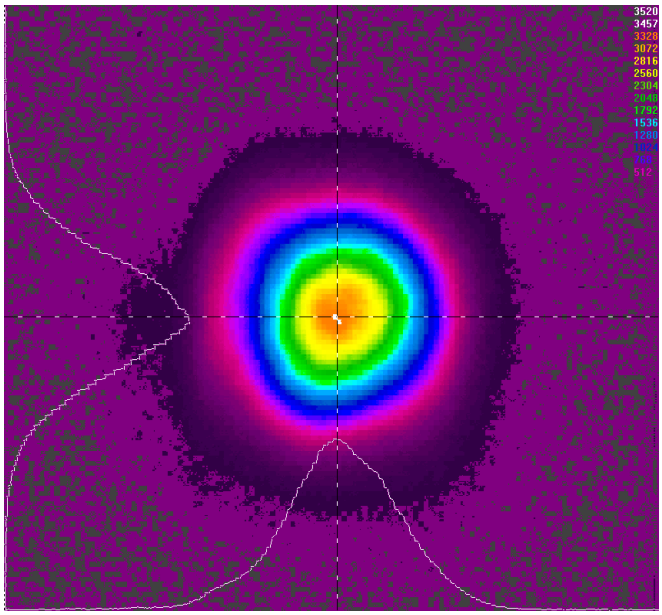

Figure 78: The beam intensity profile of the 4 µm amplified beam, as recorded by an *Ophir Spiricon Pyrocam III*.

oscillator, whose temporal behaviour could vary considerably under different pumping and pressure regimes. This was not fully characterised, however.

A beam profile of the output beam from the amplifier measured in the far field is shown in Figure 78. The beam was nearly circular-symmetric appearing Gaussian in both the X and Y axes (A fit to confirm this was not done). As the seed laser operated on $TEM_{00,}$ the seed and pump beam diameters in the amplifier were relatively well matched (Figure 65), and the beam profiles from the oscillator and amplifier also matched well (Figure 73 & Figure 78). This implied that the amplified 4 µm beam had a good beam quality. An M^2 measurement to confirm this was not taken, however.

The amplifier was also seeded with the 2 mJ laser pulses from the 4 µm oscillator which contained the intra-cavity CO_2 absorption cell. A maximum output energy of 6.5 mJ was obtained with this setup.

7.4 Discussion

It is worth noting that the HBr oscillator alone in this system delivered more than twice the previously reported record output energy for an optically pumped HBr laser (Botha et al. 2009). Up to 5.4 mJ of 4 µm laser light for 206 mJ of incident pump power was obtained with the laser emitting simultaneously at 4.20 and 4.34 µm.

However, the operating wavelengths of the free-running HBr oscillator resided in an undesirable region of the optical spectrum hampering free space propagation as it fell within a strong CO_2 absorption band. But the laser emission lines of the HBr resonator containing the intra-cavity CO_2 absorption cell (3.89, 4.13, and 4.16 µm) fell well within the atmospheric transmission band as is apparent from Figure 72. The HBr laser oscillated on these three lines simultaneously. A maximum output energy of 2 mJ was measured from the HBr oscillator when the CO_2 cell was present. This was less than with the previous setup but with the laser wavelength now lying outside the CO_2 absorption band, the energy measured over long propagation distances would be much more than for the free-running system. This would make it well suited for applications where long propagation distances are required such as LIDAR or directed infrared countermeasures.

The stand-alone oscillator approach does have scaling limitations, however, and optical damage of the input coupler, where the optical fluence was highest, was experienced during the experiment. It is interesting that the slope between the last two points in Figure 70 is considerably steeper than the slope between all the preceding data points. This can imply that cascade lasing from level v=1 to v=0 *may* have started to occur at that pump power, but this could not be determined spectrographically or otherwise. Cascade lasing is particularly difficult to achieve as the pump laser does not sufficiently empty the v=0 level for a population inversion to occur (Ratanavis et al.

2009). However, in the author's view this single data point is insufficient to confirm cascade lasing - and even if it were - it is so close to the damage threshold of the available optics that it would be of no benefit to a reliable system. To investigate this further, one would need to redesign the system to obtain higher pump fluences in the HBr while preventing optical damage to the laser components.

The HBr Master Oscillator Power Amplifier (MOPA) approach performed admirably, with the amplifier delivering up to 10.3 mJ of output energy when seeded with 2.0 mJ and pumped with 184 mJ of energy. This presented a gain factor of more than 5, but was not reproducible, probably due to gradual degradation of the optical components which were in direct contact with the HBr gas. A small-signal gain of over 30 for a 0.2 mJ seed and a near-saturated gain factor of 4 indicated that this amplifier performed well, even by the standards of bulk solid-state amplifiers as reported upon in Chapter 5.

7.5 Conclusion

Significant improvements were made over the results reported on in (Botha et al. 2009). The oscillator delivered a maximum of 5.4 mJ of 4 µm energy which is the highest energy ever reported from an optically-pumped HBr molecular laser. The amplifier delivered up to 10.3 mJ when seeded with 2 mJ from the oscillator, illustrating that a MOPA approach to further scale energy output of optically pumped HBr systems is feasible. The maximum 4 µm laser energy was 4 times higher than the previously reported work when using a master oscillator power amplifier combination.

It was also shown experimentally that an intra-cavity CO_2 absorption cell could force the HBr laser to oscillate on three lines that were all inside the atmospheric transmission window. With the added ability of wavelength tuning demonstrated in the next chapter, optically-pumped HBr systems show promise, if given sufficient attention.

8 Design & Development of an Optically Pumped Tuneable HBr Laser

An optically pumped tuneable HBr molecular laser has been demonstrated for the first time. The pump source was a single-frequency Ho:YLF laser and amplifier system which was locked to the 2064 nm absorption line of HBr. Laser oscillation was demonstrated on nineteen molecular transition lines including both the R-branch (3870 nm to 4015 nm) and the P-branch (4070 nm to 4453 nm) by the use of an intra-cavity diffraction grating. This was the first time lasing on the R-branch of HBr has been demonstrated. The highest output energy for the given input energy was 2.4 mJ at 4134 nm.

8.1 Introduction

In the previous chapter it was stated that one reason for the slow progress on optically pumped HBr lasers is the limited availability of suitable narrow-band high-energy pump lasers that must be stabilized to an absorption line of HBr. To solve this problem we developed an injection-seeded single-frequency Ho:YLF ring laser as well as appropriate amplifier systems. The ring laser was locked to the P(9) HBr absorption line at 2064.12 nm using a reference absorption cell with a Pound-Drever-Hall feedback loop (Bollig et al. 2009). The ring laser delivered output energies of up to 72 mJ in ~350 ns long pulses at a pulse repetition rate of 50 Hz (Bollig et al. 2009). These laser pulses were amplified to 200 mJ with a Ho:YLF & Ho:LuLF slab amplifier (W. Koen, H. Strauss, et al. 2010) which was pumped by a 189 W Tm:YLF slab laser (W. Koen,

H. J. Strauss, et al. 2010). Subsequent to this a two-crystal double-pass Ho:YLF slab laser was developed which delivered 330 mJ single-frequency laser pulses at a 50 Hz pulse repetition rate, as discussed in Chapter 5.

Another challenge is that while the emission lines of HBr lie within the 3-5 µm atmospheric transmission window as shown in Figure 79, most of the P-Branch transitions are within a CO_2 absorption band which limit HBr lasers' usefulness for applications requiring good free space propagation. The R-branch transitions are highly desirable though, since they fall well within the atmospheric transmission window, but no lasing has been demonstrated on the R-branch laser lines up until this work (Koen et al. 2014). This therefore makes a wavelength selectable HBr laser desirable in order to alleviate or avoid potential atmospheric absorption (Kletecka et al. 2004)

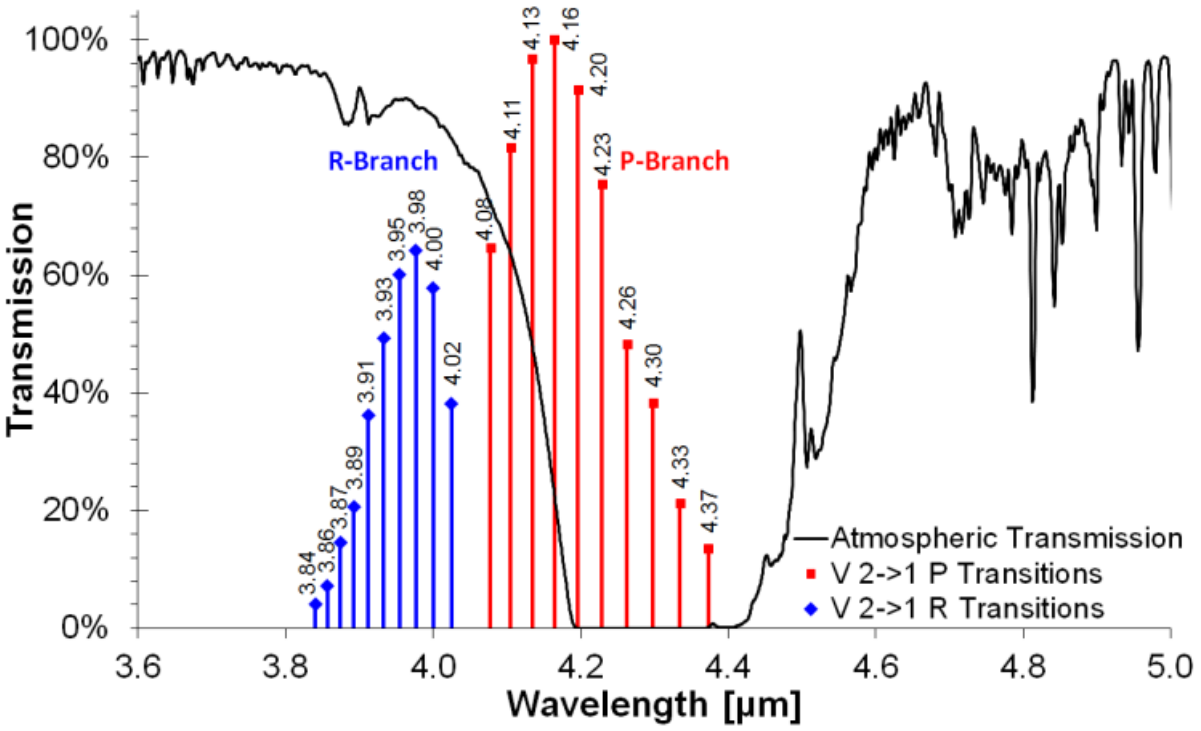

Figure 79: Atmospheric transmission in the 3.6 to 5 µm region (from space to ground at an altitude of 4.2 km) using the program IRTRANS4 (UKIRT 2013) with the emission cross sections of v=2 to v=1 transitions of HBr (Miller et al. 1994) superimposed upon it. The cross sections have been normalized such that the strongest line, P(4), equals 100 %.

and improve the prospects of using HBr lasers for applications requiring free space propagation. In this chapter the design and development of a tuneable HBr laser using an intra-cavity diffraction grating to select the HBr laser wavelength is presented. This enabled oscillation on most of the P-branch lines individually as well as the R-branch laser transitions shown in Figure 79 by merely adjusting the diffraction grating's angle.

Section 8.2 of this chapter presents the tuneable HBr laser design and setup as well as the 2 µm single-frequency pump source. The experimental results obtained from the tuneable HBr laser are presented and discussed in Section 8.3, with conclusions drawn in Section 8.4.

8.2 Experimental design and setup

The single-frequency 2 µm ring-laser and amplifier systems resided on one laboratory table while the HBr system was built on an adjacent table, as shown in Figure 59. The various aspects of the setup are discussed in the subsections below.

8.2.1 The single-frequency pump source

The HBr oscillator was optically end-pumped with 2064.12 nm pulses from the single-frequency Ho:YLF slab amplifier previously discribed in Chapter 5. This allowed pumping and subsequent lasing of a single isotope of HBr at a time as the corresponding isotope energy level mismatch between ^{79}HBr and ^{81}HBr is about 50 GHz (Ratanavis et al. 2009). With regards to the P(9) linewidth; it was previously found that a value of 430 MHz for the Doppler broadening and 8 MHz per torr for the pressure broadening gave the best fit to the experimental results (Botha et al. 2009). Pumping on the P(9) transition at 2064.12 nm has the added advantage that the pump source itself also coincides with an atmospheric transmission window. This design choice is discussed in greater detail in Section 7.2.1 of Chapter 7.

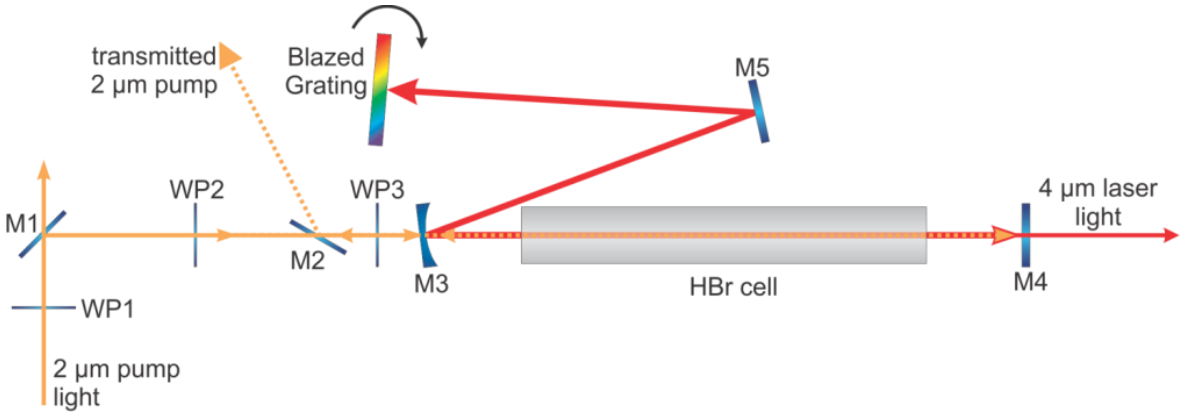

Figure 80: Experimental setup of the tuneable HBr oscillator.

The 2 µm pump pulses were approximately 360 ns long and had a maximum energy of up to 330 mJ at a 50 Hz pulse repetition rate. The 2 µm pump beam exiting the amplifier was astigmatic due to its slab configuration and was shaped with cylindrical lenses into a circular, low astigmatic beam, before being steered across several metres from the one optical table to the other, into the

HBr setup. This is discussed in greater detail in Chapter 5 and Sections 7.2.1 & 7.2.3 of Chapter 7.

8.2.2 Design and setup of the tuneable HBr laser

A diagram of the HBr oscillator setup is shown in Figure 80. The linearly polarised 2 µm pump light was split in two with a variable beam splitter consisting of a half-wave plate (WP1) and a polarisation-dependent 45° mirror (M1) that was highly reflective for the vertical polarisation (HRs) and highly transmissive for the horizontal polarisation (HTp). By rotating the first half-wave plate (WP1) the pump energy incident on the oscillator could be adjusted. For this work the incident oscillator pump power was set to 50 mJ per pulse (similar to the previous chapter so that a comparison could be made between the results) with the remaining 280 mJ of transmitted pump light earmarked for an HBr amplifier stage.

The following pump scheme was designed and implemented to prevent back-reflections into the 2 µm pump system while allowing good pump absorption in the HBr oscillator cell. A half-wave plate (WP2) changed the vertically-polarised light to horizontally-polarised. It was then transmitted through a Brewster-type thin film polariser (M2) and quarter-wave plate (WP3) after which the circularly polarised pump light was double-passed through the oscillator for maximum pump absorption by reflecting off the flat 4 µm output coupler mirror (M4) that was coated to be highly reflective for 2 µm. Back-reflections into the Ho:YLF amplifier were prevented by the quarter-wave plate (WP3) changing the circularly polarised 2 µm pump light to vertical linearly polarised light on the second pass, which was then reflected by the plate polariser (M2). The transmitted pump light could then be measured with a power meter or dumped on to a heat sink.

The HBr oscillator design was based on that presented in Chapter 7 as the pump setup was the same. The resonator output coupler mirror (M4), in addition to being highly reflective at 2 µm (for double-passing the pump light) had a reflectivity of approximately 80% around 4 µm. The dichroic input coupler mirror (M3) had a 5 m concave radius of curvature and was coated to be highly reflective at 4 µm and highly transmissive at 2 µm. The pump mirror was slightly tilted in order to reflect light onto a flat HR 4 µm, HT 2 µm mirror (M5) which in turn reflected onto the gold plane ruled diffraction grating (300 lines/mm) which was blazed at 4.29 µm. The specified grating reflectivity varied from 95 % at 3.8 µm to 85 % at 4.5 µm for the s-plane, and 47 % at

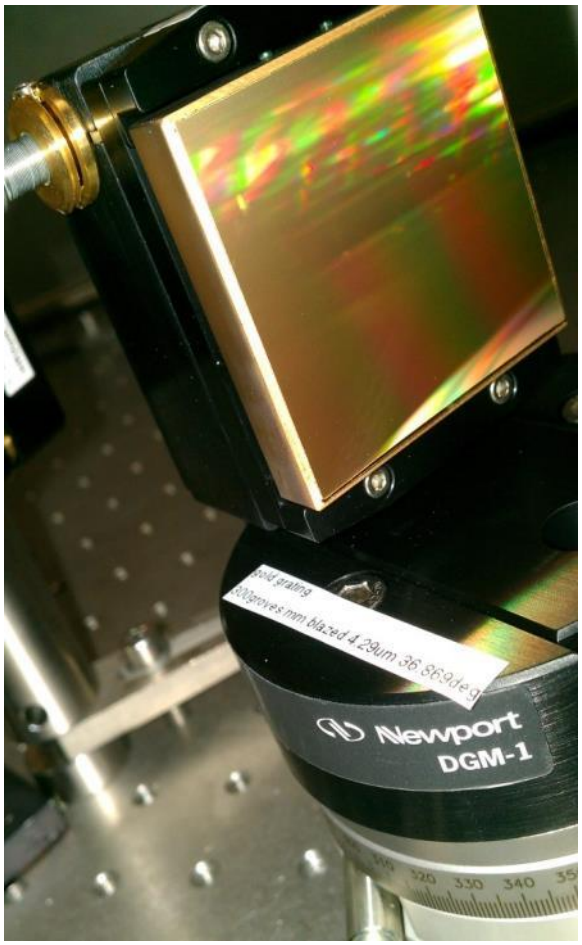

Figure 81: A photo of the ruled intra-cavity grating mounted in a rotation stage.

3.8 µm to 33 % at 4.5 µm for the p-plane respectively. This was the most appropriate grating that could be sourced for the wavelength range of interest. The cavity was designed that the diffraction grating acted as the end-mirror of the HBr resonator. The wavelength could then be selected by rotating the grating.

The HBr gas was contained in a 510 mm long absorption cell at a pressure of 73 mBar. The gas cell's outside wall was kept at a 20°C set point. No buffer gas was used and the cell contained both isotopes of HBr (assumed to be the natural occurring ratio of 50.7 % ^{79}HBr and 49.3 % ^{81}HBr). At 73 mBar, approximately 76 % (38 mJ) of the pump light was absorbed under lasing conditions. The HBr gas cell was placed 26 mm away from the output coupler mirror (M4). The cell windows were made from Cleartran®, with anti-reflective coatings for both 2 µm and 4 µm light. The pump beam was fairly collimated over the length of the tube and had an average radius of 1.5 mm, which matched the calculated fundamental resonator mode, as previously discussed in Chapter 7.

Interference from H_2O and CO_2 absorption lines was lessened by enclosing the oscillator in a box which was flushed with commercially available synthetic dry air containing no H_2O or CO_2 as previous work suggested this might be prudent in order to observe as many HBr laser transitions possible which reside in absorption bands (Experiments were done with the relative humidity below 5 %). The laser's spectral properties were measured using a *Jarrel Ash* monochromator with a photosensitive detector, while the output power was measured simultaneously with a *Gentec* power meter.

8.3 Experimental results and discussion

A total of 19 laser transitions were individually observed on the P- and R-branches. To the author's knowledge this is the first time that oscillation was observed on the R-branch of HBr. The measured output energy for each line is shown in Figure 82 and a summary of the lasing wavelengths and observed and their respective output energies are given in Table 10 at the end of this section.

Eleven of the observed lines belonged to the P-branch of the v = 2 to v = 1 transition, ranging from 4070 nm up to 4453 nm. This represented lasing on almost all transitions from P(1) to P(12), with a conspicuous absence of P(6) which could have been expected at 4229 nm. Despite using synthetic dry air containing no CO_2 to flush the laser enclosure, losses caused by residual carbon dioxide (which could not be measured with the given equipment) prevented this line from lasing

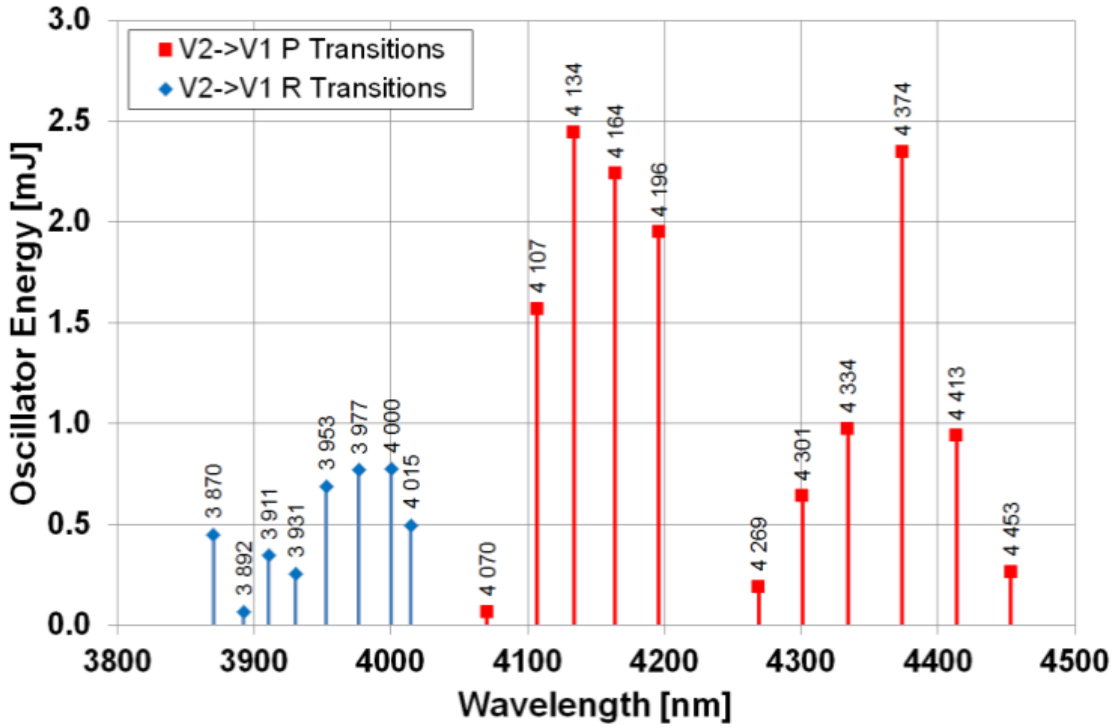

Figure 82: Laser transition lines observed by tuning the resonator cavity with the optical grating. The output energy measured for each laser transition is depicted by the square (P-branch) and diamond markers (R-branch).

in addition to affecting energy output of various other P-branch transitions.

Lasing on the P(3) (4134 nm), P(4) (4164 nm) and P(10) (4374 nm) transitions were especially strong compared to the other transitions, with output energies all exceeding 2 mJ per pulse. The highest output energy for the set 50 mJ input energy was 2.4 mJ at 4134 nm, comparing very well with the non-wavelength selected laser reported by our group previously (Botha et al. 2009) which delivered 2.5 mJ for 60 mJ of pump light at an HBr pressure of 60 mBar.

Lasing on eight R-branch transitions was also observed, a first according to literature (Weber 2000). Lasing was demonstrated from R(0) (4015 nm) to R(7) (3870 nm). In general, the laser output energy was lower when compared to lasing on a P-branch transition, as expected from the lower Einstein A-coefficients (Miller et al. 1994). The highest output energy for lasing in the R-branch was obtained from R(1) (4000 nm), R(2) (3977 nm) and R(3) (3953 nm) with a typical energy per pulse of 0.75 mJ.

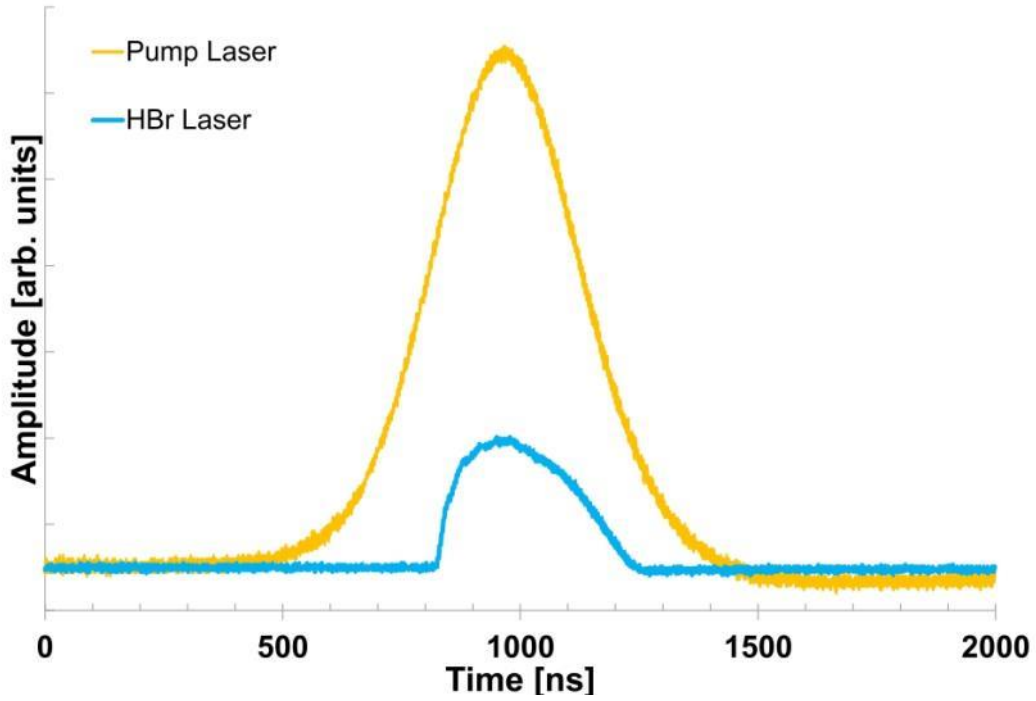

Figure 83: Temporal pulse traces of the pump laser (yellow) and the HBr laser (cyan). The pump and laser pulse intensities are arbitrary and not relative to each other.

Figure 83 shows a temporal pulse profile of the pump and HBr laser. The temporal behaviour of the laser was dependent on its output wavelength, but was not fully characterised. The pump duration (FWHM) was approximately 370 ns and the output pulse width of the HBr laser was 310 ns. The HBr pulse shape is comparable to previous work reported upon in (Botha et al. 2009) and Chapter 7.

Table 10: HBr laser transitions observed from vibrational level 2 to 1.

P branch Transitions	Measured Wavelength [nm]	Output Energy [mJ]	R branch Transitions	Measured Wavelength [nm]	Output Energy [mJ]
P(1)	4070	0.07	R(0)	4015	0.5
P(2)	4107	1.57	R(1)	4000	0.78
P(3)	4134	2.24	R(2)	3977	0.77
P(4)	4164	2.24	R(3)	3953	0.69
P(5)	4196	1.95	R(4)	3931	0.26
P(6)	not observed	-	R(5)	3911	0.35
P(7)	4269	0.19	R(6)	3892	0.07
P(8)	4301	0.64	R(7)	3870	0.45
P(9)	4334	0.98			
P(10)	4374	2.35			
P(11)	4413	0.94			
P(12)	4453	0.27			

Apart from transitions P(1) and R(0), the measured wavelengths correspond well to theory and literature (Miller et al. 1994), (Botha et al. 2009). It should be possible to demonstrate lasing on even more transitions by pumping harder as well as implementing a lower loss cavity by using an intra-cavity prism for wavelength selection instead of the optical grating. However, despite the extra loss introduced by the grating, the maximum conversion efficiency of 6.3 % with regard to absorbed pump power fell within the 5–12 % region reported upon in (Botha et al. 2009). Efficiency could be further increased if cascade lasing occurs from the v=1 to v=0 transition, but

this is particularly difficult as the pump laser does not sufficiently empty the *v*=0 level for a population inversion to occur (Ratanavis et al. 2009). Cascade lasing was not observed in this experiment as much higher pump levels than what was used would be required and the losses introduced by the intra-cavity grating were too high. Unfortunately, corrosive damage of the HBr cell windows prevented further experimentation with this setup (See Figure 84).

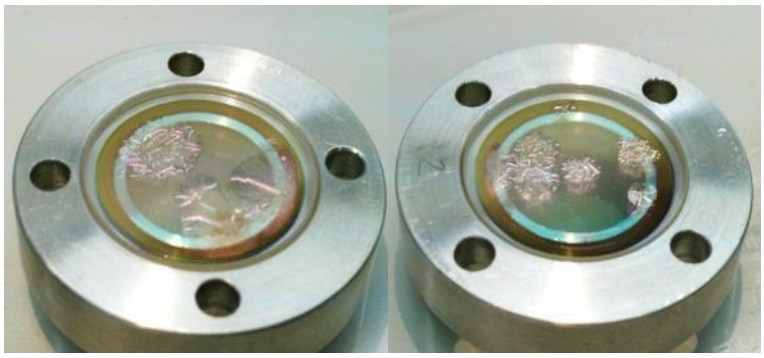

Figure 84: The HBr cell's AR coated windows damaged by corrosion.

8.4 Conclusion

In summary, tuneable mid-infrared oscillation in the 3 to 5 µm region was demonstrated for HBr on nineteen molecular transition lines for both the R-branch (from 3870 nm to 4014 nm) and the P-branch (from 4070 nm to 4453 nm). The highest output energy for the given input energy was 2.4 mJ at 4134 nm when pumped with 50 mJ. It is also noteworthy that this demonstration represents a tuning range of 583 nm, with numerous transitions below the strong CO_2 atmospheric absorption feature between 4.2 and 4.4 µm. This makes HBr a feasible alternative to optical parametric generation for free space propagation, with good energy scaling potential, as previously demonstrated in Chapter 7.

9 Closing Remarks

This chapter concludes the dissertation by providing a summary of the significant experimental results reported on in the preceding chapters. The work is briefly reviewed in the context of results reported prior to this work. The various challenges experienced and how they were overcome are discussed. Conclusions are drawn and recommendations given with regard to improvements that can be made in future work. An outlook on these technologies' future is also provided.

9.1 Summary of significant results

9.1.1 Efficient 45 W Ho:YLF Laser Pumped by a Tm:fibre Laser

A compact and efficient high-power Ho:YLF laser which was pumped by a commercially available thulium fibre laser was presented in Chapter 3. The 2064 nm holmium laser delivered 45.1 W in a near diffraction-limited beam when pumped with 84.7 W of 1940 nm unpolarised laser light. This record optical-to-optical efficiency of 53 % compared favourably with similar Ho:YAG lasers which are historically more efficient than Ho:YLF lasers. These high average output powers in conjunction with high optical-to-optical efficiencies from a three level laser were made possible with a design approach allowing high pump intensities by using a small pump diameter, while obtaining good unpolarised pump light absorption from birefringent crystals, whose absorption is highly polarisation dependent, through the use of a-cut Ho:YLF crystals.

While this approach proved highly successful, in this instance for cw and high repetition rate Q-switched operation, power scaling of this stand-alone laser using multiple intra-cavity crystals would ultimately be limited by optical damage at lower repetition rates and higher pump powers due to the increased fluence. A good approach to scale these outputs further would be to implement one or more amplifier stages, as was demonstrated subsequently in Chapter 4.

9.1.2 60 W Ho:YLF Oscillator-Amplifier System

In Chapter 4 a compact Ho:YLF oscillator–amplifier system producing 60.2 W of output power at 2064 nm, when pumped by two 54 W unpolarised Tm:fibre lasers, was developed and demonstrated. The seed laser of the MOPA delivered a maximum output of 24 W with an M^2 of 1.06. The two-crystal, single-pass amplifier delivered a gain of 2.5, and an M^2 of 1.09. The amplifier utilised the transmitted pump from the seed's single fibre laser in addition to a second fibre laser, resulting in an optical-to-optical efficiency of 55.5%. Under Q-switched operation, laser pulse lengths of between 43 and 113 ns at repetition rates from 15 to 40 kHz were measured respectively.

This system scaled the pumping scheme demonstrated in the previous chapter further using a multiple crystal amplifier stage which not only effectively used the unpolarised pump light from its fibre laser but also the unused pump light transmitted by the seed laser. This approach led to a compact portable system with high optical-to-optical efficiencies, which also included an optical switching system and two state of the art optical parametric oscillators (OPO's) that were pumped by the Ho:YLF MOPA (The OPO's were not presented in this dissertation, but may be reported on in later publications).

Further work on this MOPA design would entail a more engineering-based approach, ruggedizing the system while striving to make it even more compact. An investigation in passive cooling

techniques might also prove beneficial as this may improve the portability and thus versatility of such a system, opening up various applications for such a system in various industries. Passive cooling should not prove too challenging as the heat load comprised of less than 15 W from the laser's AOM in addition to the unconverted pump light which was less than 50 W.

9.1.3 High-energy, Single-frequency Ho:YLF Slab Amplifier

Chapter 5 contained collaborative work done by the author and his colleagues. A Ho:YLF slab amplifier which delivered ~350 ns long single-frequency pulses of up to 330 mJ at 2064 nm, with a maximum M^2 of 1.5 at a PRF of 50 Hz was developed. The amplifier was end-pumped with an in-house developed diode-pumped Tm:YLF slab laser and seeded with up to 50 mJ of single-frequency laser pulses from an injection-seeded Ho:YLF ring-laser. For effective pumping of the Ho:YLF amplifier crystals the Tm:YLF laser had to be redesigned to efficiently operate at 1890 nm, taking various issues such as polarisation-dependent cross sections, thermal lensing, and cavity losses into account.

This amplifier system was used to pump the HBr systems which were presented in the subsequent Chapters 7 and 8 and illustrated how one may go from one domain of laser research to another (namely bulk solid-state to optically-pumped molecular lasers) in order to achieve a specific goal; which in this case was the generation of laser light in the 3-5 µm region. It should also be noted that the complete Ho:YLF ring-laser and 330 mJ amplifier system were in nearly daily use over numerous months (and years in the case of the ring-laser) without failing.

9.1.4 Optically Pumped Mid-Infrared HBr Master Oscillator Power Amplifier System

This dissertation also included extensive work done on a lesser studied type of laser; namely mid-infrared optically pumped molecular gas lasers based on HBr. In Chapter 7 the world's first optically end-pumped HBr master oscillator power amplifier was developed and demonstrated. This HBr system was pumped by the 330 mJ single-frequency amplifier reported on in Chapter 5. The oscillator alone produced record output energies of up to 5.4 mJ per pulse of laser output at a PRF of 50 Hz, twice that of the previous reported record. The amplifier produced up to 10.3 mJ at 4.20 and 4.34 µm when seeded with 2 mJ of laser light from the oscillator. With near-saturated gains of between 4 and 5 obtained from a single-pass pump, single-pass seed amplifier, energy scaling using optically pumped HBr gas amplifiers seems a very promising approach for laser light in the 4 µm region.

Wavelength selection in HBr lasers with the use of an intra-cavity CO_2 absorption cell was also demonstrated experimentally for the first time, forcing the oscillator to emit at 3.89, 4.13 and 4.16 µm simultaneously, with a maximum output energy of 6.5 mJ per pulse after amplification.

9.1.5 Optically Pumped Tuneable HBr Laser

In the last experimental chapter of the dissertation (Chapter 8), an optically pumped tuneable HBr molecular laser was developed and demonstrated for the first time. The pump source was the same single-frequency Ho:YLF laser and amplifier system reported on in Chapter 5 which was locked to the 2064.12 nm absorption line of HBr. With the use of an intra-cavity ruled diffraction grating, laser oscillation was demonstrated on nineteen molecular transition lines including both the R-branch (3870 nm to 4015 nm) and the P-branch (4070 nm to 4453 nm). This was also the first time lasing on the R-branch of a molecular HBr laser has been demonstrated experimentally.

The highest output energy for the given input energy was 2.4 mJ at 4134 nm, which compared very favourably to the highest energy from a free running HBr OPML reported in (Botha et al. 2009). I may also comment that the ease of tuning the HBr laser by merely adjusting the diffraction grating angle was very similar to commercial tuneable CO_2 lasers I have worked with in the past; making this a promising versatile laser source in the 3.8-4.5 µm region.

Unfortunately it was also observed that prolonged exposure to HBr gas degraded the AR-coated HBr cell windows and stainless steel cells. This may be avoided by rather using Brewster windows in future and exclusively using materials that resist corrosion caused by HBr, as reported in (Rutt 1979).

9.2 Conclusion

In the beginning of the dissertation it was stated that the need remains to improve mid-infrared laser sources in the 2-5 µm region with regard to size, brightness, efficiency, and wavelength range. Throughout this dissertation these issues were addressed by designing and implementing a diverse selection of novel lasers and amplifiers, both bulk solid-state (Tm:YLF & Ho:YLF) as well as molecular (optically pumped HBr).

Considering the high output powers, high efficiencies and compact form factors of the Ho:YLF laser systems which were presented in this dissertation, it is clear that this technology has been researched, developed and improved to the point where commercialization of these 2 µm laser sources should be considered in earnest. Such new coherent high-energy, high-power sources at 2 µm will without a doubt be of great benefit to both the research community and industry. The pump, resonator, and amplifier design approaches which led to these results could also be applied to other promising bulk solid-state laser materials, particularly those exhibiting quasi-three level behaviour, as they may benefit the most.

When compared to the bulk solid-state laser systems reported in this dissertation; and the model predictions made by various other groups, it is apparent that optically pumped molecular HBr lasers and amplifiers require significantly more research to reach their full potential. The promising results, especially with regards to the first optically pumped HBr amplifier as well as the first tuneable HBr oscillator, indicate that the research community may soon have a new versatile high-energy laser source in the 4 μm region should this work be pursued further.

However, various challenges such as the lack of readily available narrow-band pump sources, lower than anticipated conversion efficiencies, and the corrosive nature of HBr need to be addressed. This may be as simple as using HBr in conjunction with resilient components and architectures, such as HBr-flushed holey fibres or HBr-filled Ho-doped crystal fibres (a hybrid co-doped approach that may have some merit), or more traditional waveguides that can tolerate the fluences and absorption lengths required for efficient operation. The prospects are only limited by our ingenuity, and Physics itself.

10 References

Bai, Y. et al., 2009. High Repetition Rate and Frequency Stabilized Ho:YLF Laser for CO2 Differential Absorption Lidar. In *Advanced Solid-State Photonics*. p. WB22.

Bai, Y. et al., 2007. Highly efficient Q-switched Ho:YLF laser pumped by Tm:fiber laser. In *Conference on Lasers and Electro-Optics*. p. CTuN5.

Bai, Y. et al., 2011. Tm: Fiber Laser Resonantly-Pumped Ho: YLF Laser for air/space borne lidar application. In *Fiber Laser Applications*. p. FWC3.

Bollig, C. et al., 2009. 70 mJ Single-Frequency Q Switched Ho: YLF Ring Laser-Amplifier System Pumped by a Single 82-W Tm Fibre Laser. *Middle-Infrared Coherent Sources, Trouville, France*, pp.8–12.

Botha, L. et al., 2009. Ho: YLF pumped HBr laser. *Optics express*, 17(22), pp.20615–20622.

Burtsev, A. et al., 2005. Lasing of molecular HBr in the four micron region pumped by a DF-laser. In J. Kodymova, ed. *XV International Symposium on Gas Flow, Chemical Lasers, and High-Power Lasers*. Proc. of SPIE Vol. 5777, pp. 528–530.

Chang, T.Y. & Wood, O.R., 1972. Optically pumped atmospheric CO2 laser. *Applied Physics Letters*, 21, pp.19–21.

Chang, Y.-A. & Kuo, Y.-K., 2002. Optical performance of Ho: YLF Q-switched Tm: YAG laser system. In *Photonics Asia 2002*. pp. 510–521.

Chicklis, E.P. et al., 1971. High-Efficiency Room Temperature 2.06 micron Laser using sensitized Ho:YLF . *Applied Physics Letters*, 19(119).

Clarkson, W., 2001. Thermal effects and their mitigation in end-pumped solid-state lasers. *Journal of Physics D: Applied Physics*, 34(16), p.2381.

Collett, O.J.P., 2013. *Modelling of end-pumped Ho:YLF amplifiers*.

Dergachev, A. et al., 2007. 3.4 micron ZGP RISTRA nanosecond optical parametric oscillator pumped by a 2.05 micron Ho: YLF MOPA system. *Optics express*, 15(22), pp.14404–14413.

Dergachev, A. et al., 2008. High-power, high-energy ZGP OPA pumped by a 2.05 micron Ho: YLF MOPA system. In *Lasers and Applications in Science and Engineering*. pp. 687507–687507.

Dergachev, A. & Moulton, P.F., 2003. High-power, high-energy diode-pumped Tm:YLF-Ho:YLF-ZGP laser system. In *Advanced Solid-State Photonics*. p. 137.

Dergachev, A., Moulton, P.F. & Drake, T.E., 2005. High-power, high-energy Ho: YLF laser pumped with Tm: fiber laser. In *Advanced Solid-State Photonics*. p. 608.

Deutsch, T.F., 1967. Molecular laser action in hydrogen and deuterium halides. *Applied Physics Letters*, 10, pp.234–236.

Ede, A., 2006. *The chemical element: a historical perspective*, Greenwood Publishing Group.

Elder, I., 2009. Thulium fibre laser pumped mid-IR source. In *SPIE Defense, Security, and Sensing*. p. 73250I–73250I.

Esser, M., 2010. *Mid-infrared diode-pumped solid-state lasers*.

Esser, M.D. et al., 2009. Diode-end-pumped Tm: GdVO4 laser operating at 1818 and 1915 nm. *Applied Physics B*, 97(2), pp.351–356.

Fan, T.Y. et al., 1988. Spectroscopy and diode laser-pumped operation of Tm,Ho:YAG. *IEEE Journal of Quantum Electronics*, 24(6), pp.924–933.

Fan, T.Y. & Byer, R.L., 1987. Modeling and CW operation of a quasi-three-level 946 nm Nd: YAG laser. *Quantum Electronics, IEEE Journal of*, 23(5), pp.605–612.

Feaver, R., Peterson, R. & Powers, P., 2013. Longwave-IR optical parametric oscillator in orientation-patterned GaAs pumped by a 2 micron Tm, Ho: YLF laser. *Optics express*, 21(13), pp.16104–16110.

Fonnum, H., Lippert, E. & Haakestad, M.W., 2013. 550 mJ Q-switched cryogenic Ho: YLF oscillator pumped with a 100 W Tm: fiber laser. *Optics letters*, 38(11), pp.1884–1886.

Gibert, F. et al., 2014. 2 micron high-power multiple-frequency single-mode Q-switched Ho: YLF laser for DIAL application. *Applied Physics B*, 116, pp.967–976.

Gillies, A. et al., 2000. PSST! Photonics Simulation Software for Teaching.

Hayward, R., Clarkson, W. & Hanna, D., 2000. High-power room-temperature intracavity-pumped Ho: YAG laser. In *Lasers and Electro-Optics Europe, 2000. Conference Digest. 2000 Conference on*. p. 1–pp.

Inrad, 2015. Inrad ZGP Data Sheet. Available at: www.inradoptics.com [Accessed 2015].

IPG, 2015. Thulium Fiber Laser Specifications. Available at: http://www.ipgphotonics.com/products_tlm_flm.htm [Accessed 2015].

Jacobs, C. et al., 2009. Electronic Stabilization of Continuous-Wave and Pulsed Lasers Based on Macroscopic Rate-Equation Modelling. *IEEE journal of quantum electronics*, 45(9-10), pp.1221–1231.

Jacobs, C., 2013a. EXAG: Excel ABCD Gaussian Beam Propagation III v0.10 closed BETA software.

Jacobs, C., 2013b. SimuLaser modelling library.

Johnson, L., Boyd, G. & Nassau, K., 1962a. Optical maser characteristics of Ho3+ in CaWO4. *Proc. IRE*, 50(87).

Johnson, L., Boyd, G. & Nassau, K., 1962b. Optical maser characteristics of Tm3+ in CaWO4. *Proc. IRE*, 50(86).

Kean, S., 2011. *The Disappearing Spoon...and other true tales from the Periodic Table*, Random House.

Kieleck, C. et al., 2015. 6.5 W mid-infrared ZnGeP2 parametric oscillator directly pumped by a Q-switched Tm3+-doped single oscillator fiber laser. In *SPIE LASE*. p. 93470O–93470O.

Kletecka, C. et al., 2004. Cascade lasing of molecular HBr in the four micron region pumped by a Nd:YAG laser. *Quantum Electronics, IEEE Journal of*, 40(10), pp.1471–1477.

Kletecka, C. et al., 2002. Cascade lasing of molecular HBr in the four micron region pumped by a Nd:YAG laser. In C.R. Phipps, ed. *High-Power Laser Ablation IV*. Proc. of SPIE Vol. 4760, pp. 594–601.

Koen, W., Strauss, H., et al., 2010. 200mJ Single Frequency Ho:YLF & Ho:LuLF Slab Amplifier System. *Hamburg, Germany*.

Koen, W. et al., 2015. 60W Ho: YLF oscillator-amplifier system. In *SPIE LASE*. p. 93421Y–93421Y.

Koen, W. et al., 2010. Compact fibre-laser-pumped Ho: YLF oscillator-amplifier system. *Applied Physics B*, 99(1), pp.101–106.

Koen, W., Strauss, H.J., et al., 2010. High-power diode-end-pumped Tm:YLF slab laser delivering 189 W at. In *The 55th Annual Conference of the South African Institute of Physics*. p. 205.

Koen, W. et al., 2014. Optically pumped tunable HBr laser in the mid-infrared region. *Opt. Lett.*, 39(12), pp.3563–3566. Available at: http://ol.osa.org/abstract.cfm?URI=ol-39-12-3563.

Koen, W.S. et al., 2013. Efficient Ho:YLF Laser Pumped by a Tm: fiber Laser. In *Mid-Infrared Coherent Sources*. p. MW1C–6.

Koen, W.S., 2010. *End-pumped solid-state lasers*.

Kwiatkowski, J. et al., 2012. A highly efficient resonantly pumped Ho:YAG laser. In *SPIE Photonics Europe*. p. 84331J–84331J.

Kwiatkowski, J., Zendzian, W., et al., 2014. Continuous-wave and high repetition rate Q-switched operation of Ho: YLF laser in-band pumped by a linearly polarized Tm: fiber laser. *Optics \& Laser Technology*, 63, pp.66–69.

Kwiatkowski, J., Swiderski, J., et al., 2014. Resonantly pumped, Q-switched Ho: YLF laser with output energy of 5 mJ at 1 kHz. *Photonics Letters of Poland*, 6(1), p.pp–5.

Kwiatkowski, J., Jabczynski, J.K. & Zendzian, W., 2015. An efficient continuous-wave and Q-switched single-pass two-stage Ho:YLF MOPA system. *Optics & Laser Technology*, 67, pp.93–97.

Lagatsky, A. et al., 2011. Femtosecond Tm-Ho codoped double tungstate lasers around 2060 nm. In *Advanced Solid-State Photonics*. p. ATuA3.

Lippert, E., Fonnum, H., Arisholm, G., et al., 2010. A 22-watt mid-infrared optical parametric oscillator with V-shaped 3-mirror ring resonator. *Optics express*, 18(25), pp.26475–26483.

Lippert, E., Fonnum, H. & Stenersen, K., 2010. High power multi-wavelength infrared source. In *Security + Defence*. p. 78360D–78360D.

Miller, H.C., Radzykewycz Jr, D. & Hager, G., 1994. An optically pumped mid-infrared HBr laser. *Quantum Electronics, IEEE Journal of*, 30(10), pp.2395–2400.

Nicholson, J. & Neumann, D., 2001. *Cost effective, scalable optically pumped molecular laser*, AFRL.

Payne, S.A. et al., 1992. Infrared cross-section measurements for crystals doped with Er 3+, Tm 3+, and Ho 3+. *Quantum Electronics, IEEE Journal of*, 28(11), pp.2619–2630.

Pires, H. et al., 2015. Ultrashort pulse generation in the mid-IR. *Progress in Quantum Electronics*, 43, pp.1–30.

Ratanavis, A. et al., 2008. Optically pumped HBr gas laser operating in regions of high atmospheric transmission. In C.R. Phipps, ed. *High Power Laser Ablation VII*. Proc. of SPIE vol. 7005.

Ratanavis, A., 2011. Optically pumped molecular gas lasers in mid infrared region. *The Journal of Applied Science*, 10(2), pp.95–102.

Ratanavis, A. et al., 2009. Performance and spectral tuning of optically overtone pumped molecular lasers. *Quantum Electronics, IEEE Journal of*, 45(5), pp.488–498.

Rustad, G. & Stenersen, K., 1996. Modeling of laser-pumped Tm and Ho lasers accounting for upconversion and ground-state depletion. *Quantum Electronics, IEEE Journal of*, 32(9), pp.1645–1656.

Rutt, H., 1979. A high-energy hydrogen bromide laser. *Journal of Physics D: Applied Physics*, 12(3), p.345.

Sato, A., Asai, K. & Mizutani, K., 2004. Lasing characteristics and optimizations of a diode-side-pumped Tm, Ho: GdVO< sub> 4</sub> laser. *Optics letters*, 29(8), pp.836–838.

Schellhorn, M., 2011. A comparison of resonantly pumped Ho: YLF and Ho: LLF lasers in CW and Q-switched operation. In *Advanced Solid-State Photonics*. p. AWA8.

Schellhorn, M. et al., 2007. High repetition rate mid-infrared laser source. *Comptes Rendus Physique*, 8(10), pp.1151–1161.

Schellhorn, M. & Eichhorn, M., 2015. Ho: YLF non-planar ring laser with fractional image rotation. In *SPIE LASE*. p. 93420D–93420D.

Schellhorn, M., Ngcobo, S. & Bollig, C., 2009. High-power diode-pumped Tm: YLF slab laser. *Applied Physics B*, 94(2), pp.195–198.

Shen, D., Cooper, L. & Clarkson, W., 2004. Highly efficient Ho: YLF and Ho: YAG lasers pumped by Tm-doped silica fibre laser.

So, S. et al., 2006. A power-scaling strategy for longitudinally diode-pumped Tm: YLF lasers. *Applied Physics B*, 84(3), pp.389–393.

Sorokina, I.T. & Vodopyanov, K.L., 2003. *Solid-state mid-infrared laser sources*, Springer Science & Business Media.

Stoneman, R. & Esterowitz, L., 1995. Efficient 1.94 micron Tm: YALO laser. *Selected Topics in Quantum Electronics, IEEE Journal of*, 1(1), pp.78–81.

Strauss, H. et al., 2013. 330 mJ single-frequency Ho: YLF slab amplifier. *Optics letters*, 38(7), pp.1022–1024.

Strauss, H. et al., 2011. Ho: YLF & Ho: LuLF slab amplifier system delivering 200 mJ, 2 micron single-frequency pulses. *Optics express*, 19(15), pp.13974–13979.

Urata, Y. et al., 2005. Diode-pumped continuous wave Tm, Ho: GdVO 4 laser in room temperature. In *Lasers and Electro-Optics Europe, 2005. CLEO/Europe. 2005 Conference on*. p. 57.

Walsh, B.M., Barnes, N.P. & Di Bartolo, B., 1998. Branching ratios, cross sections, and radiative lifetimes of rare earth ions in solids: application to Tm3+ and Ho3+ ions in LiYF4. *Journal of applied physics*, 83(5), pp.2772–2787.

Weber, M.J., 2000. *Handbook of lasers*, CRC press.

Zhang, X. et al., 2013. Passively Q-switched Tm, Ho: LuLiF4 laser with near constant pulse energy and duration. *Applied Physics B*, 111(2), pp.165–168.

Zhang, X. et al., 2012. Single frequency optical bistability operation in end-pumped Tm, Ho: YLF lasers. *Applied Physics B*, 108(3), pp.565–569.

Zhu, G. et al., 2010. High-power, high-quality ZGP OPO pumped by a Tm, Ho: GdVO4 laser. *Laser Physics*, 20(6), pp.1341–1343.

11 List of Publications

International Publications and Conferences:

Wayne Koen, Cobus Jacobs, Lorinda Wu, and Hencharl J. Strauss, "60W Ho:YLF oscillator-amplifier system," Solid State Lasers XXIV: Technology and Devices, edited by W. Andrew Clarkson, Ramesh K. Shori, Proc. of SPIE Vol. 9342 93421Y-1 (2015), ISBN: 9781628415131, doi: 10.1117/12.2078786, http://proceedings.spiedigitallibrary.org.

Wayne S. Koen, Cobus Jacobs, Oliver Collett, Daniel Esser, "Efficient Ho:YLF Laser Pumped by a Tm: fiber Laser," Mid-Infrared Coherent Sources, Marriott Paris Rive Gauche Hotel and Convention Center, Paris, France, 27 October - 01 November 2013, Optical Society of America, paper MW1C. 6, ISBN 978-1-55752-9824.

Wayne Koen, Cobus Jacobs, Lourens Botha, Christoph Bollig, H. J. Strauss, and M J Daniel Esser, "Optically pumped tuneable HBr laser in the mid-infrared region," Optics Letters, Vol. 39, No.12, posted 05/05/2014; Doc. ID 209055, http://www.opticsinfobase.org/ol/upcoming_pdf.cfm?id=209055.

W. Koen, C. Bollig, H. Strauss, M. Schellhorn, C. Jacobs, and M.J.D. Esser, "Compact Fibre-Laser-Pumped Ho:YLF Oscillator-Amplifier System," Journal of Applied Physics B, Volume 99, Issue 1, Page 101, 2010, URL: http://www.springerlink.com/content/m823265551470079, DOI: 10.1007/s00340-009-3819-y.

H. J. Strauss, **W. Koen**, C. Bollig, M. J. D. Esser, C. Jacobs, O. J. P. Collett, and D. R. Preussler, "Ho:YLF & Ho:LuLF slab amplifier system delivering 200 mJ, 2 μm single-frequency pulses," Optics Express, Vol. 19, Issue 15, pp. 13974-13979 (2011), http://dx.doi.org/10.1364/OE.19.013974.

Wayne Koen, Cobus Jacobs, Christoph Bollig, Hencharl J. Strauss, Lourens Botha, M.J. Daniel Esser, "Demonstration of a wavelength selected optically pumped HBr laser," Technologies for Optical Countermeasures IX, edited by David H. Titterton, Mark A. Richardson, Proc. of SPIE Vol. 8543, 85430E (Nov 2012), doi: 10.1117/12.974710, ISBN: 0819492841 / ISBN-13: 9780819492845.

R. C. Botha, H. J. Strauss, C. Bollig, **W. Koen**, O. Collett, N. V. Kuleshov, M. J. D. Esser, W. L. Combrinck, and H. M. von Bergmann, "High average power 1314 nm Nd:YLF laser, passively Q-switched with V:YAG," Optics Letters, Vol. 38, Issue 6, pp. 980-982 (2013), http://dx.doi.org/10.1364/OL.38.000980.

H. J. Strauss, D. Preussler, M. J. D. Esser, **W. Koen**, C. Jacobs, O. J. P. Collett, and C. Bollig, "330 mJ single-frequency Ho:YLF slab amplifier," Optics Letters, Vol. 38, Issue 7, pp. 1022-1024 (2013), http://dx.doi.org/10.1364/OL.38.001022

Wayne S. Koen, Cobus Jacobs, Oliver Collett, Daniel Esser, "Efficient Ho: YLF Laser Pumped by a Tm: fiber Laser," Mid-Infrared Coherent Sources, Marriott Paris Rive Gauche Hotel and Convention Center, Paris, France, 27 October - 01 November 2013, Optical Society of America, paper MW1C. 6, ISBN 978-1-55752-9824.

Cobus C. Jacobs, Hencharl J. Strauss, **Wayne S. Koen**, Dieter Preussler, Lourens R. Botha, Oliver J.P. Collett, Chistoph Bollig, "High-energy laser research for infrared countermeasures," SPIE Security + Defence, Edinburgh International Conference Centre, Edinburgh, United Kingdom, 24-27 September 2012 **(invited paper).**

Wayne Koen, Cobus Jacobs, Christoph Bollig, Hencharl J. Strauss, Lourens Botha, M.J. Daniel Esser, "Demonstration of a wavelength selected optically pumped HBr laser," SPIE Security + Defence, Edinburgh International Conference Centre, Edinburgh, United Kingdom, 24-27 September 2012.

M. J. D. Esser, C. Jacobs, **W. Koen**, H. Strauss, D. Preussler, L. R. Botha, O. J. P. Collett and C. Bollig "High-Energy 2 μm Solid-State Laser Development" Fourteenth Annual Directed Energy Symposium, Directed Energy Professional Society, 14-18 November 2011, La Jolla, California (invited) (2011).

M. J. D. Esser, **W. Koen**, H. J. Strauss, C. Jacobs, L. R. Botha, and C. Bollig "An HBr Oscillator-amplifier Pumped by a High-energy Ho:YLF Laser System" in CLEO/Europe and EQEC 2011 Conference Digest, OSA Technical Digest (CD) (Optical Society of America, 2011), paper CA1_3 (2011).

C. Bollig, H.J. Strauss, **W. Koen**, M.J.D. Esser, C. Jacobs, O.J.P. Collett, D.R. Preussler and L.R. Botha, "High-Energy Narrow-Band Mid-Infrared Laser Systems", 20th International Laser Physics Workshop (LPHYS '11) Sarajevo, July 11-15, 2011, Talk #4.5.2. (invited paper) (2011).

H.J. Strauss, D. Preussler, O.J.P. Collett, M.J.D. Esser, C. Jacobs , C. Bollig, **W. Koen,** and K. Nyangaza, "330 mJ, 2 μm, Single Frequency, Ho:YLF Slab Amplifier," in Advanced Solid-State Photonics (ASSP), Istanbul, Turkey, ATuA4, ISBN: 978-1-55752-904-6, (2011).

W. Koen, H.J. Strauss, C. Bollig, M.J.D. Esser, C. Jacobs, O.J.P. Collett, K. Nyangaza, and D. Preussler, "200 mJ Single Frequency Ho:YLF & Ho:LuLF Slab Amplifier System at 2064 nm," in 4th EPS-QEOD Europhoton Conference, Hamburg, Germany, WeC4, Europhysics Conference Abstract Volume 34C, ISBN 2-914771-64-9, (2010).

M.J.D. Esser, H.J. Strauss, **W. Koen (Presenting author)**, O.J.P. Collett and C. Bollig, "End-pumped Ho:YLF & Ho:LuLF Slab Laser," in 4th EPS-QEOD Europhoton Conference, Hamburg, Germany, WeP29, Europhysics Conference Abstract Volume 34C, ISBN 2-914771-64-9, (2010).

C. Bollig, H.J. Strauss, M.J.D. Esser, **W. Koen**, M. Schellhorn, D. Preussler, K. Nyangaza, C. Jacobs, E.H. Bernhardi and L.R. Botha, "Compact Fibre-Laser-Pumped Ho:YLF Oscillator-Amplifier System,"
CLEO Europe, Munich, Germany, 14-19 June, 2009.

C. Bollig, M. J. D. Esser, C. Jacobs, **W. Koen**, D. Preussler, K. Nyangaza and M. Schellhorn, "70 mJ Single-Frequency Q-Switched Ho:YLF Ring Laser-Amplifier System Pumped by a Single 82W Tm Fibre Laser," Middle-Infrared Coherent Sources, Trouville, France, 8-12 June, 2009 **(invited).**

M. J. Daniel Esser, H. Strauss, **W. S. Koen**, D. Preussler, K. Nyangaza and C. Bollig, "Q-switched Ho:YLF Laser Pumped by a Tm:GdVO4 Laser," Middle-Infrared Coherent Sources, Trouville, France, 8-12 June, 2009.

H. J. Strauss, **W. Koen**, C. Bollig, M. J. D. Esser, D. Preussler, K. Nyangaza and C. Jacobs, "Efficient Fiber-Laser-Pumped Ho:YLF Oscillator and Amplifier Utilizing the Transmitted Pump Power of the Oscillator," CLEO, Baltimore, USA, 31 May - 5 June, 2009.

C. Bollig, **W. Koen**, H. Strauss, E.H. Bernhardi, R. Botha, M.J.D. Esser and D. Preussler, "Exploiting the natural doping gradient of Nd:YLF crystals for high-power end-pumped lasers," In Proceedings of the 3rd EPS-QEOD Europhoton Conference, Paris, France, 31 August - 5 September, 2008.

M.J.D. Esser, C. Bollig, D. Preussler, C. Jacobs, **W. Koen** and E.H. Bernhardi, "High power diode and pumped Tm:GdVO4 laser operating at 1818 nm and 1915 nm," In Proceedings of the Marie Curie Chair Conference Recent advances in laser spectroscopy and laser technology, Lodz, Poland, 29-31 May, 2007.

National Conference Papers

Wayne Koen, Cobus Jacobs, Oliver Collett and M.J. Daniel Esser, "Efficient Ho:YLF laser pumped by a Tm:fiber laser," in South African Institute of Physics 58th annual Conference, hosted by University of Zululand, Richard's Bay Campus, 8-12 July 2013, paper 250.

Wayne Koen, Cobus Jacobs, Daniel Esser, Hencharl Strauss, "Mid-Infrared doubly-resonant Optical Parametric Oscillator based on $ZnGeP_2$," in South African Institute of Physics 57th annual Conference, hosted by University of Pretoria, 9-13 July 2012, paper 346.

Cobus Jacobs, **Wayne Koen**, Hencharl Strauss, Oliver Collett, Daniel Esser, "Challenges in developing a Holmium slab laser to pump a rod OPO," in South African Institute of Physics 57th annual Conference, hosted by University of Pretoria, 9-13 July 2012, paper 428.

Wayne Koen, Hencharl Strauss, Daniel Esser, Cobus Jacobs, Lourens Botha, "Demonstration of a wavelength tunable mid-IR molecular laser," in South African Institute of Physics 56th annual Conference, hosted by Unisa, 12-15 July 2011, paper 158.

Daniel Esser, **Wayne Koen**, Hencharl Strauss, Cobus Jacobs, Lourens Botha, Christoph Bollig, Shaun Burd, "2 um pumped Hbr Oscillator-amplifier," in South African Institute of Physics 56th annual Conference, hosted by Unisa, 12-15 July 2011, paper 354.

Hencharl Strauss, Daniel Esser, Cobus Jacobs, Christoph Bollig, **Wayne Koen**, Oliver Collett, Kwanele Nyangaza, Diter Preussler, "2 um Ho doped amplifiers," in South African Institute of Physics 56th annual Conference, hosted by Unisa, 12-15 July 2011, paper 150.

Wayne Koen, Hencharl Strauss, Christoph Bollig and Daniel Esser, "High-power diode-end-pumped Tm:YLF slab laser delivering 189 W at 1890 nm," in South African Institute of Physics 55th annual conference, CSIR, Pretoria, September 2010, paper 205, (2010).

Cobus Jacobs, Hencharl Strauss, Christoph Bollig, Daniel Esser, **Wayne Koen**, Oliver Collett, Kwanele Nyangaza and Dieter Preussler, "Single Frequency 2µm MOPA delivering 200mJ at 50Hz," in South African Institute of Physics 55th annual conference, CSIR, Pretoria, September 2010, paper 280, (2010).

Hencharl Johan Strauss, Shaun Burd, **Wayne Koen**, Cobus Jacobs, Oliver Collett, Kwanele Nyangaza, Dieter Preussler and Christoph Bollig, "Multi pass 1.9 µm Tm:YLF slab laser pump source," in South African Institute of Physics 55th annual conference, CSIR, Pretoria, September 2010, paper 247, (2010).

M. J. D. Esser, C. Jacobs, **W. Koen**, H. Strauss, D. Preussler, L.R. Botha, O. J. P. Collett and C. Bollig, "Development of High-Energy 2 µm Solid-State Lasers," CSIR conference "Science: real and relevant," August 2010.

C. Bollig, M. J. D. Esser, C. Jacobs, **W. Koen**, D. Preussler and K. Nyangaza, "High-energy single-frequency Q-switched 2-μm Ho:YLF oscillator-amplifier system pumped by a thulium fibre laser," in South African Institute of Physics 54th annual conference, University of KwaZulu-Natal, KwaZulu-Natal, July, 2009.

C. Jacobs, C. Bollig, M. J. D. Esser and **W. Koen**, "Electronic feedback control to stabilise a high-energy Ho:YLF ring laser," in South African Institute of Physics 54th annual conference, University of KwaZulu-Natal, KwaZulu-Natal, July, 2009.

M. J. D. Esser, C. Jacobs, S. Ngcobo, **W. Koen**, H. Strauss, D. Preussler, L.R. Botha and C. Bollig, "Development of high-energy 2 μm solid-state lasers," in South African Institute of Physics 54th annual conference, University of KwaZulu-Natal, KwaZulu-Natal, July, 2009.

M.J.D. Esser, C. Bollig, D. Preussler, **W.S. Koen**, E. H. Bernhardi, H.J. Strauss, and M. Schellhorn "Tm:GdVO4 Laser as Pump Source For a Ho:YLF Laser Oscillator," in South African Institute of Physics 53rd annual conference, University of Limpopo, Polokwane, July, 2008.

W. Koen, C. Bollig, H. Strauss, R. Botha, E. Bernhardi, and M. J. D. Esser, "Power Scaling of a High-Power End-Pumped Nd:YLF Laser," in South African Institute of Physics 53rd annual conference, University of Limpopo, Polokwane, July, 2008.

H. J. Strauss, C. Bollig, M. J. D. Esser, M. Schellhorn, D. Preussler, C. Jacobs, K. Nyangaza and **W. Koen**, "High energy fibre laser pumped Ho:YLF 2 μm laser," in South African Institute of Physics 53rd annual conference, University of Limpopo, Polokwane, July, 2008.

C. Bollig, D. Preussler, M. J. D. Esser, S. Ngcobo, C. Jacobs, R. C. Botha, **W. S. Koen**, E. H. Bernhardi, A. R. Sarmani and L. R. Botha, "Solid-state laser source research at the CSIR - National Laser Centre," in South African Institute of Physics 52nd annual conference, University of the Witwatersrand, Johannesburg, July, 2007.

M.J.D. Esser, C. Bollig, D. Preussler, C. Jacobs, **W. Koen** and E.H. Bernhardi, "Diode-end-pumped Tm:GdVO4 laser at selected wavelengths," in Proceedings of the 52nd South African Institute of Physics Conference, University of the Witwatersrand, Johannesburg, South Africa, July, 2007.

W. S. Koen, C. Bollig, A. Forbes, A. R. Sarmani, R. C. Botha and M. J. D. Esser, "Ultra short-pulse (USP) laser development," in South African Institute of Physics 52nd annual conference, University of the Witwatersrand, Johannesburg, July, 2007.

R. C. Botha, C. Bollig, **W. S. Koen**, A. R. Sarmani, L. R. Botha and C. Jacobs, "Energy scaling techniques in ultra-short pulse lasers," in South African Institute of Physics 52nd annual conference, University of the Witwatersrand, Johannesburg, July, 2007.

R. C. Botha, C. Bollig, **W. S. Koen** and N. V. Kuleshov, "High-Power Continuous-Wave and Passively Q-switched 1314 nm Nd:YLF laser," in South African Institute of Physics 50th annual conference, Pretoria, 2005.